

**UNCLASSIFIED**

**AD 410441**

**DEFENSE DOCUMENTATION CENTER**

**FOR**

**SCIENTIFIC AND TECHNICAL INFORMATION**

**CAMERON STATION, ALEXANDRIA, VIRGINIA**



**UNCLASSIFIED**

NOTICE: When government or other drawings, specifications or other data are used for any purpose other than in connection with a definitely related government procurement operation, the U. S. Government thereby incurs no responsibility, nor any obligation whatsoever; and the fact that the Government may have formulated, furnished, or in any way supplied the said drawings, specifications, or other data is not to be regarded by implication or otherwise as in any manner licensing the holder or any other person or corporation, or conveying any rights or permission to manufacture, use or sell any patented invention that may in any way be related thereto.

SSD-TDR-63-76

N-63-4-3  
REPORT NO.  
TDR-169(3240)TN-1

①

AD No. \_\_\_\_\_  
DDC FILE COPY 410441

# Materials and Structures Program

SEMIANNUAL TECHNICAL NOTE

(1 July - 31 December 1962)

*Seeley*

20 MAY 1963

Prepared by MATERIALS SCIENCES LABORATORY

Prepared for COMMANDER SPACE SYSTEMS DIVISION

UNITED STATES AIR FORCE

Inglewood, California

JUL 29 1963

410441



LABORATORIES DIVISION • AEROSPACE CORPORATION  
CONTRACT NO. AF O4(695)-169

11.50

18  
19  
SSD TDR 63/76

4 11.50

5 17505 7-8 NA

14  
Rept. No.  
TDR 169/3240 TN/1

6 MATERIALS AND STRUCTURES PROGRAM.

9 SEMIANNUAL TECHNICAL notes  
(1 Jul - 31 Dec 1962)

10 NA  
11 20 May 63  
12 IV. 13 NA  
16 + 17 NA

Prepared by  
Materials Sciences Laboratory

20 W  
21 NA

AEROSPACE CORPORATION  
El Segundo, California

Fdc

15 Contract AF 04/695/169

20 May 1963

Handwritten signature

Prepared for  
COMMANDER SPACE SYSTEMS DIVISION  
UNITED STATES AIR FORCE  
Inglewood, California

## GENERAL ABSTRACT

Progress during the report period on the study of the fundamental principles of crystal growth and the preparation of single crystals of laser and electronic materials for research purposes is reported in ~~Laser and Electronic Materials~~. Studies on <sup>the</sup> effect of structure (crystal lattice and defects) on certain physical properties such as superconductivity, semiconductivity, laser activity, and mechanical behavior, are reported in ~~Materials Physics~~. The study of crystal growth is reported in ~~Inorganic Chemistry~~. Results for electrochemical methods used in the study of foreign metal ions in ionic solids are described in ~~Electrochemistry of Solids~~. Work in High Temperature Chemistry during the report period consisted of studies in polymer synthesis and polymer mechanical properties and studies of the combustion of tetrafluoroethylene, which is the monomer and chief pyrolysis product of Teflon. Physical Measurements covers property changes in pyrolytic graphite for ballistic re-entry heat shields, space environment effects on prospective satellite thermal control surface materials, and laser effects on materials. Progress in studies on refractory metals, refractory metal carbides, and refractory oxides during the report period is reviewed in ~~Metallurgy and Ceramics Research~~.

## GENERAL CONTENTS

I.	LASER AND ELECTRONIC MATERIALS . . . . .	1-1
A.	INTRODUCTION . . . . .	1-1
B.	TECHNIQUES . . . . .	1-2
C.	DISCUSSION . . . . .	1-3
D.	THEORETICAL PROBLEMS IN CRYSTAL GROWTH . . . . .	1-4
E.	OTHER ELECTRONIC MATERIALS. . . . .	1-5
F.	EXPERIMENTAL RESULTS - LASER CRYSTALS . . . . .	1-6
G.	REFERENCES . . . . .	1-15
II.	MATERIALS PHYSICS . . . . .	2-1
A.	INTRODUCTION . . . . .	2-1
B.	DISCUSSION . . . . .	2-1
C.	MECHANICAL PROPERTIES . . . . .	2-5
D.	REFERENCES . . . . .	2-16
III.	INORGANIC CHEMISTRY . . . . .	3-1
A.	INTRODUCTION . . . . .	3-1
B.	CRYSTAL GROWTH . . . . .	3-3
C.	PHASE TRANSITION IN SINGLE CRYSTAL $ZrO_2$ . . . . .	3-4
D.	EFFECT OF PRESSURE ON THE MONOCLINIC- TETRAGONAL TRANSITION IN $ZrO_2$ . . . . .	3-5
E.	REFERENCES . . . . .	3-7
IV.	ELECTROCHEMISTRY OF SOLIDS . . . . .	4-1
A.	INTRODUCTION . . . . .	4-1
B.	EXPERIMENTAL METHODS AND RESULTS . . . . .	4-2
C.	REFERENCES . . . . .	4-4

GENERAL CONTENTS (Continued)

V.	HIGH TEMPERATURE CHEMISTRY . . . . .	5-1
	A. INTRODUCTION . . . . .	5-1
	B. SYNTHETIC WORK TOWARD HIGH TEMPERATURE POLYMERS . . . . .	5-2
	C. MECHANICAL PROPERTIES OF THREE- DIMENSIONAL POLYMER NETWORKS . . . . .	5-4
	D. THE REACTION OF TETRAFLUOROETHYLENE WITH OXYGEN . . . . .	5-5
	E. REFERENCES . . . . .	5-8
VI.	PHYSICAL MEASUREMENTS . . . . .	6-1
	A. PYROLYTIC GRAPHITE . . . . .	6-1
	B. SPACE ENVIRONMENTAL EFFECTS . . . . .	6-7
	C. EMISSIVITY STUDIES . . . . .	6-11
	D. EFFECT OF LAZER BEAMS ON MATERIALS . . . . .	6-21
	E. REFERENCES . . . . .	6-24
VII.	METALLURGY AND CERAMICS RESEARCH . . . . .	7-1
	A. INTRODUCTION . . . . .	7-1
	B. REFRACTORY METALS . . . . .	7-1
	C. REFRACTORY CARBIDES . . . . .	7-24
	D. REFRACTORY OXIDES . . . . .	7-34

**LASER AND ELECTRONIC MATERIALS**

(JO 3240-10)

Prepared by

J. W. ROWEN

R. W. WILCOX

## ABSTRACT

The purpose of the Laser and Electronic Materials Program is to study the fundamental principles of crystal growth and to prepare single crystals of laser and electronic materials for research purposes. To accomplish these objectives the following methods have been put into effect: the flame fusion method, the metal oxide flux method, the Czochralski method, and the zone refining method. With these techniques the following potential laser single crystals have been prepared: ruby, chromium-doped gallium oxide, gallium-yttrium garnets containing rare earths, and barium fluoride. The absorption and fluorescence spectra of some of these materials have been examined. The preparation and properties of other electronic materials such as superconductors and semiconductors have also been considered.

Theoretical studies have been made on the selection of optimum types of laser host crystals and on the heat and mass transfer problems associated with crystal growth.

#### ACKNOWLEDGMENTS

The authors wish to acknowledge the substantial contributions of Judith A. Osmer and Hugh S. Guthrie to this program. Also, they are especially indebted to Dr. Harry H. Tippins for the fluorescence measurements of Fig. 6. Acknowledgment is also given to Drs. Hans Conrad and Milton Birnbaum for many stimulating discussions.

#### ACKNOWLEDGMENTS

The authors wish to acknowledge the substantial contributions of Judith A. Osmer and Hugh S. Guthrie to this program. Also, they are especially indebted to Dr. Harry H. Tippins for the fluorescence measurements of Fig. 6. Acknowledgment is also given to Drs. Hans Conrad and Milton Birnbaum for many stimulating discussions.

## CONTENTS

ABSTRACT .....	1-i
A. INTRODUCTION .....	1-1
B. TECHNIQUES .....	1-2
1. The Flame Fusion Method .....	1-2
2. The Flux Method .....	1-2
3. The Czochralski Technique .....	1-2
4. The Zone Refining Method .....	1-3
C. DISCUSSION .....	1-3
D. THEORETICAL PROBLEMS IN CRYSTAL GROWTH .....	1-4
1. Heat Transfer in Crystal Pulling .....	1-4
2. Incomplete Mixing in Fractional Crystallization from the Melt .....	1-4
E. OTHER ELECTRONIC MATERIALS .....	1-5
1. Superconductors .....	1-5
2. Semiconductors .....	1-6
F. EXPERIMENTAL RESULTS - LASER CRYSTALS .....	1-6
1. Aluminum Oxide Host (Ruby) .....	1-6
2. Gallium Oxide Host .....	1-6
3. Dislocations in Growth of Ruby .....	1-7
4. Garnet Hosts .....	1-7
5. Fluoride Hosts .....	1-7
6. Low-Melting Hosts .....	1-8
G. REFERENCES .....	1-15

## FIGURES

1	Modified Flame Fusion Apparatus . . . . .	1-9
2	Temperature versus Various Gas Mixtures . . . . .	1-10
3	Temperature versus Various Gas Flow Rates . . . . .	1-11
4	Seven Ruby Boules at Two Crystal Orientations . . . . .	1-12
5	Chromium-Doped Gallium Oxide Crystals. . . . .	1-13
6	Sharp Line Fluorescent Intensity of Chromium-Doped Gallium Oxide . . . . .	1-14

## I. LASER AND ELECTRONIC MATERIALS

### A. INTRODUCTION

The Laser and Electronic Materials Program has a twofold objective. The first objective is to study the fundamental principles of crystal nucleation and growth at elevated temperatures. The second part deals with the use of these growth principles to obtain improved understanding and performance of laser and electronic materials. The program is closely coupled with related Air Force investigations of high gain radiation systems, amplifiers, oscillators, computers and similar devices in the Electronics Research Laboratory. It will be seen below that this approach is based in part upon the hypothesis that the improved understanding of stimulated emission of coherent radiation may be obtained through the preparation, characterization and study of transitional metal and rare earth metal ions appropriately placed in the oxides of metals of the third group of the periodic table and in the alkaline earth halide crystals.

To study the significant parameters which control crystal defects and crystal growth, it is necessary first to devise and to install methods of crystal growth. These steps will make possible not only the observation of significant parameters of heat and mass transfer in the growth process, but also the relaxation mechanisms which accompany the origin of imperfections and cracking in the final crystal. These imperfections may have an important bearing upon the efficiency of the quantum process of stimulated emission. The cracking, on the other hand, has an important bearing upon the cost and utilization of these crystalline materials. Part I, therefore, deals with the planning, installation and application of the following four types of techniques: (1) the flame fusion method, (2) the metal oxide flux method, (3) the Czochralski method, and (4) the zone refining technique.

## B. TECHNIQUES

### 1. The Flame Fusion Method

One of the most widely used methods of preparing large single crystals of metal oxides, garnets and ferrites utilizes the flame fusion apparatus. Therefore, a modified flame fusion apparatus has been assembled, calibrated and put into operation as shown in Fig. 1. In Fig. 2 a number of gradients are shown which were obtained with the apparatus shown in Fig. 1; Figure 3 shows a moderate range of gas flow rates and a flexibility of temperature control in this same apparatus.

This preparation method exposed the problem of cracking, upon completion of growth, of the single crystals of ruby. Consideration of this problem led to experiments (Ref. 1) which have since provided a better understanding of the role of the temperature gradients and of flame profiles in annealing and in avoiding the accumulation of "built-in" strains in ruby crystals (Ref. 2).

### 2. The Flux Method

A special Super Kanthal furnace and programmer, operating with good temperature control ( $\Delta t = 2^{\circ}\text{C/hr}$ ) over the range of 1300 to 500 $^{\circ}\text{C}$ , accompanying platinum crucibles (500 cc), and boats were obtained and installed. With this furnace it was possible to grow single crystals of  $\text{Cr}^{+3}$ -doped  $\text{Ga}_2\text{O}_3$  crystals which are described in Part II of the Experimental Results.

### 3. The Czochralski Technique

The only large dislocation-free crystals reported thus far were made by the Czochralski, or crystal-pulling, process (Refs. 4, 5). Although these crystals were germanium and silicon, it is expected that large laser crystals of high perfection can be grown by the same technique which has been slightly modified. Accordingly, a Czochralski apparatus and accessories similar to those used for growing semiconductor crystals have been purchased. The equipment is being made ready for operation.

#### 4. The Zone Refining Method

Zone refining is a useful tool not only for purification of starting materials for crystal growth studies, but under proper conditions it can also produce single crystals. At present, two zone refiners are available. For materials melting up to 1500°C, a platinum (20 percent rhodium) wound reciprocating multipass zone refiner has been constructed which is similar to that described by Pfann (Ref. 6). Five zones are available with travel rates down to 1/16-inch per hour. In early runs the graphite boat was pushed back and forth by push rods inside the surrounding furnace tube. This tube, on which the platinum (20 percent rhodium) is wound, has cracked and another liner tube is being placed inside the furnace. The boat will be placed in this new tube and the whole liner tube moved back and forth. A Fisher Zone Refiner is also available for crystals which melt between room temperature and 1000°C. As supplied, the motion of the refiner was too rapid (~1/4 in. /hr) and it has been modified for speeds of less than 1/16 in. /hr. A Sola constant-voltage transformer is employed to stabilize the heat input and, hence, the zone size.

#### C. DISCUSSION

The original program plan (Ref. 3) called for the study of group three metal oxide hosts but was later extended to include mixtures of gallium and aluminum, yttrium, lanthanum and gadolinium oxides, as well as the alkaline earth halides containing rare earth ions. The two forms of gallium oxide ( $\alpha$ - and  $\beta$ -forms) have certain similarities and differences when they are compared with the successful laser host, aluminum oxide (ruby). The differences relate to crystal symmetry and metal ion radii, whereas the similarities relate to the melting point, mechanical properties, and lattice point group. For these same reasons the mixed gallium-aluminum oxides,  $\text{Ga}_x\text{Al}_{2-x}\text{O}_3$  ( $0.7 \leq x \leq 1.3$ ) and the gallium-yttrium garnets ( $\text{Ga}_5\text{Y}_3\text{O}_{12}$ ) are also of interest.

The alkaline earth fluorides are relatively simple crystal structures which may be good hosts for paramagnetic ions such as cerium<sup>+3</sup> and which also may be useful for study and clarification of the above-mentioned growth principles.

#### D. THEORETICAL PROBLEMS IN CRYSTAL GROWTH

##### 1. Heat Transfer in Crystal Pulling

Two necessary factors in the growth of high perfection crystals by the Czochralski technique are low thermal stresses and a controlled solid-liquid interface shape (Ref. 7). Both factors depend on the temperature distribution in the solid which, in principle, can be calculated. Because the shape of the freezing interface initially is unknown, this represents a free-boundary problem and is very difficult to solve. The location of the interface is specified by two conditions. Each point on the interface must be at the melting point. Second, the heat flux normal to the interface in the solid at each point must be equal to the sum of the rate of liberation of latent heat of freezing at that point and the heat conducted from the melt. Solution of this problem has been undertaken by the authors in conjunction with A. R. Sims et al. of the Aerospace Computation Department. Initially, the problem has been simplified by ignoring the heat carried in the solid by its own movement (due to growth) and by assuming constant properties and constant heat transfer coefficients from crystal to surroundings and to the melt.

##### 2. Incomplete Mixing in Fractional Crystallization from the Melt

The final distribution of doped ions in laser crystals grown from the melt is an important parameter. In prediction of the distribution the degree of mixing in the melt must be considered. The boundary-layer assumption corresponds closely to actual conditions. In this case the bulk of the melt is assumed to be completely mixed while a thin layer on the freezing interface is completely stagnant. This treatment has been used by Burton, Prim, and Slichter (Ref. 8) for the case of constant distribution coefficient.

We have extended this work to simple eutectic and other systems. We also have calculated the initial transient that previously had been ignored. This treatment will be covered more fully in a subsequent report. (Ref. 9).

Two additional problems have appeared during the course of this work and are being considered. The first problem is the dependence of the crystal growth rate in the flux method upon the temperature range and the number of cycles. The second problem is the dependence of the crystallization rate upon the surface free energy of a nonplanar face containing a dislocation.

#### E. OTHER ELECTRONIC MATERIALS

In addition to the work on growth of laser crystals, a limited amount of work has been done on other electronic materials.

##### 1. Superconductors

One hypothesis explaining hard superconductivity is the thin-film or filament theory. This theory holds that a superconductor will be hard if one of its dimensions is of the order of the penetration thickness. An attempt is being made to prepare thin layers of superconductors by electroplating. Two methods are being employed: (1) alternate plating of two different materials in separate baths, and (2) plating an alloy of alternate layers of two metals deposited from a single bath<sup>1</sup>. Preliminary experiments have been carried out on the plating of alternate thin layers of copper and lead from fluorborate baths onto copper wire. An alloy of lead and tin has also been plated from a fluorborate bath. These materials will be tested for their superconducting properties by the Electronics Research Laboratory of Aerospace Corporation.

---

<sup>1</sup>For example, alternate layers of tin and copper may be plated from a stannate cyanide bath under proper conditions (Ref. 10).

## 2. Semiconductors

Analyses of radiotracer data on the diffusion of gold into silicon have shown that the mechanism involves a vacancy-controlled interstitial-substitutional equilibrium combined with rapid interstitial diffusion (Ref. 11). In addition, a value for the self-diffusion coefficient of silicon was determined from the calculation. (The self-diffusion coefficient for silicon cannot be measured directly because no suitable silicon radiotracer is available,)

In analytical solutions for diffusions performed in manufacturing semiconductor devices, the repeated integral of the error function complement sometimes appears. This Laboratory has derived a new method of determining these functions, and, thereby, has calculated a series of values over the range of usual interest (Ref. 12).

The internal heating problem for an interdigitated power transistor has been solved analytically for the first time (Ref. 13).

## F. EXPERIMENTAL RESULTS - LASER CRYSTALS

### 1. Aluminum Oxide Host (Ruby)

It was possible to grow high quality single crystals of chromium ( $\text{Cr}^{+3}$ ) doped aluminum oxide (ruby) with the flame fusion apparatus described above. Examples of seven of these boules at two different crystal growth orientations are shown in Fig. 4. As a result of this exploratory work it was possible to describe (Ref. 1) an objective, reproducible crystal growing procedure. A description of this procedure has been prepared so that it may be used as an operator's manual for the growing of single crystals of synthetic sapphire, ruby, gallium-rich rubies, rare earth oxides and other electronic materials.

### 2. Gallium Oxide Host

Single crystals of chromium-doped gallium oxide, 3 x 10 by 1 mm, have been grown by the flame fusion and flux methods described above. These

crystals are shown in Fig. 5. The sharp line fluorescence of other samples has been measured, in collaboration with members of the Electronics Research Laboratory, by employing the high resolution grating (resolving power  $\geq 0.05 \text{ \AA}$ ) of the Jarrell Ash spectrometer. An example of the sharpening of the  $R_1$  and  $R_2$  lines in chromium-doped gallium oxide is shown in Fig. 6. The Figure shows that the fluorescence is shifted to shorter wavelengths when the temperature is lowered from room temperature to  $77^\circ\text{K}$ . This temperature change causes the half width of the bands to decrease from a range of  $25\text{-}27 \text{ \AA}$  to  $4 \text{ \AA}$  in the case of the  $R_1$  line ( $6956 \text{ \AA}$ ), and to  $12 \text{ \AA}$  in the case of the  $R_2$  line ( $6885 \text{ \AA}$ ). The relationship of these lines and their shifts to the ruby lines and shifts will be discussed in a future publication.

### 3. Dislocations in Growth of Ruby

A study of the possible importance of growth parameters upon the density of dislocations in ruby crystals is well under way.

### 4. Garnet Hosts

Additional work during the reporting period in gallium-yttrium garnets doped with 0.2 to 20 percent europium<sup>+3</sup> showed sharp line spectra, and this work is being pursued. There are now available extremely pure samples of  $\alpha$ -gallium oxide doped with chromium,  $\beta$ -gallium oxide doped with chromium and gallium-aluminum oxide doped with chromium.

### 5. Fluoride Hosts

The alkaline earth fluorides,  $\text{BaF}_2$ ,  $\text{SrF}_2$  and  $\text{CaF}_2$  have been chosen for crystal growth by the Czochralski technique. Previous work has demonstrated that these fluorides are suitable host materials for rare earth fluoride doping to give laser crystals (Ref. 14 to 16). Also, an etch-pit technique to determine dislocations in calcium fluoride has been developed by Philips (Ref. 17). Therefore, we hope not only to grow new laser crystals from these fluorides but also to learn about the growth processes which will lead to more perfect crystals.

To purify the starting materials the reciprocating multi-pass zone refiner is being used. Preliminary runs on reagent grade (~99 percent pure) barium and strontium fluorides have been made. A single zone pass on strontium fluoride segregated graphite from the boat, but gave milky white crystals. The remaining impurity is thought to be principally strontium oxide. Two zone passes on barium fluoride gave clear crystals, part of which were yellow colored, indicating some iron impurity. Both fluoride crystals cracked into several large pieces soon after the boat was removed from the furnace.

#### 6. Low-Melting Hosts

It would be convenient if the laser crystal as-grown were perfectly cylindrical. This would eliminate the usual elaborate polishing involved in preparing a laser from a crystal. One way of accomplishing this growth is to grow the crystal in a cylindrical cavity. If the walls of the container were optically clear the crystal would not have to be removed from it. Accordingly, the growth of low melting crystals in Pyrex and quartz tubing in the Fisher Zone Refiner has been attempted. Lanthanum nitrate (hydrate), magnesium nitrate (hydrate), and strontium nitrate have been tried so far in 9 mm I. D. Pyrex and Vycor tubing. The lanthanum nitrate gave only milky crystals. The melt was very viscous and showed a great tendency to supercool to a glass when initially filling the tubes. The strontium nitrate gave only milky crystals and, in addition, attacked the Vycor tubing. Although the solid was white, the melt was yellow, probably indicating dissolved nitrogen oxides. Upon melting in an open crucible, some brown gas is evolved. The magnesium nitrate gave clear crystals at the low speed (<1/16 in/hr). Single crystals were obtained when the zone was started at a constriction made in the tube to select a single nucleus for growth. Growth in larger diameter tubes has not been successful. The solid had a tendency to pull away from the glass, to crack, and to form several crystals instead of one.

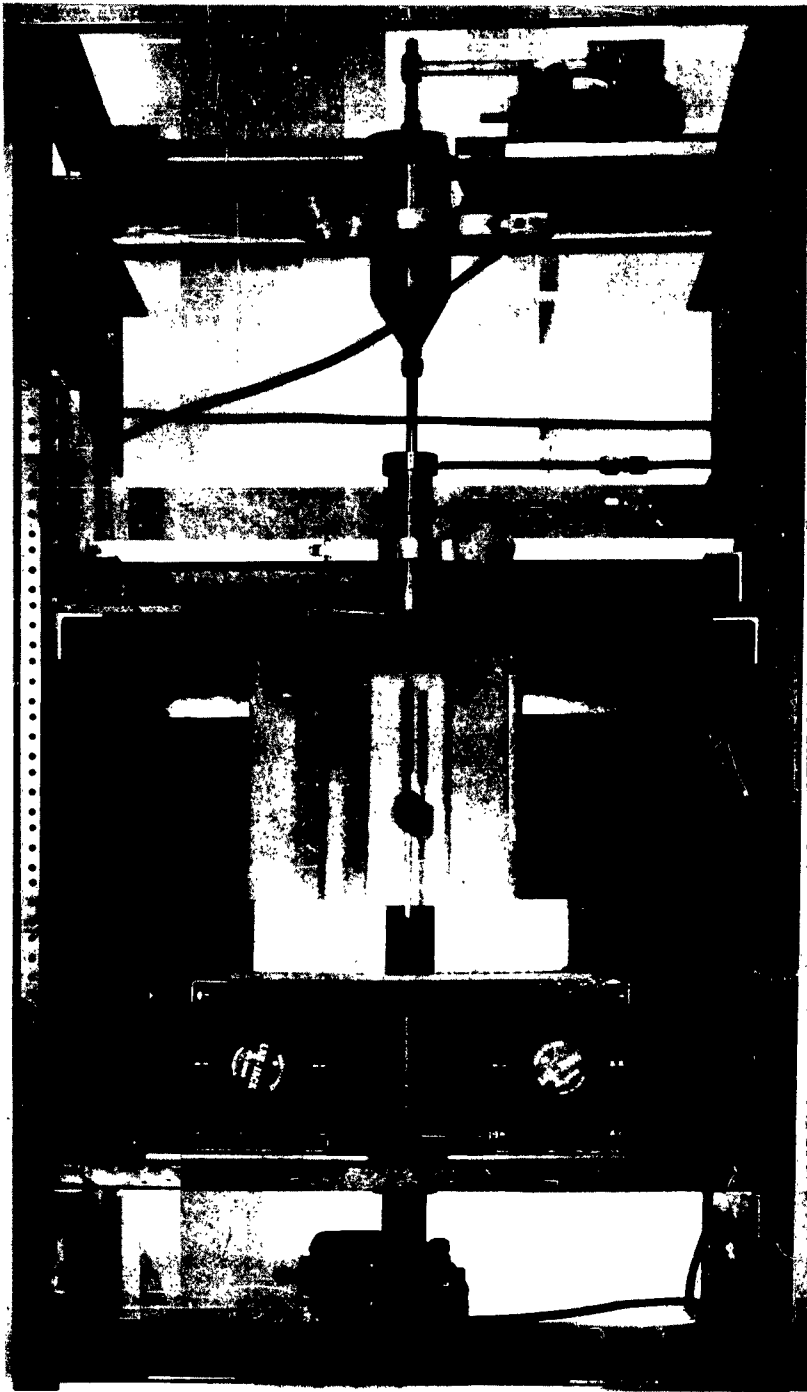


Figure 1. Modified Flame Fusion Apparatus

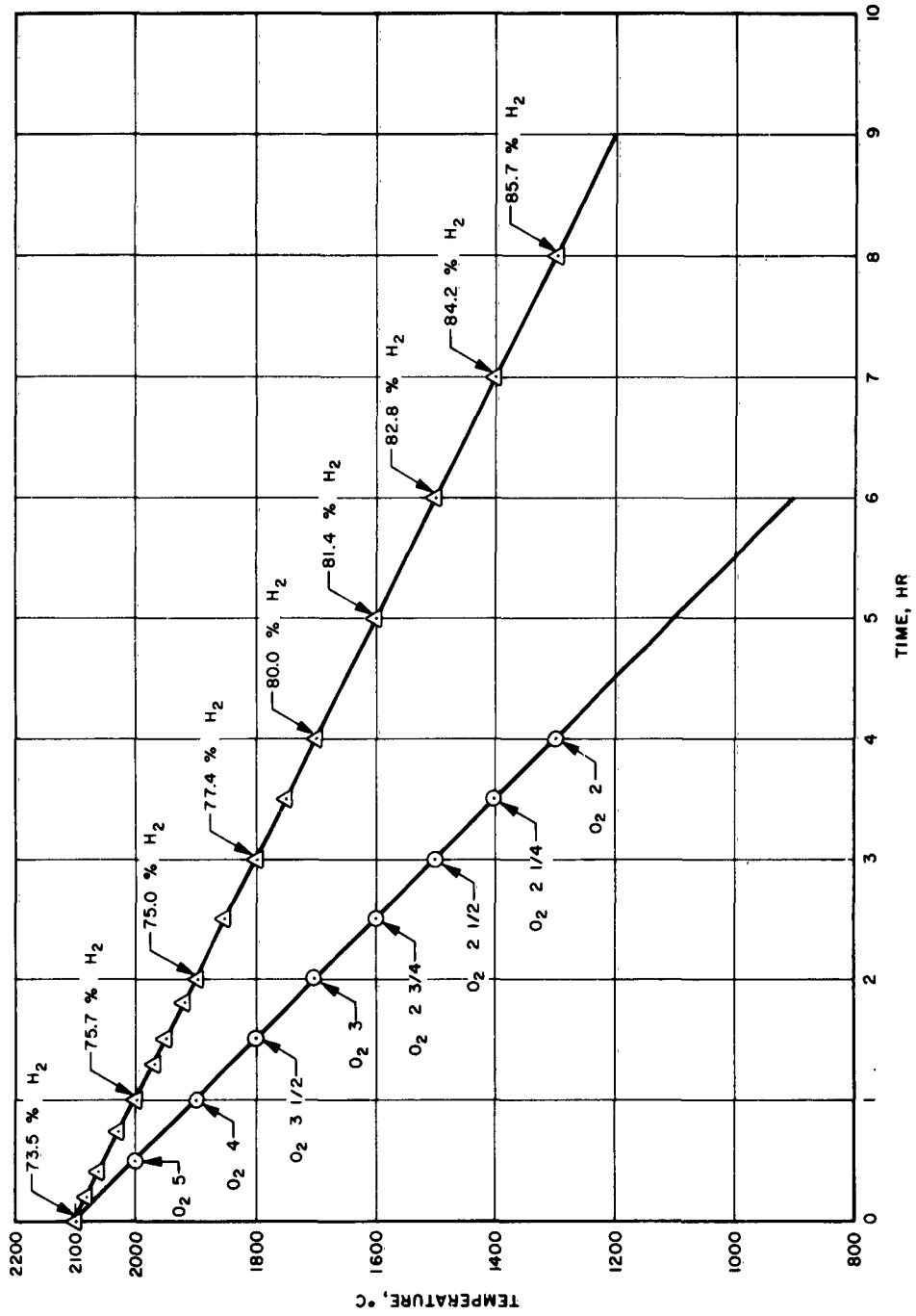


Figure 2. Temperature versus Various Gas Mixtures

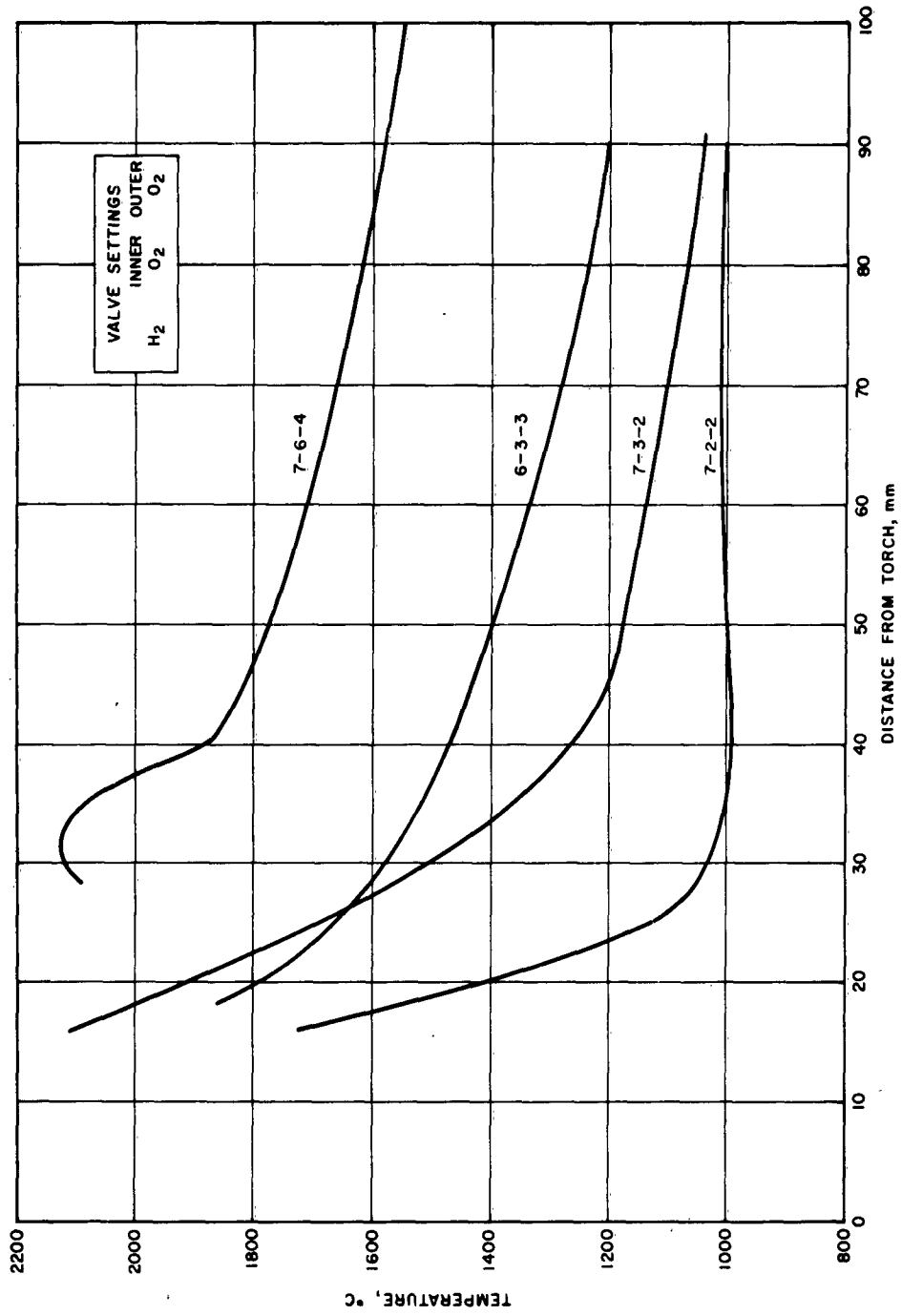


Figure 3. Temperature versus Various Gas Flow Rates

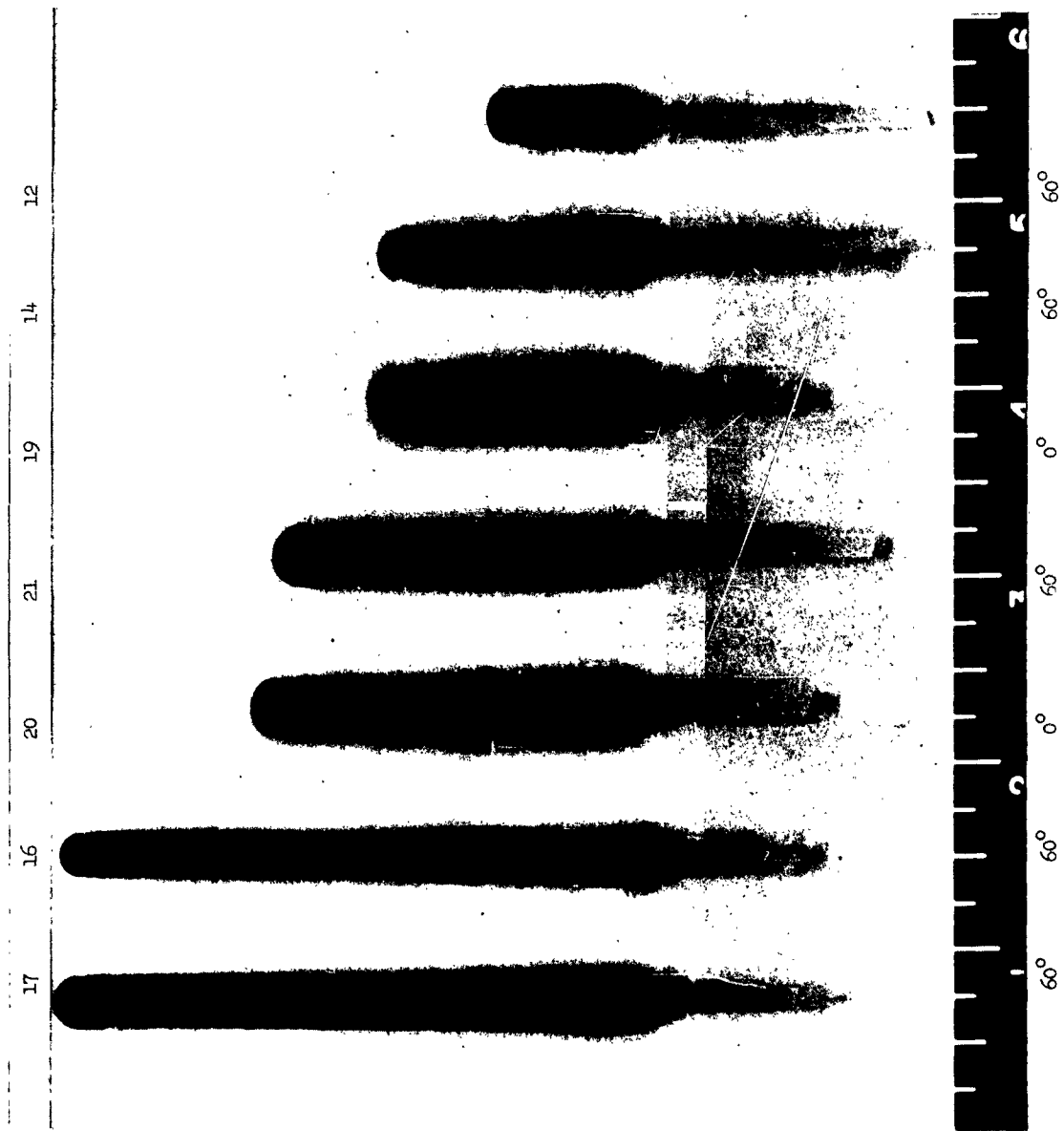


Figure 4. Seven Ruby Boules at Two Crystal Orientations



Figure 5. Chromium-Doped Gallium Oxide Crystals

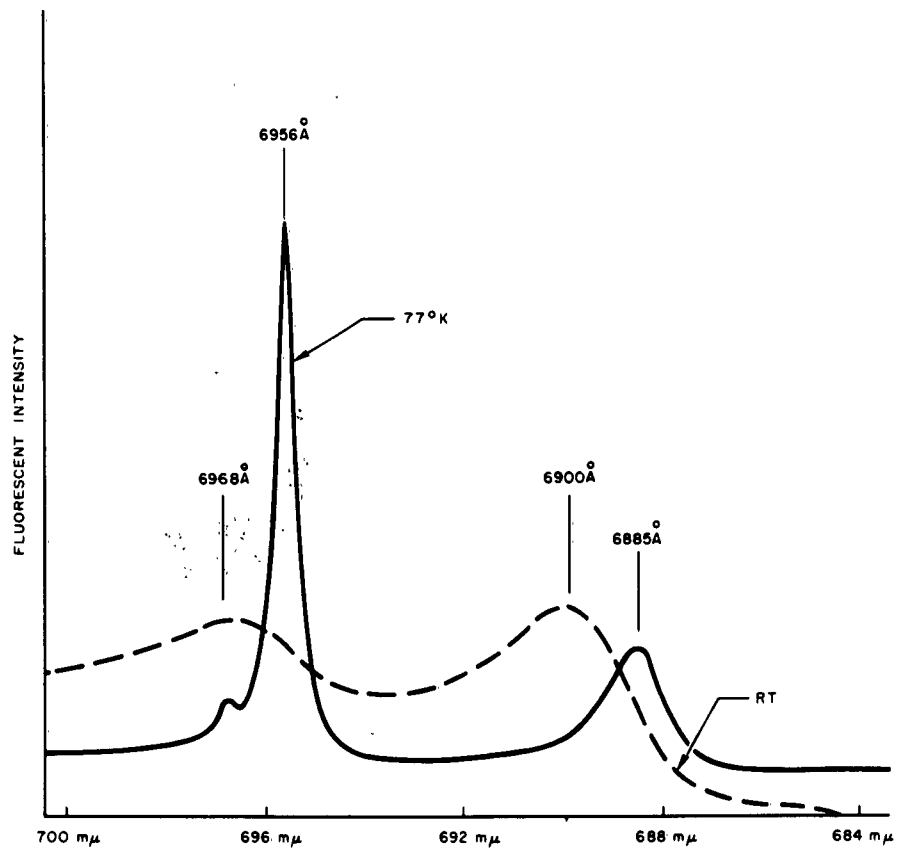


Figure 6. Sharp Line Fluorescent Intensity of Chromium-Doped Gallium Oxide

## G. REFERENCES

1. J. W. Rowen, J. A. Osmer, and H. S. Guthrie, "Calibration and Operation of a Modified Flame Fusion Apparatus," Aerospace Report No. TDR-169(3240-10)TR-1 (Oct. 26, 1962).
2. J. W. Rowen, "Current Laser Materials Research at Six Governmental and Non-Governmental Establishments," memorandum to H. Conrad dated 30 July 1962.
3. Laser and Electronic Materials Program of the Program Plan of the Materials Sciences Laboratory (1 July 1962).
4. W. C. Dash in Growth and Perfection of Crystals, ed. Doremus, Roberts, Turnbull (Wiley, 1958), pp. 372-385.
5. F. D. Rosi, "Effect of Crystal Growth Variables on Electrical and Structural Properties of Germanium," RCA Review 19, 349 (1958).
6. W. G. Pfann, Zone Melting (J. Wiley and Sons, Inc., 1958) 70, Fig. 4.8(d).
7. D. T. J. Hurle, Progress in Materials Science 10, ed. Bruce U. Chalmers (Pergamon Press, 1962), p. 140.
8. J. A. Burton, R. C. Prim and W. P. Slichter, "The Distribution of Solute in Crystals Grown from the Melt" J. Chem. Phys. 21, 1987 (1953).
9. W. R. Wilcox, "Incomplete Mixing in Crystallization from the Melt," report in preparation.
10. W. T. Lee, "Bronze Plating from Modified Stannate Cyanide Baths," Trans. Inst. Metal Finishing 36, 51 (1958-59).
11. W. R. Wilcox, and T. J. LaChapelle, "Mechanism of Gold Diffusion into Silicon," in preparation, to be submitted to J. Appl. Phys.
12. W. R. Wilcox, "Computation of the Repeated Integrals of the Error Function Complement," TDR-169(3240-10)TR-2 (Jan. 1963), submitted to Math of Comp.
13. W. R. Wilcox, "Heat Transfer in Power Transistors," Aerospace Report No. TDR-169(3240-10)TR-3 (February 1963), submitted to IRE Trans. Elect. Devices.

14. P. P. Sorokin, et al., "Spectroscopy and Optical Maser Action in  $\text{SrF}_2:\text{Sm}^{2+}$ " Phys. Rev. 127, 503 (1962).
15. G. G. B. Garrett, W. Kaiser, D. L. Wood, "Fluorescence and Optical Maser Effects in  $\text{CaF}_2:\text{Sm}^{++}$ ," Phys. Rev. 123, 766 (1961).
16. H. Guggenheim, "Growth of Single-Crystal Calcium Fluoride with Rare Earth Impurities," J. Appl. Phys. 32, 1337 (1961).
17. W. C. Phillips, Jr., "Deformation and Fracture Processes in Calcium Fluoride Single Crystals," J. Am. Ceram. Soc. 44, 499 (1961).

**MATERIALS PHYSICS**

**(JO 3240-11)**

**Prepared by**

**H. CONRAD**

**R. B. BENSON**

**S. F. FREDERICK**

**K. R. JANOWSKI**

**E. J. STOFEL**

## ABSTRACT

The objective of this program is to establish the effect of structure (crystal lattice and defects) on certain physical properties such as superconductivity, semiconductivity, laser activity, and mechanical behavior. The first three areas represent new research activities, and the work during the past six months consisted principally of establishing the necessary equipment and developing the techniques of sample preparation and property measurement. Work on mechanical properties had been underway previous to this report period and significant additional progress was made during the past six months. The major accomplishments were:

- (1) The Peierls-Nabarro stress and energy and the kink energy were calculated for the b.c.c. transition metals (V, Nb, Ta, Cr, Mo, W, Fe) from yielding and flow data at low temperatures.
- (2) Dislocation densities and the change in deformation cell size with strain were calculated for f. c. c. and b. c. c. metals on the basis that the effect of grain size on the yield and flow stresses of metals is associated with the average distance that dislocations move during deformation.
- (3) The high temperature mechanical property data for three superalloys (N-155, René 41 and L-605) were correlated using Weertman's dislocation climb model of high temperature creep.
- (4) The effect of chromium on the dislocation structure of nickel deformed by rolling at room temperature was established.

## CONTENTS

ABSTRACT . . . . .	2-i
A. INTRODUCTION . . . . .	2-1
B. DISCUSSION . . . . .	2-1
1. Superconductivity . . . . .	2-1
2. Semiconductor Radiation Damage . . . . .	2-2
3. Laser Activity . . . . .	2-3
C. MECHANICAL PROPERTIES . . . . .	2-5
1. Yielding and Flow of the B.C.C. Transition Metals at Low Temperatures . . . . .	2-5
2. Effect of Grain Size on the Yield and Flow Stress of Metals . . . . .	2-6
3. Correlation of High Temperature Mechanical Properties of Certain Superalloys . . . . .	2-7
4. Effect of Stacking-Fault Energy on the Creep of Ni-Base Alloys . . . . .	2-8
5. The Nickel-Chromium System . . . . .	2-8
a. Alloy Preparation . . . . .	2-8
b. Stacking-Fault Energy Measurements . . . . .	2-9
D. REFERENCES . . . . .	2-16

## FIGURES

1. Comparison of the Calculated Average Distance Moved by Dislocations during Each 10 Percent Increment of Strain, $s_1$ , with Measured Deformation Cell Size . . . . .	2-12
2. Dislocation Structures of Ni-Cr Alloys Deformed Approximately 10 Percent by Rolling at Room Temperature . . . . .	2-13

TABLES

1	Comparison of Counted and Calculated Dislocation Densities . . . . .	2-7
2	Electropolishing Conditions for the Preparation of Thin- Films of Ni-Cr Alloys for Electron Transmission Studies . . . . .	2-10

## II. MATERIALS PHYSICS

### A. INTRODUCTION

Many of the physical properties (both mechanical and electronic) are structure sensitive, that is, they are sensitively dependent upon the microstructure (phase and grain distribution) and on crystal defect structure (impurities, vacancies, and dislocations). To predict the behavior of materials and to design new materials with desired properties, it is essential to know what structure and defects are present and to what degree they affect a particular property. The objective of the Materials Physics Program is to identify the structure (defect and microstructure) of materials to be used in space and missile systems and to determine the effect of this structure on desired physical properties. Some of the properties under consideration are superconductivity, semiconductivity, laser activity, plastic flow and fracture.

### B. DISCUSSION

#### 1. Superconductivity

An experimental investigation was initiated to study the effect of grain size on the superconducting properties in a material at a given impurity level. The thermal treatments used to produce different grain sizes may also produce a variation in the distribution and density of dislocations; therefore, if dislocations and grain boundaries act as superconducting filaments, then the superconducting properties will be a function of the grain size. An attempt will then be made to distinguish the contribution due to grain boundaries from that due to dislocations.

Electropolished specimens of various grain sizes were prepared from commercial grade niobium wire. The critical current and field of these specimens at 4.2°K are now being determined by the Electronics Research Laboratory. The detailed defect structure of these specimens will be determined by optical and electron transmission microscopy and will be correlated with changes in the superconducting properties.

If the filamentary properties of dislocations are caused by their stress fields, then the segregation of interstitial impurities to dislocations, which changes the stress field around a dislocation, should produce a change in the superconducting properties. To examine this, a series of niobium specimens with a high interstitial impurity level and a fixed grain size were strained through the Luders strain to a strain of approximately 0.06. They were then aged at various temperatures in the range of 100 to 500°C for one hour. The maximum percentage increase in flow stress after aging was 5 percent. These specimens have been submitted to the Electronics Research Laboratory for determination of the critical current and field at 4.2°K both before and after the aging treatment.

Research has been initiated to relate the dislocation and subgrain structure, which were produced by various mechanical and thermal treatments to the macroscopic superconducting properties in niobium of a fixed impurity level. Again, the detailed structure will be determined by optical and electron transmission microscopy.

For this research activity a method has been developed for producing electron transmission films from sheet material. In addition, equipment has been built and methods are being developed for preparing electron transmission specimens from wires. Also, a vacuum annealing furnace has been built for the thermal treatment of specimens and for purifying niobium strip by resistance heating to 2000°C.

A titanium-40 percent niobium superconducting alloy which had a total reduction in area of 240 times was obtained from Atomics International. A method of preparing specimens from this alloy for transmission electron microscopy was developed. The structure that could be resolved by electron transmission microscopy consisted of an equiaxed dislocation cellular network.

## 2. Semiconductor Radiation Damage

A program has been directed toward understanding radiation effects in semiconducting materials. During the past six months familiarity was gained with

many of the techniques required for studying electronic properties of semiconductors. Preparations have been made to use infrared absorption techniques which permit a detailed spectral study of radiation induced damage.

In addition to the conventional methods of measuring electrical properties, a recently discovered (Rinder, Raytheon Co.) strong electromechanical effect in P/N junctions is being considered for use as a sensitive detector of local variations of crystal defect structures in the vicinity of junctions. By lightly pressing a diamond-tipped needle against the surface near the junction, a distortional stress is produced over a very small region of the junction. The resulting change of the electrical properties at this distorted region is sufficiently large to be readily measured. The magnitude of this electromechanical effect is dependent upon the lattice perfection of the region under stress. This method is applicable only to P/N junctions that are parallel and very near ( $< 2\mu$ ) the probed surface, such as exist for silicon solar cells. Within this limitation, however, the method provides a useful new analytical tool for studying lattice defects near junctions.

The lack of suitable high energy irradiation facilities at Aerospace has proved to be a greater difficulty in conducting significant research in radiation damage of semiconductors than had originally been anticipated. To avoid undesirable annealing effects, specimens must usually be maintained at cryogenic temperature between the time they are irradiated and the time damage measurements are made, a factor which limits the distance that it is practical to transport specimens. The few sources of high energy radiation in Southern California which are available for contracted research programs are usually quite busy and require a long lead time when scheduling experiments. However, the use of these facilities is being considered.

### 3. Laser Activity

The initial effort on the laser program has been to determine the defect structure of materials used as laser crystals. To accomplish this, single crystals of rubies have been examined by the etch-pit technique to determine

the dislocation substructure. The initial work was done on sapphire or undoped ruby, using  $H_3PO_4$  as the etching agent. The end of a sapphire rod of a known orientation was held in an oxy-acetylene flame until it melted and formed a hemisphere. This was then placed in  $H_3PO_4$ , and the etchant was heated to  $390^\circ C$  for approximately 1 hour. The specimen was then removed and observed microscopically. Triangular etch pits were observed at four areas of the hemisphere, which corresponded to the basal plane and the 3 rhombohedral planes of the  $\{2021\}$  type. No etch pits of other planes were found.

Another ruby specimen was cut and polished to expose a polished basal plane, a polished rhombohedral plane, and a polished prismatic plane of the  $\{11\bar{2}0\}$  type. The specimen was placed in  $H_3PO_4$  and heated to  $400^\circ C$ . The specimen was removed and examined at  $300^\circ C$  and thereafter at  $20^\circ C$  intervals. Etch pits first appeared on the basal plane at  $340^\circ C$ . At  $380^\circ C$ , etch pits appeared on the rhombohedral face. There was no evidence of etch pits on the prismatic face.

To determine if the pattern of pits was reproducible, the basal plane was re-polished to remove the pit pattern and re-etched with  $H_3PO_4$  at  $340^\circ C$ . The same general pit pattern with slight differences in pit positions was produced. The specimen was again re-polished and a new etchant,  $KHSO_4$ , was used. The  $KHSO_4$  was heated to  $700^\circ C$  and the specimen immersed for 35 seconds. The same general pit pattern recurred, indicating that the pit structure was the same after re-etching, regardless of the etchant.

The etch-pit technique was subsequently refined. The optimum etching conditions to obtain etch pits on the basal plane have been established as follows: (1) mechanically polish the basal plane of the crystal, finishing with a 1 micron diamond polish followed by a 0.05 micron alumina abrasive, (2) chemically polish the surface in  $H_3PO_4$  at  $425^\circ C$  for 2 min, and (3) etch in  $KHSO_4$  at  $700^\circ C$  for 8-10 sec. In addition, it was found that by etching in  $KHSO_4$  at  $800^\circ C$  etch pits could be observed on the prismatic faces of ruby crystals.

Studies are currently underway to determine a suitable method for changing the dislocation density and substructure of ruby. The most promising method appears to be possible through the proper application of thermal cycling. Ruby specimens will be given thermal cycling treatments and then etched to determine the conditions under which the dislocation structure and density can best be changed.

Photographs at magnifications as high as 230X have been taken of the ends of ruby crystals as they undergo laser action as a preliminary step in the microscopic examination of lasers with known defect structures. Correlations will be made between this defect structure and the laser pattern.

### C. MECHANICAL PROPERTIES

The scientific papers completed during the past six months are given in Refs. 1 to 3. Papers currently in preparation are given in Refs. 4 to 8. The following is a summary of the more significant results presented in these papers:

#### 1. Yielding and Flow of the B.C.C. Transition Metals at Low Temperatures

Additional work supported the earlier conclusion that overcoming the Peierls-Nabarro stress was the rate controlling dislocation mechanism during yielding and flow of the b. c. c. (body centered cubic) metals at low temperature ( $T < 0.2 T_m$ ). The activation energy  $H$ , activation volume  $v^*$ , and frequency factor  $\nu$  were determined as a function of the thermal component of the stress  $\tau^*$  for the Group VA (V, Nb, Ta), Group VIA (Cr, Mo, W) metals and iron. For these metals it was found that  $H_0$  ( $\tau^* = 1 \text{ kg/mm}^2$ )  $\approx 0.1 \mu b^3$ , where  $\mu$  is the shear modulus and  $b$  is the Burgers vector, and  $v^* \approx 50 b^3$  at  $\tau^* = 2 \text{ kg/mm}^2$ , increasing rapidly to values in excess of  $100b^3$  at lower stresses and decreasing to  $2-5 b^3$  at high stresses ( $\tau^* = 50 - 60 \text{ kg/mm}^2$ ) and  $\nu = 10^6 - 10^{12} \text{ sec}^{-1}$ , the higher values of  $\nu$  generally being associated with the purer materials.  $H$  and  $v^*$  as a function of stress were independent of structure. This and other observations indicated that thermally-activated overcoming of the Peierls-Nabarro stress is rate

controlling. The values of  $H_0$  and the change in  $H$  with stress at low stresses are in agreement with those predicted by Seeger's model for the nucleation of kinks. The Peierls-Nabarro stress and kink energy derived from the experimental data are approximately  $10^{-2} \mu$  and  $4 \times 10^{-2} \mu b^3$ , respectively.

## 2. Effect of Grain Size on the Yield and Flow Stress of Metals

Additional work supported the earlier suggestion that the increase in yield and flow stresses with decrease in grain size was associated with the smaller average distances that dislocations move in fine-grained material as compared to the coarse-grained material. From data in the literature on the variation of dislocation density and stored energy with grain size for b. c. c. and f. c. c. (face centered cubic) metals, it was found that  $s$  can be related to the grain size by

$$s \approx k d^n \quad (2-1)$$

where  $d$  is the grain size and  $k$  and  $n$  are constants which decrease with strain. From this relationship and the basic dislocation equation

$$\epsilon = a_1 \rho b s \quad (2-2)$$

where  $\epsilon$  is the tensile strain,  $a_1$  is a geometric constant of value 1.4 relating tensile strain to shear strain,  $\rho$  is the density of dislocations which have participated in the deformation, and  $b$  is the Burgers vector, dislocation densities were calculated for Cu and Ag which were in good agreement with actual dislocation counts (see Table 1). Also, a calculation of the deformation cell size as a function of strain for b. c. c. and f. c. c. metals on the basis of Eqs. (2-1) and (2-2) was in good agreement with the experimentally measured values (see Fig. 1).

Table 1. Comparison of Counted and Calculated Dislocation Densities

Material	Grain Size, mm	Author	Strain	$\rho$ Counted $\text{cm}^{-2}$	$\rho$ Calculated $\text{cm}^{-2}$
Cu	0.015	Gordon <sup>a</sup>	17.5	$3 \times 10^{10}$	$2.2 \times 10^{10}$
			30.0	$5.7 \times 10^{10}$	$7.9 \times 10^{10}$
Ag	0.020	Bailey and Hirsch <sup>b</sup>	11.0	$2.2 \times 10^{10}$	$1.0 \times 10^{10}$
			21	$5.2 \times 10^{10}$	$2.4 \times 10^{10}$
			32	$6.8 \times 10^{10}$	$8.8 \times 10^{10}$

<sup>a</sup>P. Gordon, Trans. AIME 203 1043 (1955). Counts on Gordon's copper are unpublished results of J. Bailey.

<sup>b</sup>J. Bailey and P. Hirsch, Phil Mag. 5, 485 (1960).

3. Correlation of High Temperature Mechanical Properties of Certain Superalloys

High temperature mechanical property data (tensile and compressive proportional limit, 0.2 percent yield strength, flow stress, tensile strength, creep rate, and time to rupture) for an iron-base (N-155), a nickel-base (René 41) and a cobalt-base (L-605) superalloy were analyzed to evaluate the equation which correlates the data and to identify the dislocation mechanism which is rate-controlling. The data correlated through the relationship

$$\dot{\epsilon} = \frac{A}{T} \exp -(H_c/RT) f(\sigma) \approx kt_r$$

where  $\dot{\epsilon}$  is the strain rate,  $t_r$  is the time to rupture,  $H_c$  is the activation energy for deformation, A and k are constants, and  $f(\sigma)$  is a stress function, which was  $f(\sigma) = \sigma^n$  with  $n = 4 - 5$  at stress below about  $10 \text{ kg/mm}^2$  (15,000 psi). The values of  $H_c$  were 100, 215, and 120 kcal/mole, respectively, for

N-155, René 41 and L-605. These values are higher than those for self-diffusion of the base metals of these alloys.

The form of the above equation, especially in regard to the stress law, is in agreement with Weertman's dislocation climb model of high temperature creep. It was suggested that the higher values of  $H_c$  represent either changes in structure with temperature or the interaction of solute atoms or precipitates with dislocations during climb.

#### 4. Effect of Stacking-Fault Energy on the Creep of Ni-Base Alloys

Other than the alloys based on the refractory metals, the nickel-base superalloys have the highest service temperatures for structural uses. In general, these superalloys are strengthened by precipitation hardening which, however, is limited to temperatures below about 1900°F because of re-solution and agglomeration of the precipitates. While work has been done with the use of insoluble particles such as aluminum oxide, there may be other types of strengthening mechanisms.

High temperature creep rates are usually considered to be controlled by climb of dislocations over obstacles. Anything that will retard this process will improve the creep strength. A possibility is to lower the stacking-fault energy by alloying which leads to the separation of dislocations into ribbons of stacking-faults bounded by partial dislocations. Energy must then be supplied to constrict the stacking-fault before it can climb. This research program was initiated to determine the effectiveness of this mechanism by establishing the effect of several alloying elements on the stacking fault energy and high temperature creep behavior of nickel. Because of its extensive use in commercial alloys, the Ni-Cr system was chosen for initial study.

#### 5. The Nickel-Chromium System

##### a. Alloy Preparation

Nickel-chromium alloys with nominal chromium contents up to 31 percent have been prepared by electroplating chromium on 0.002- or 0.004-inch

high-purity nickel sheet and annealing for 24 hours at 1300°C. From the diffusivity of Cr in Ni (Ref. 9), this should provide less than 95 percent saturation at the center. The difficulties mentioned in the previous progress report (Ref. 10) in providing a suitable atmosphere during the anneal were eliminated by using dried hydrogen gas. Even with the use of hydrogen, great care was necessary in purging the furnace before the specimen was heated. Chemical analyses for Cr and Ni were accomplished by x-ray fluorescence of an electropolishing solution.

b. Stacking-Fault Energy Measurements

From a survey of the literature on methods of measuring stacking-fault energies, two methods were selected. The first method is the measurement of dislocation network node radii in thin film specimens observed by transmission electron microscopy (Refs. 11, 12). This is the only method which gives a direct determination of stacking-fault energy with a minimum of assumptions. It is limited, however, to rather low energies. Because pure nickel has a rather high stacking-fault energy, a second method for high-nickel alloys must be used and the technique of thermal grooving of twin boundaries was selected (Ref. 13). This method involves the measurement of equilibrium root angles developed at high temperatures where a twin boundary meets the surface. From this angle, the interfacial energy of the twin can be related to the surface energy which, in turn, can be measured by a separate experiment. Then, since a stacking-fault may be considered as two one-layer twins, the twin energy is estimated to be one-half the stacking-fault energy. This technique is an indirect method and is based on what may be a dubious assumption (Ref. 14). Nevertheless, it was felt that since two methods were being used on a single alloy system, there would be enough overlap to make a correction to the less reliable values.

Thin films of pure nickel and nickel-chromium alloys for electron transmission were prepared by a modification of the point-cathode technique (Ref. 15). Several polishing solutions were used, depending on the alloy. Table 2 lists the solutions and polishing conditions. Representative electron micrographs

Table 2. Electropolishing Conditions for the Preparation of Thin-Films of Ni-Cr Alloys for Electron Transmission Studies

Alloy	Solution	Current Density, amp/10 <sup>2</sup>	Voltage, volts	Temperature
Pure Ni	H <sub>2</sub> SO <sub>4</sub> 580 cc	0.26	4	R. T.
Ni+<5% Cr	Paratoluene-sufonic acid 5 gm H <sub>2</sub> O 435 cc			
Ni+5-10% Cr	Above solution 80% Glycerol 20%	0.26	4	R. T.
Ni+10-31% Cr	H <sub>3</sub> PO <sub>4</sub> 45 cc H <sub>2</sub> SO <sub>4</sub> 30 cc H <sub>2</sub> O 25 cc	1.6	6	R. T.

obtained so far are shown in Fig. 2. In most cases, the specimens were deformed approximately 10 percent by rolling before polishing. As seen from the micrographs, the dislocation structure changes with increasing chromium content in a manner similar to that observed in copper-aluminum alloys (Ref. 16) and indicates a decrease in stacking-fault energy with increase in Cr. The dislocation distribution changes from a heavily tangled network to long rows of pile-ups as the chromium content is increased. Tangles indicate extensive cross slip, while pile-ups indicate that cross-slip is difficult, which would be expected if the dislocations were extended. As yet, no extended nodes have been observed, so the stacking-fault energy has not been measured. A number of extended dislocations were observed in the 31 percent Cr alloy; however, stacking-fault energies calculated from the separation of the partials assuming equilibrium were so low that this assumption could not be considered valid.

The initial work on thermal grooving was done using the 0.004 inch foil procured for the thin-film work. However, the surface was not sufficiently flat for adequate precision when using the interferometric method to measure the groove angles. It is hoped that with the electron-beam melting unit now available, high-purity nickel can be produced and alloys in the form of heavy sheet can be made for this phase of the program.

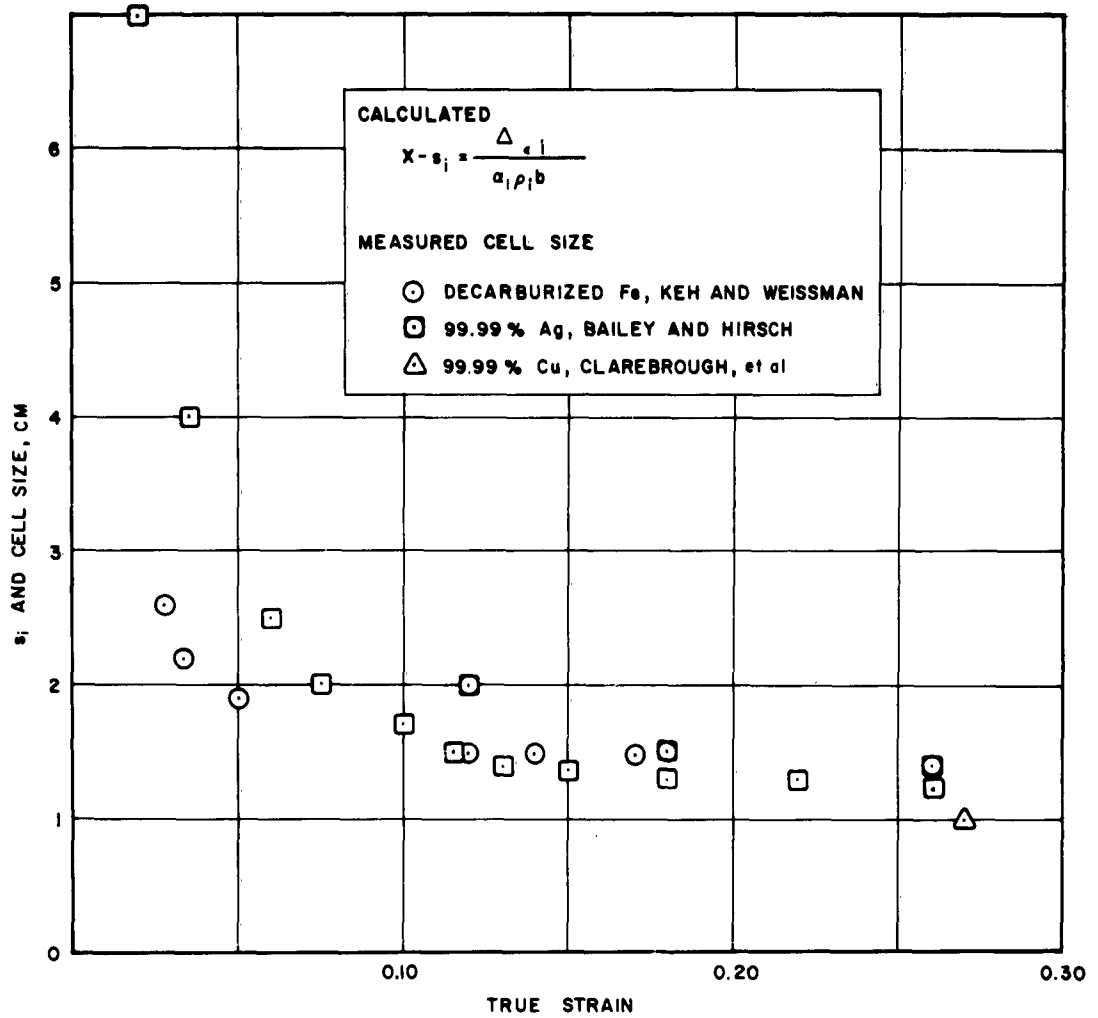


Figure 1. Comparison of the Calculated Average Distance Moved by Dislocations during Each 10 Percent Increment of Strain,  $s_i$ , with Measured Deformation Cell Size

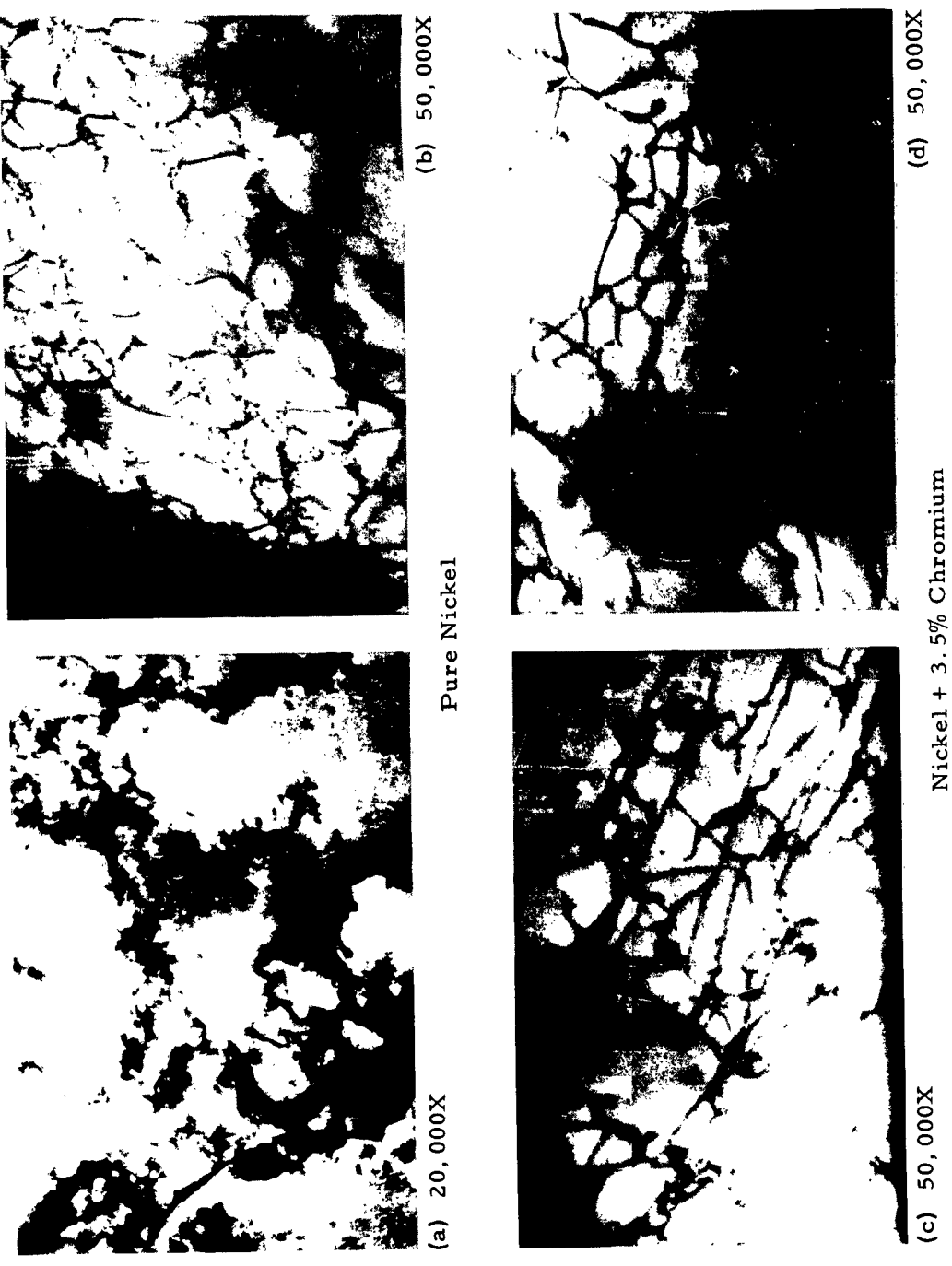


Figure 2. Dislocation Structures of Ni-Cr Alloys Deformed Approximately 10 Percent by Rolling at Room Temperature



Nickel + 19% Chromium

(e) 50,000X



(f) 20,000X



(g) 50,000X

Nickel + 26% Chromium

Figure 2. (continued)



(h) 20,000X



(i) 20,000X



Nickel + 31% Chromium

(j) 50,000X

Figure 2. (continued)

#### D. REFERENCES

1. H. Conrad, "Yielding and Flow of the B.C.C. Metals at Low Temperatures," Aerospace Report No. TDR-169(3240-11)TN-5 (7 March 1963); to be published in N.P.L. Symposium on "The Relation between Structure and Properties of Metals."
2. H. Conrad and B. Christ, "Variation of Dislocation Density and Stored Energy with Grain Size," Aerospace Report No. TDR-169(3240-11)TN-6 (21 February 1963); to be published in AIME/ Interscience Book, "Recovery and Recrystallization of Metals."
3. H. Conrad, J. White, and E. Bernett, "Correlation and Interpretation of High Temperature Mechanical Properties of Certain Superalloys," Aerospace Report No. TDR-169(3240-11)TN-1 (20 February 1963); to be published in ASME, IME and ASRM volume, "Joint International Conference on Creep and Fracture."
4. E. Stofel and H. Conrad, "Brittle Fracture of Ceramics," in preparation and under consideration as a chapter in a book entitled, "Ceramics in Aerospace Technology."
5. H. Conrad, G. Stone, and D. Clausing, "Yielding and Flow of Nb at Low Temperatures"; to be submitted to Acta Met.
6. H. Conrad and K. Janowski, "Yielding and Flow of Sapphire Crystals"; to be submitted to Trans. AIME.
7. H. Conrad and G. Thomas, "Yielding and Plastic Flow of the B.C.C. Metals"; to be published in Progress in Materials Science.
8. S. Frederick, "A Simple Temperature Controller"; submitted to J. Scientific Instruments.
9. P. L. Gruzin and G. B. Fyedorov, Dokladi Akad, Nauk 105, 264 (1955).
10. H. Conrad, "Materials and Structures Study and Improvement of Superalloys"; Aerospace Report No. ATN-62(9214)-1, (27 September 1962).
11. M. J. Whelan, Proc. Roy. Soc. 249, 114 (1959).
12. A. Howie and P. R. Swann, Phil Mag., 6, 1215 (1961).
13. R. L. Fullman, J. App. Phys. 22, 448 (1951).

I

14. P. R. Thornton, T. E. Mitchell, and P. B. Hirsch, Phil Mag. 7, 80, 1349 (1962).
15. G. Thomas, "Transmission Electron Microscopy"; (J. Wiley and Sons, New York, 1962).
16. P. R. Swann and J. Nutting, J. Inst. Metals 50, 133 (1961-62).

INORGANIC CHEMISTRY

(JO 3240-20)

Prepared by

W. S. GINELL

## ABSTRACT

Progress in the study of crystal growth is described. A technique for observing the quasi-martensitic phase transition in  $ZrO_2$  single crystals is discussed. Initial experiments on the effects of very high hydrostatic pressures and elevated temperatures on the monoclinic-tetragonal transition indicate that appreciable stabilization of the tetragonal phase does not occur.

CONTENTS

ABSTRACT .....	3-i
A. INTRODUCTION .....	3-1
B. CRYSTAL GROWTH .....	3-3
C. PHASE TRANSITION IN SINGLE CRYSTAL $ZrO_2$ .....	3-4
D. EFFECT OF PRESSURE ON THE MONOCLINIC- TETRAGONAL TRANSITION IN $ZrO_2$ .....	3-5
E. REFERENCES .....	3-7

TABLES

1	Temperature at Onset of Transition in $ZrO_2$ Platelets .....	3-4
2	Effect of Pressure on Phase Transition in $ZrO_2$ .....	3-6

### III. INORGANIC CHEMISTRY

#### A. INTRODUCTION

Zirconium and hafnium oxides are two of the more promising refractory materials suitable for use under oxidizing conditions at temperatures in excess of 1700°C. Because of their high melting points, low thermal conductivity, and fairly high spectral emittance, zirconia and hafnia may find extensive applications as thermal barrier materials. The oxides have low vapor pressures, low dissociation pressures, and low reactivities toward molten metals and glasses at elevated temperatures and, therefore, may be used as inert containers in many applications. However, each of the pure oxides is subject to destructive phase changes: ZrO<sub>2</sub> at about 1100°C, and HfO<sub>2</sub> at about 1700°C. This effect has been overcome by the addition of specific stabilizers selected from among the refractory oxides having cation radii similar to that of Zr<sup>+4</sup> (i. e., 0.80 Å). In the case of addition of the di- and trivalent cations Ca<sup>+2</sup>, Y<sup>+3</sup>, Dy<sup>+3</sup>, oxygen ion vacancies are created in the lattice with the result that at temperatures above 750°C zirconium oxide becomes an ionic conductor (Ref. 3-1). At lower temperatures, the electronic transport number becomes appreciable, reaching 74 percent at 300°C (Ref. 3-2). The identification of the current carriers in stoichiometric and oxygen-deficient single crystal zirconium oxide is necessary for the clarification of the conduction mechanism in pure and stabilized zirconia. Single crystals would be required for ionic self-diffusion studies.

The monoclinic-tetragonal phase transition in zirconium oxide has been extensively investigated (Ref. 3-3). Recent work by Wolten (Ref. 3-4) at Aerospace has established that the transition is in many ways very similar to the well-known martensite transformation. The predominantly athermal nature of the transformation, the large hysteresis loop obtained on temperature cycling, and the insuppressibility of the reaction all tend to indicate a diffusionless phase change in this system.

It has been postulated that the austenite-martensite transformation in iron alloys requires the presence of martensite embryos of finite size which are stabilized by dislocations. The suggestion also has been advanced that the embryos themselves are dislocation arrays which increase in size with decreasing temperature up to a critical radius and suddenly initiate the formation of martensite at some lower temperature. The effect of hydrostatic pressure on the austenite-martensite transformation in iron alloys has been studied by Kaufman (Ref. 3-5). It was possible to reduce the transformation temperature such that the high temperature phase could be recovered at room temperature. The assumption was made that the application of pressure at elevated temperature followed by quenching resulted in the freezing-in of smaller embryos which in turn lowered the transformation temperature.

Whitney (Ref. 3-6) calculated the effect of pressure on the monoclinic-tetragonal phase transition in zirconium oxide with the assumption that at a given temperature and pressure, equilibrium existed between the two phases such that  $-\Delta F(P, T) = \int_1^P \Delta V(P, T) dP$ , where  $\Delta V$  is the molar volume change, and  $\Delta F$  is the chemical free energy change. However, he did not take into account the quasi-martensitic nature of the transformation and hence omitted contributions due to nonchemical free energy such as surface and strain energy. For the tetragonal-nonclinc transition to occur, it is not only necessary that  $\Delta F$  be positive, but it must be sufficiently positive to overcome the nonchemical free energy.

In the study of the phase transition in zirconium oxide and the effect of pressure on the transformation, the availability of single crystals of high purity and known crystallographic orientation would greatly simplify the interpretation of the experimental data. The direct optical observation of the transition at temperature would permit identification of habit, orientation, macroscopic displacement, and twin formation in the two phases. Linear expansion coefficients also could be determined and it could be possible to observe and identify the embryonic structures in the optically transparent crystal.

## B. CRYSTAL GROWTH

The growth of zirconium oxide single crystals is complicated by the fact that growth must take place at temperatures below the tetragonal-monoclinic transition temperature. In pure, hafnium-free zirconium oxide this temperature is in the range of 850-900°C. In the hafnium oxide-zirconium oxide solid solutions system, the transition temperature is higher, that is, it is probably a linear function of concentration up to ~ 1700°C. Growth from solution or via a vapor transport technique are two of the more favorable approaches.

Zirconium oxide single crystals have been grown from molten borate and phosphate glasses and from molten polymolybdates. Techniques included (1) cooling a saturated solution at rates between 1 and 30°C/hr, (2) mass transport along a suitable temperature gradient, and (3) pulling from solution. Crystals which formed at temperatures below 900°C were often optically clear, six-sided monoclinic platelets or rectangular cross-section monoclinic needles. Numerous, small severely cracked crystals which exhibited a tetragonal habit were also obtained. These crystals presumably formed at temperatures above the transition temperature or within the hysteresis region and subsequently fractured on cooling. Long polycrystalline dendrites which served as nucleation centers for clear platelets were very frequently observed. The occurrence of dendrites is to be expected in molten glass systems because of the extreme tendency toward supercooling. Nucleation at the walls results in rapid growth along the most favorable crystallographic growth direction and toward a region of high solute concentration. Apparently, the polycrystalline dendrites grew above the transition temperature and attained significant lengths owing to the relatively low melt viscosities at the higher temperatures. At lower temperatures platelets grew at right angles to the dendrite axis, but growth was limited due to the higher melt viscosities, low diffusion rates, and low residual solubilities.

Attempts were made to increase the solubility of zirconium oxide and to decrease the melt viscosity by the addition of chloride and fluoride ions. Experiments were carried out in sealed platinum containers to minimize additive loss by volatilization. No appreciable solubility increase was obtained although some decrease in viscosity was noted. The crystals obtained were of high quality with few inclusions or voids. Further studies of this system are warranted.

C. PHASE TRANSITION IN SINGLE CRYSTAL  $ZrO_2$

The monoclinic-tetragonal phase transition in single crystal,  $ZrO_2$  platelets was observed visually with the aid of a stereomicroscope and a platinum filament hot stage. The crystal, which rested on the junction of a calibrated platinum-platinum 13 percent rhodium thermocouple, was cycled through the transition temperature range at a linear rate of  $10^{\circ}C/min$ . The onset of the transformation was marked by a slight clouding of the initially transparent crystal caused by the appearance of slip or twin lines parallel to one of the crystal edges. Continued heating resulted in a step-wise spreading of the cloudiness across the face of the crystal. On cooling, the reversal of the transition was accompanied by further changes in the distribution and size of the translucent areas. Listed in Table 3-1 are the temperatures at which the indicated transition was first observed.

Table 1. Temperature at Onset of Transition in  $ZrO_2$  Platelets

Cycle	Monoclinic→Tetragonal, $^{\circ}C$	Tetragonal→Monoclinic, $^{\circ}C$
Initial Heating and Cooling Cycle	1195 - 1199	1022
Subsequent Heating and Cooling Cycles (5 Cycles)	1182	1052 - 1068

The hysteresis observed in the initial heating and cooling cycle was consistently and significantly wider than in subsequent cycles. This may be due in part to the greater strength of a single crystal as opposed to a polycrystalline body and to the formation of embryos of requisite size.

Examination under the polarizing microscope of a crystal which had undergone thermal cycling revealed numerous polysynthetic twinned monoclinic regions randomly arranged parallel and normal to the long ( $C_o$ ) axis of the crystal. Naturally occurring  $ZrO_2$  (baddeleyite) is almost invariably found in the form of polysynthetic twins, rather than in the form of growth twins; this may indicate that crystallization occurred above the transition temperature.

The transition temperature in spectrographic grade  $HfO_2$  as determined by Wolten (Ref. 3-4) occurs in the vicinity of  $1700^\circ C$ . Observation of this transition and the tetragonal-cubic transition in  $ZrO_2$  will be carried out on a tungsten filament hot stage.

#### D. EFFECT OF PRESSURE ON THE MONOCLINIC-TETRAGONAL TRANSITION IN $ZrO_2$

In a preliminary experiment, it was shown that metastable tetragonal  $ZrO_2$  could be converted to the monoclinic form by the application of hydrostatic pressure at room temperature. This experiment and subsequent experiments were conducted in a tetrahedral anvil apparatus. The sample of powdered tetragonal  $ZrO_2$  was enclosed in a cylindrical platinum tube heater which was capped at both ends by platinum foil-covered steel end plugs. A platinum-platinum 13 percent rhodium thermocouple contacted the outer surface of the heater. Sample temperatures were estimated to be ten percent lower than the heater temperature. A pyrophyllite tetrahedron served as the pressure transmitting medium. Tests were carried out at 50 kilobars for the indicated times and temperatures (Table 3-2) and the system was quenched to room temperature before release of the pressure. Samples were examined microscopically and the phases were identified by x-ray diffraction analysis.

Table 2. Effect of Pressure on Phase Transition in  $ZrO_2$

Sample	Pressure, k bar	Temperature, °C	Time, min	Phases Present
0	0.001	25	--	tetragonal and trace monoclinic
1	50	25	30	monoclinic and trace tetragonal
2	50	1800	1	monoclinic
3	50	1250	30	monoclinic
4	50	1000	30	monoclinic
5	50	750	25	monoclinic and trace tetragonal

Samples 1, 4 and 5 exhibited no observable grain growth and appeared as high density, coherent, compacted cylinders. Samples 2 and 3 showed appreciable recrystallization and grain growth. The polyhedral grains showed no coherence and were easily detached from the mass.

It was apparent that tetragonal  $ZrO_2$  formed at the higher temperatures but reverted to the monoclinic form within approximately the same temperature region as that observed for the atmospheric pressure reaction.

Because extensive design modifications to the high pressure apparatus were necessary, further experiments were not carried out.

E. REFERENCES

1. K. Kiukkola and C. Wagner, J. Electro. Chem. Soc. 104, 379 (1957).
2. Systems Research Laboratories Report 203-4 (September 1961)  
AD 263 962.
3. B. C. Weber, J. Am. Ceram. Soc. 45, (12) 614 (1962).
4. G. M. Wolten, "Diffusionless Phase Transformations in Zirconia and Hafnia," Aerospace Report No. ATN-63(9213)-2; also to be published in J. Am. Ceram. Soc.
5. L. Kaufman, A. Leyenaar, J. S. Harvey, Acta Met. 8, 270 (1960).
6. E. D. Whitney, J. Am. Ceram. Soc. 45, (12) 612 (1962).

ELECTROCHEMISTRY OF SOLIDS

(JO 3240-21)

Prepared by

T. S. LEE

F. M. WACHI

W. H. CHILDS

## ABSTRACT

Electrochemical methods have been developed for the study of foreign metal ions in ionic solids. These methods provide information on chemical activity and mobility and are sensitive to concentrations of foreign ions as low as 20 parts per million.

The methods were used to investigate the following metal ions in solid potassium iodide at room temperature: mercury, copper, silver, lead, cadmium, thallium, and zinc ions. The data showed that these ions in potassium iodide form complexes, the properties of which are remarkably similar to the iodide complexes of the same metals in aqueous solutions. Movement of the metal ions through the solid was shown to occur by the process of linear diffusion.

New methods, based on the variation of electrode potential with time, were studied and were found to be applicable to solids of high resistivity. In the future these methods will be applied to non-ionic solids.

## CONTENTS

ABSTRACT . . . . .	4-i
A. INTRODUCTION . . . . .	4-1
B. EXPERIMENTAL METHODS AND RESULTS . . . . .	4-2
1. Chemical Activity of Foreign Metal Ions in Potassium Iodide . . . . .	4-2
2. Diffusion . . . . .	4-3
3. Sensitivity . . . . .	4-3
4. Constant Current Methods . . . . .	4-4
C. REFERENCES . . . . .	4-4

## IV. ELECTROCHEMISTRY OF SOLIDS

### A. INTRODUCTION

The Electrochemistry of Solids Program includes an experimental study of phenomena that occur when electric current is passed across the boundary between a metal and a solid. The research was undertaken (1) to develop new techniques for the study of solids, and (2) to study the chemical behavior and the diffusion of trace constituents in certain solid materials.

Since trace constituents frequently influence the properties of solids and since there are to date few methods by which trace constituents of solids may be studied selectively and in situ, the research described here is of great value to the Air Force materials program. The methods that have been evolved in this Laboratory have been applied thus far only to salts. In principle, the methods are applicable to a variety of materials, and in the future they will be applied to non-ionic solids. In addition, the studies of mechanisms of electrode reactions give information that may lead to a better understanding of slow degradation reactions that occur in transistors, in dry capacitors, and at the surfaces of electrical contacts.

The current work is based on an interpretation of current versus voltage curves. These curves were obtained by applying voltage to a cell consisting of a pellet of salt held between two sheets of metal. In the technique most frequently used the emf that was applied to the cell was varied linearly with time (linear potential scan) and the current that passed through the cell was recorded. Each electro-reducible or electro-oxidizable constituent in the solid produced a peak in the current-voltage curve at a characteristic potential. The position and the height of the peaks provided information on the thermodynamic activities and on the mobilities of the individual constituents.

The relation of this investigation to published research has been described and a list of references has been given (Ref. 4-1). In summary, no prior studies in this area have been reported, except those related to solid state batteries and semiconductors.

Research completed on this program prior to July 1962 was described completely in Ref. 4-1. A detailed description of subsequent research is being prepared for publication in the Journal of the Electrochemical Society (Ref. 4-2).

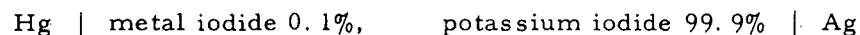
## B. EXPERIMENTAL METHODS AND RESULTS

Experimental procedures were discussed in detail in Ref. 4-1. Subsequently, several new procedures have been adopted for the elimination of traces of water and for minimizing background current. In one procedure, the cell assembly is kept in a vacuum oven prior to and during the period when electrical measurements are made. In addition, a dry box has been installed which allows the solids to be ground, mixed, and pressed to 10,000 psi in a dry, inert atmosphere.

A technique has been devised that allows platinum and gold electrodes to be replaced by liquid mercury electrodes. This change has reduced the background current and increased the sensitivity of the current-voltage methods.

### 1. Chemical Activity of Foreign Metal Ions in Potassium Iodide

A study of the cells of the type



showed that the chemical activity of metal ions in solid solution in potassium iodide closely parallels the chemical activity of the same ions in aqueous saturated potassium iodide solution. In contrast, there is no correlation of the chemical activity of metal ions in solid potassium iodide with the chemical activity of the same ions in aqueous solutions that do not contain iodide. It is concluded that the metal ions form iodide coordination complexes in solid solution just as they do in aqueous solution. Although there is a large difference

in the chemical activities of the aquo and the iodide complexes, a relatively small difference is caused by whether the solvent is water or solid potassium iodide. The examined metals were mercury, copper, silver, lead, cadmium, thallium and zinc.

## 2. Diffusion

To learn more about the nature of the movement of traces of foreign metal ions in salts, current-voltage curves were compared with curves calculated from Fick's first and second laws. Close agreement of theoretical values with experimental values was found. Similar comparisons were made of current versus time curves at constant potential, and potential versus time curves at constant current. In each case, theoretical values agreed with experimental values. It is concluded that the foreign metal ions move by the process of linear diffusion. Conversely, it was concluded that the electric field does not appreciably influence the movement of the ions. Moreover, the foreign ions are not located in the particles of a separate phase in a potassium iodide matrix, but they are dispersed uniformly. These results and diagnostic electrochemical tests showed that the foreign metal ions were present in solid solution. The studied metals were those mentioned in Section 1, and the concentration range was 0.002 to 0.02 weight percent foreign metal.

## 3. Sensitivity

Experiments with platinum and gold electrodes revealed that oxides on these surfaces contributed to background current. An appreciable background current was caused by as little as one-twentieth of a monolayer of oxygen on the metal, as calculated from Faraday's law. The use of mercury as an electrode metal, in place of platinum or gold, greatly reduced the background current, provided that oxygen was completely removed from the cell chamber before admission of mercury. The use of mercury extended the sensitivity of the electrochemical methods of investigation to the parts per million range.

#### 4. Constant Current Methods

A study was made of the variation of electrode potential with time under the condition that the cell current was held constant. Reduction potentials and diffusion coefficients were calculated from the experimental potential-time curves, just as in the case of current-voltage curves. However, the constant current technique was found to have the advantage of being applicable to solids of much higher resistivity. Theoretical potential-time curves, calculated on the assumptions of linear diffusion and thermodynamically reversible electrode reactions, were compared with the experimental curves. Close agreement was found except in one respect; namely, the experimental curves corresponded to an apparent value of 1 electron consumed in the reduction of one mole of cadmium ion. The real value is, of course, two. The discrepancy is being investigated.

The constant current method has promise of being more sensitive and more widely applicable than the current-voltage method.

#### C. REFERENCES

1. T. S. Lee, and F. M. Wachi, "Materials and Structures, Materials and Processes Analysis Program, Electrochemistry of Solids, Semiannual Technical Report," (1 January - 30 June, 1962) Aerospace Report No. TDR-69(2240-53)TR-2, (12 September 1962).
2. T. S. Lee, F. M. Wachi, and W. H. Childs, "Electrochemistry of Solids: Metal Iodides in a Matrix of Potassium Iodide," Aerospace Report No. TDR-169(3240-21)TN-1, in preparation.

HIGH TEMPERATURE CHEMISTRY

(JO 3240-22)

Prepared by

J. E. COLWELL

T. J. DUDEK

R. G. NEVILLE

F. M. WACHI

M. T. O'SHAUGHNESSY

## ABSTRACT

Work in High Temperature Chemistry during the report period consisted of (1) studies in polymer synthesis and polymer mechanical properties, and (2) studies of the combustion of tetrafluoroethylene ( $C_2F_4$ ), the monomer and chief pyrolysis product of Teflon.

Synthetic polymer work consisted of exploration of the possibilities of obtaining polymers of high thermal stability by condensation of bi- or polyfunctional formylphenoxy silanes with amines to form polymeric Schiff bases. Several model condensation products were prepared and have shown encouraging thermal stability.

Physical chemical work on polymers consisted of the preliminary detailed investigation of the properties of three-dimensional polymers and their relationship to structure. Work during the report period dealt with the effects of time, temperature, and crosslink density on the stress-strain properties of ethylene-propylene rubber. Large deviations from ideal rubbery behavior were observed; explanation of these deviations is being sought. A literature survey of mechanical properties studies on epoxy resins was conducted in preparation for experimental work. A report on basic concepts in polymer chemistry has been issued.

In the studies of Teflon monomer combustion, conditions were determined under which the reaction of tetrafluoroethylene with oxygen can be investigated in diffusion flames or in premixed flames. Spectrographic data were obtained that show that the luminosity of these flames is of low intensity and consists chiefly of continua, overlaid in some spectral regions by relatively faint molecular band spectra. Experiments were initiated to study the degree of ionization in the flame front and in the burnt gases.

## CONTENTS

ABSTRACT .....	5-i
A. INTRODUCTION .....	5-1
B. SYNTHETIC WORK TOWARD HIGH TEMPERATURE POLYMERS .....	5-2
1. Substituted Silicon Isocyanates and Isothiocyanates .....	5-2
2. Organometallic Schiff Bases .....	5-3
C. MECHANICAL PROPERTIES OF THREE- DIMENSIONAL POLYMER NETWORKS .....	5-4
D. THE REACTION OF TETRAFLUOROETHYLENE WITH OXYGEN .....	5-5
1. Spectroscopy of the $C_2F_4-O_2$ Flame .....	5-5
2. Stability Measurements .....	5-6
3. Ionization Phenomena in Flames .....	5-7
E. REFERENCES .....	5-8

## V. HIGH TEMPERATURE CHEMISTRY

### A. INTRODUCTION

The area of responsibility of the Chemistry Department in the Materials Sciences Laboratory is the study of organic materials for aerospace applications and of related chemical problems. In High Temperature Chemistry, work is being done on polymers, with high temperature serviceability as the ultimate objective, and also on reactions of heat shield ablation products with atmospheric gases.

The polymer studies include synthesis and also investigations of the relationship of fundamental properties to structure in three-dimensional polymer systems. The synthetic work to date has consisted of exploration of possible routes to high temperature plastics through the polycondensation of appropriately substituted monomers derived from, or related to, the highly stable substance tetraphenylsilane. The mechanical properties studies were begun in October 1962 with an investigation of the effect of rate of strain, temperature, and crosslink density on the stress-strain properties of ethylene-propylene rubbers. Simultaneously, a literature survey of fundamental mechanical studies of epoxy resins was undertaken in an effort to extend the experimental work to representative members of this class. For numerous reasons there has been little fundamental work done on the mechanical and electrical properties of epoxy resins, although a great many engineering measurements have been made. The basis on which this area of investigation has been chosen is the belief that a phenomenological description of the fundamental properties of members of a resin system, and the explanation of these properties in terms of internal structural parameters, provides the soundest basis for the intelligent application of the resins in question, and also provides for guidance in synthetic research toward their improvement. Due to its extensive and growing use in heat shields, it is believed that the epoxy system is the most important class with which to extend studies of this type into the field of nonelastomeric structural plastics.

The high-temperature gas phase chemistry of ablation product combustion has been centered on tetrafluoroethylene ( $C_2F_4$ ), the monomer and chief pyrolysis product of Teflon. Teflon has been used extensively as an experimental noncharring low-surface-temperature heat-shield material. To predict the effects of  $C_2F_4$  in the boundary layer and wake of re-entering bodies and to interpret observations, we must identify the individual step reactions occurring in Teflon combustion and establish the way in which these individual steps are combined in the overall reaction mechanism. Work during the period consisted of establishing conditions for the investigation of the combustion of  $C_2F_4$  in premixed and diffusion flames, together with spectrographic observation of these flames. Preparations for the study of ionization in these flames and in burnt gases are being made. The most important question to be answered is the degree to which chemi-ionization occurs in  $C_2F_4$  combustion. This phenomenon is well known in hydrocarbon combustion and can lead to electron concentrations several orders of magnitude higher than would be expected if thermodynamic equilibrium prevailed. It is expected that work of this sort will, in time, be extended to other heat-shield materials.

The following sections of this report describe, more or less briefly, the experimental work conducted during the report period. Most of the results will be reported in greater detail in separate technical documents and journals.

## B. SYNTHETIC WORK TOWARD HIGH-TEMPERATURE POLYMERS

### 1. Substituted Silicon Isocyanates and Isothiocyanates

Details on these compounds and the reasons for studying them in a high temperature program are contained in Ref. 1. It was discovered in the course of work that the ureidosilanes are unstable hydrolytically and are cleaved by moisture to mono-substituted ureas or thioureas and gelatinous silica. The ramifications and potentialities for synthesis of this hydrolysis reaction have been investigated during this report period, and it has been

established that the reaction of silicon pseudohalides [e. g.,  $\text{Si}(\text{NCO})_4$  and  $\text{Si}(\text{NCS})_4$ ] with aliphatic, aromatic, and heterocyclic primary and secondary mono-, di-, and polyamines leads to the formation, in essentially theoretical yields, of the corresponding N-mono- or N, N-di-substituted ureas or thioureas. A paper describing this work has been prepared for publication.

## 2. Organometallic Schiff Bases

A discussion of the reasons for studying compounds of this type is also given in Ref. 1. During the period covered by the present report, details have been worked out for the synthesis in 80-90 percent yield of the following formylphenoxy silanes:

- a) o, m, p-formylphenoxytrimethylsilanes
- b) bis(o, m, p-formylphenoxy)dimethylsilanes
- c) bis(o, m, p-formylphenoxy)methylvinylsilanes
- d) o, m, p-formylphenoxytriphenylsilanes

All are new compounds except o-formylphenoxytrimethylsilane. The compounds under a), b), and c) have been characterized by their infrared spectra and by typical aldehyde derivatives (e. g., the phenylhydrazones, 2, 4-dinitrophenylhydrazones). Their reactivity toward a variety of aliphatic and aromatic mono- and diamines has been investigated; approximately 50 compounds of various types have been synthesized. In every case, the ortho- and paraformyl compounds were found to be significantly more reactive towards amines than were the corresponding metaformylphenoxy compounds.

The following compounds were prepared as model substances for Schiff base polymers and preliminary studies of their thermal stability were carried out:

- a) N, N'-bis[2(trimethylsiloxy)benzylidene]-o-phenylenediamine
- b) bis[2(trimethylsiloxy)benzylideneamino] diphenyl
- c) bis[2(4-tritylphenyliminomethyl)phenoxy]dimethylsilane

- d) bis[ 4(2-trimethylsiloxybenzylideneamino)phenyl] methane
- e) bis[ 4(2-trimethylsiloxybenzylideneamino)] diphenyl ether
- f) 2(4-tritylphenyliminomethyl)phenoxytrimethylsilane

Although each of these compounds darkened when heated to 400°C (as anticipated from the thermochromic behavior of Schiff bases), none gave any evidence of decomposition when held at this temperature for 5-10 min. Current laboratory work emphasizes the preparation of formylphenoxyphenylsilanes (which would be expected to show still greater stability) and the preparation of polymers.

#### C. MECHANICAL PROPERTIES OF THREE-DIMENSIONAL POLYMER NETWORKS

The following summary of results covers work carried out in October-December 1962 on a program on the relation between structure and mechanical properties of network polymers. A literature survey on epoxide resins and an experimental investigation of the stress-strain behavior and ultimate properties of elastomers were initiated.

A special dynamometer was constructed which is suitable for studying the constant strain rate stress-strain behavior of polymeric materials over a range of strain rate and temperature. Experiments were undertaken to clarify the molecular mechanisms contributing to the tensile properties of elastomers.

Stress-strain curves to rupture for ethylene-propylene (EPR) rubbers of varying crosslink density were obtained over a temperature range of 25°-100°C at two strain rates (1.25 min<sup>-1</sup> and 0.060 min<sup>-1</sup>). The initial shapes of the stress-strain curves (to about 150 percent elongation) were determined by the degree of crosslinking and the strain rate, and were almost independent of temperature. The portions of the curves at elongations approaching the ultimate elongation are strongly dependent on temperature as well as on strain rate and crosslink density. The results obtained on highly swollen samples of the vulcanizates have been compared

with those obtained on unswollen samples. The swollen samples yield stress-strain curves which are independent of strain rate and, hence, close to equilibrium for the networks as they exist in the swollen condition. It is thought that physical molecular entanglements present in the vulcanized rubber networks behave as mobile crosslinks and they can slip rather easily as the network is strained and thus relieve the stress on highly-stressed chains. A qualitative consideration of the effect of these "chain-entanglement crosslinks" on stress-strain behavior is consistent with the experimental results. A more quantitative description of this process is being sought. A detailed report of this work is planned for the near future.

The literature survey of epoxy resins has revealed that, while many engineering data exist, very little fundamental work has been done to characterize the detailed mechanical properties as functions of time and temperature on an epoxy resin system of well-characterized structure. We plan to undertake experimental work on these systems in the near future.

#### D. THE REACTION OF TETRAFLUOROETHYLENE WITH OXYGEN

This work was begun in Spring 1962 (Ref. 2) after a literature survey revealed that the details of the combustion of Teflon monomer are essentially unknown. Work during the period covered by the present report consists of spectrographic observations, flame stability measurements, and preparations for studies of flame ionization.

##### 1. Spectroscopy of the $C_2F_4-O_2$ Flame

Spectroscopic observations of the radiation emitted from a tetrafluoroethylene/oxygen diffusion flame were made with a Bausch and Lomb 1.5-m spectrograph and Eastman 103A-O and 103A-F film with a Wratten 2B filter. The slot burner was similar to one described by Skirrow and Wolfhard (Ref. 3) and was mounted in a Pyrex cross fitted with a sapphire window. Burner slots were 1 mm x 13 mm each, and the flame was viewed end-on through an image rotator so that the vertical axis of the flame fell across the slit. This technique allows one to obtain a cross section of the

flame zone and eliminates self-absorption effects which occur with the usual concentric burners. Argon was introduced around the burner at the base of the cross to reduce recirculation of burnt gases. Ignition was accomplished with a Tesla coil arcing to the burner.

Tetrafluoroethylene for the flame is generated by vacuum pyrolysis of Teflon. A Teflon rod is driven at a constant rate against a flat spiral heater formed from an Inconel-sheathed nichrome resistance wire. The tetrafluoroethylene passes through a Pyrex wool filter to remove fine polymer particles, then to a mechanical vacuum pump where it is pumped to atmospheric pressure, and finally to the burner through a metering system. When the generator is operated at 5 mm Hg pressure, the products are 95 percent tetrafluoroethylene. Tetrafluoroethylene flow-rates up to about 240 ml/min have been used so far. Mixture ratios of fuel and oxidizer have been approximately stoichiometric, i. e., 1:1.

In appearance the tetrafluoroethylene/oxygen diffusion flame itself is light blue and is of low intensity; there is an incandescent region between the tetrafluoroethylene gas and the flame zones when the mixture ratio is near 1:1. The incandescence indicates the occurrence of significant amounts of pyrolysis as the tetrafluoroethylene diffuses into the flame. However, the incandescence disappears on admixture of inert gas with the tetrafluoroethylene or oxygen streams.

Spectroscopic observations show that the radiation from the flame contains very little contribution from band spectra. Continua are observed in the blue and near ultraviolet regions, with a very weak band structure superimposed. The structure has not been sufficiently clearly defined in experiments conducted so far to permit wavelength measurements to be made.

## 2. Stability Measurements

A few flash-back and blow-off limits for the tetrafluoroethylene/oxygen flame have been determined with cylindrical tube burners of 0.080 and

0.092 in. id. This was done primarily to determine stable regions for operation of premixed burners. The measurements are not complete at this time and will be presented in detail in a future report.

### 3. Ionization Phenomena in Flames

A literature survey on techniques for measuring ionization density in flames has been conducted so that we may determine the applicability of these techniques for measuring electron and ion densities in a laminar premixed  $C_2F_4-O_2$  flame. Some of the techniques used for such ionization measurements are: electrostatic probes (Refs. 4 and 5), deflection of the flame by an electric field (Ref. 6), microwave attenuation (Refs. 7 and 8), use of a self-resonant coil (Refs. 9 and 10), and flame conductivity (Ref. 11). Each of these methods has been found to be applicable over a limited range of ionization density and to have certain characteristic ambiguities in its response to an ionized-gas system. The choice of technique for ionization density measurements appears to be dependent upon the relative simplicity of interpretation of the data obtained and upon the particular properties of the medium of interest. For the measurement of ionization density in the laminar premixed  $C_2F_4-O_2$  flame, the electrostatic probe, conductivity, and self-resonant coil methods have been selected. Reasons for selection of these methods are given in the following paragraphs.

Although the interpretation of the data obtained by the electrostatic probe technique is complicated by the aerodynamic, thermal, and electrical disturbances it introduces into the ionized-gas system, this device has been chosen because it is technically the simplest to construct and use for exploratory studies of the  $C_2F_4-O_2$  flame. By this technique one can measure the ionization density, the translational electron temperature, and the apparent thickness of the flame front at atmospheric and subatmospheric pressures. The results from the probe measurements will be used as the basis for selecting more sophisticated methods for future experiments. Presently, three sets of probes are being fabricated from iridium and iridium/40% rhodium wires of 0.127-, 0.254-, and 0.406-mm diameter.

These values were selected so that the effect of probe diameter on ion concentration could be investigated concurrently with the ionization density measurements.

The conductivity method has been selected because it specifically measures the ionization density of the flame front in the absence of flame-front perturbations by quenching effects. However, the determination of three additional flame parameters (the thickness and temperature of the flame front, and the velocity of flame propagation) is required for this technique in order to interpret the conductivity measurements. A rectangular slit burner has been designed and constructed, and much of the instrumentation required to make the conductivity measurements has been assembled. Attempts are being made to obtain the necessary equipment required for the evaluation of the three additional flame parameters.

The self-resonant coil technique has been chosen because it can provide information which will help to determine whether the process of electron decay in hot flame gases is predominantly controlled by recombination reactions or electron attachment reactions. This method has been selected in preference to the more sophisticated microwave attenuation techniques because it is applicable over a wider range of electron concentration. Much of the instrumentation required was assembled during the period of this report and experiments since the end of the period have resulted in considerable progress toward application of this technique.

#### E. REFERENCES

1. R. G. Neville and J. J. McGee, "Materials and Structures-Macromolecule Research Program," TDR-69(2240-54)TR-2 Aerospace Corporation, El Segundo, California (31 August 1962).

2. S. A. Greene and J. E. Colwell, "Materials and Structures-Molecular Structure and Thermodynamics Program," TDR-69(2240-51)TR-3, Aerospace Corporation, El Segundo, California (30 August 1962).
3. G. Skirrow and H. G. Wolfhord, "Studies of Chlorine Trifluoride Flames," Proc. Roy. Soc. A232, 78 (1955).
4. H. F. Calcote and I. R. King, Fifth Symposium (International) on Combustion, Reinhold Publishing Corp., New York (1955), p. 423.
5. T. Kinbara, J. Nahamura, and H. Ikegami, Seventh Symposium (International) on Combustion (Butterworths Scientific Publications, London (1959), p. 263.
6. H. F. Calcote, Third Symposium on Combustion, Flame, and Explosion Phenomena, The Wilkins and Wilkins Company, Baltimore (1949), p. 245.
7. R. E. Andrew, D. W. E. Oxford, and T. M. Sugden, Trans. Faraday Soc. 44, 427 (1948).
8. D. E. Shuler and J. Weber, J. Chem. Phys. 22, 491 (1954).
9. H. Smith and T. M. Sugden, Proc. Roy. Soc. (London) A211, 31 (1952).
10. H. Williams, Seventh Symposium (International) on Combustion, Butterworths Scientific Publications, London, (1959), p. 269.
11. A. van Tiggelen, J. N. Bertrand and H. Philippaerts, "Experimental Investigations of Ionization Processes in Flames," ASTIA AD-258-050, (May 1961), p. 16.

PHYSICAL MEASUREMENTS

(JO 3240-30)

Prepared by

J. D. McCLELLAND

## ABSTRACT

During the report period studies were undertaken on selected properties of materials that may prove limiting to BSD-SSD systems capability. Major projects included property changes in pyrolytic graphite for ballistic re-entry heat shields, space environment effects on prospective satellite thermal control surface materials, and laser effects on materials.

Studies on pyrolytic graphite were directed toward determining the kinetics of structural changes that occur at temperatures in excess of the fabrication temperature. These changes may prove limiting to the use of pyrolytic graphite in advanced ballistic re-entry systems. Preliminary data are reported.

Design and construction of a chamber to simulate space environmental conditions, combining vacuum of about  $10^{-10}$  torr and ultraviolet radiation, are described.

Equipment for measurements of spectral and total emissivity also is described. Studies will be conducted on materials for both re-entry vehicles and satellite thermal control surfaces.

The proposed experimentation for determining the effect of laser radiation on selected materials is outlined.

## CONTENTS

ABSTRACT .....	6-i
A. PYROLYTIC GRAPHITE .....	6-1
1. Introduction .....	6-1
2. Background .....	6-1
3. Experimental .....	6-2
B. SPACE ENVIRONMENTAL EFFECTS .....	6-7
1. Introduction .....	6-7
2. Background .....	6-7
3. Experimental .....	6-8
C. EMISSIVITY STUDIES .....	6-11
1. Introduction .....	6-11
2. Background .....	6-12
3. Experimental .....	6-15
D. EFFECT OF LAZER BEAMS ON MATERIALS .....	6-21
1. Introduction .....	6-21
2. Background .....	6-21
3. Experimental .....	6-22
E. REFERENCES .....	6-24

## FIGURES

1	Diffraction Furnace . . . . .	6-2
2	Elongation versus Time at Temperature . . . . .	6-5
3	$C_0$ Spacing versus Time at Temperature . . . . .	6-6
4	Ultra-High Vacuum System . . . . .	6-10
5	Thermocouple Welds. . . . .	6-18
6	Emissometer Vacuum System . . . . .	6-20

## VI. PHYSICAL MEASUREMENTS

### A. PYROLYTIC GRAPHITE

#### 1. Introduction

Pyrolytic graphite is of interest as a material for re-entry nose-caps, leading edges, and rocket nozzle inserts. However, severe dimensional changes at high temperature occur which can limit its usage in such applications. Preliminary experiments have been performed to study such changes at temperatures up to 3000°C, and times ranging from 10 sec to 8 min.

#### 2. Background

Previous experimental work showed that pyrolytic graphite undergoes severe dimensional changes at temperatures above its deposition temperature. Four-hour exposure to temperatures of 2800°C results in contractions of about 9 percent in the "c" direction and an expansion of about 4 percent in the "a" direction (Ref. 1). This change arises from two different mechanisms. The first is the ordering of the individual graphite crystallites. The second is the straightening of the spherical surface which results from the radial growth of the cone structure.

During ballistic re-entry, and in most rocket nozzle applications, the pyrolytic graphite will be at these high temperatures for only a short period. Bragg and Parker (Ref. 2) have shown that the changes due to ordering are effectively completed between 10-100 minutes, depending on temperature. It is difficult, however, to extrapolate these data to the short times that are of engineering interest. Experiments will be described in this report in which the temperature excursions of the pyrolytic graphite were limited to relatively short times from 10 sec to 8 min. To separate the two phenomena which occur, we measured both  $C_o$  spacing and gross dimensional changes.

### 3. Experimental

#### a. Equipment

The furnace utilized for both the dimensional measurements and the x-ray studies is shown in Fig. 1. It consists of two water-cooled sample chucks, one of which is electrically insulated from the horizontally adjustable base.

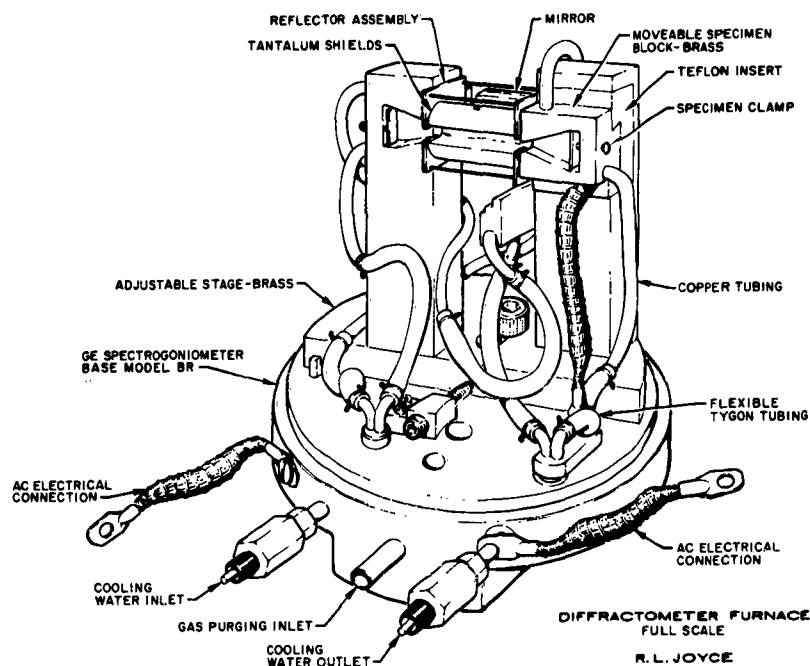


Figure 1. Diffractometer Furnace

The cooling water outlet tubing, insulated from the base with cast epoxy, conducts electrical current to the right specimen clamp. Flexible braid provides for clamp movement during the heating cycle. Insulation for this clamp is provided by a teflon dovetail slide. This unit was designed to mount on a General Electric XRD-5 x-ray diffractometer and may be used to obtain diffractograms at high temperatures. In this study, however, measurements were made at room temperature after the sample had been heated.

Specimens used in this study were cut from a 1/8-in. zone parallel to the "a" plane in the center of a 3/4-in. thick block of pyrolytic graphite. This material was made by High Temperature Materials Company, Boston, Massachusetts. Each specimen was machined so that the "a" planes of the graphite were parallel to its major surface. The triangular ends of the specimen were clamped firmly in the furnace chucks so that the "a" planes were in good electrical contact with the chucks. The central portion then could be heated with alternating current of 60-80 amp at 5-7 v.

A pyrex cover, tightly seated on the base flange, contained the argon atmosphere. A 180-deg window was cut in the front of the cover and a 0.0035-in. thick nickel foil was cemented in place. This foil permitted x-ray irradiation of the sample and retained the inert gas. (Nickel foil was chosen because it accomplished  $K_{\beta}$  filtration of the copper x-radiation without external filters.) The top of the cover was fitted with a prism for viewing the temperature of the "a" surface of the specimen and a 0.010 sq in. vent to permit a flow of argon through the furnace.

Power was supplied to the furnace by means of a 10 v-200 amp transformer, the primary of which was connected to a variable autoformer. A clock timer in series with the autoformer controlled the lengths of pulses.

A separate sample was used to obtain an approximate relationship between autoformer voltage and the sample temperature. In operation, the sample was inserted and aligned either with respect to the extensometers or the x-ray diffractometer, the cover was installed, and the furnace was purged with argon at approximately 6 cfh.

After an initial extensometer or diffractometer measurement was made, the autoformer was set to the voltage approximating the temperature desired, and the timer was actuated. Final adjustment of the autoformer to achieve the precise temperature desired was made in the initial 5 sec of the run. The specimen was allowed to cool after the pulse prior to measurement.

Two extensometers capable of measuring to  $2 \times 10^{-5}$  in. were used to measure the expansion along the "a" axis after each pulse. The difference between the location of scribe marks on each end of the surface was noted before and after the heat pulse. The determination of the  $C_0$  spacing was made, using standard x-ray techniques. A 1-deg beam slit was used which irradiated the central 0.4 in. of the sample.

b. Experimental Data

When pyrolytic graphite specimens are heated by a passage of current, the temperatures of the "a" and "c" surfaces (as read by an optical pyrometer) differ appreciably due to the effects of anisotropy in emissivity, thermal conductivity, and pyrolytic structure. The low values of emissivity of the "c" surface reported in the literature and the large thermal gradients in the "c" direction make it difficult to determine a temperature for this surface with any degree of certainty at this time. Values for the spectral emissivity of the "a" surface have been reported in the literature to be between 0.85-0.97, the most recent value being 0.95 (Refs. 3 and 4). Such high values for emissivity need only minor temperature corrections in order to obtain a reliable surface temperature. The values of temperature listed in this report were read by a micro-optical pyrometer; they are of the "a" surface.

Two problems were encountered during preliminary measurements. It was discovered at the outset that the "c" surface assumed a mottled appearance at large magnifications. Terminal faces of the pyrolytic growth cones appeared much cooler than the interstices between the cones. A difference of  $82^{\circ}\text{C}$  was read between these two areas at an average temperature of  $2400^{\circ}\text{C}$ . At low magnifications, however, the surface assumed a temperature approximating that of the cones occupying the major portion of the field of view as seen through the pyrometer. Reasons for the higher temperatures read in the interstices could either be: (1) a higher emissivity in this region; or (2) greater power generated in interstices than in the cones because of higher resistance due to the pyrolytic graphite structure.

Above 2500°C, a grey deposit began to form on the "a" surfaces of the specimen. Below this temperature, no apparent surface changes were noted even after extended periods of time at temperature. The speed at which the deposit formed increased with temperature. At temperatures above 3000°C the material began to sublime and deposited itself on the interior of the furnace. At 3100°C the field of view was totally obscured within 15 sec.

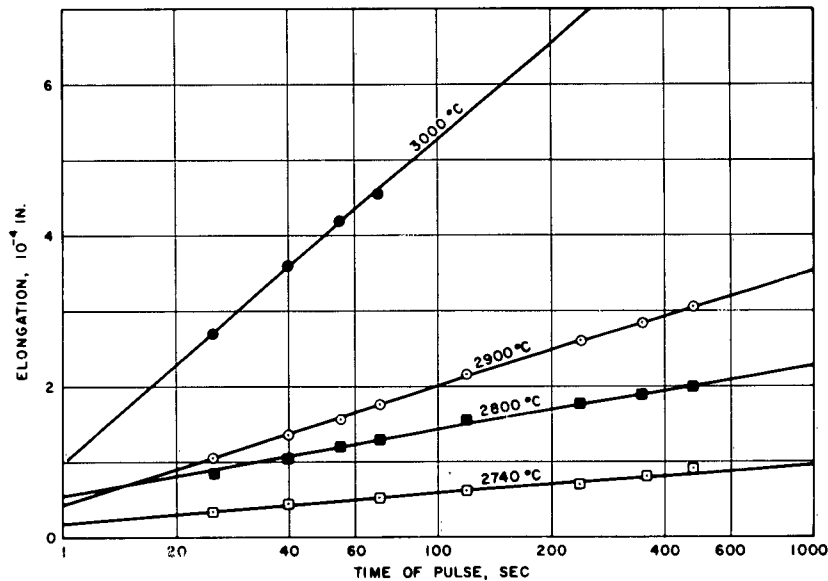


Figure 2. Elongation versus Time at Temperature

Expansion in the "a" plane is shown in Fig. 2 at temperatures ranging from 2740°C-3000°C. The curves are characterized by a rapid rate of change at times below one minute, followed by a region of more gradual changes. Plotting the expansion as a function of  $\log t$  yields a series of straight lines whose slopes increase with increasing temperature. At 2600°C no significant changes were noted. At 2740°C, a change of  $5 \times 10^{-4}$  in. was noted after 1 min, while at 3000°C a change of  $4.6 \times 10^{-3}$  in. was noted. Since there

was a severe temperature profile across the specimen, it is difficult to assess a mean gauge length by which these dimensional changes can be normalized. The present data should be considered only for qualitatively indicating the changes that occur.

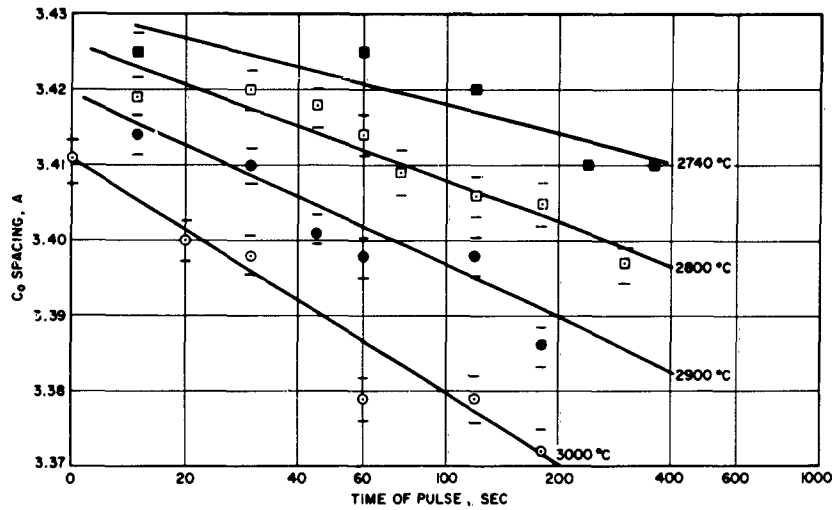


Figure 3.  $C_0$  Spacing versus Time at Temperature

The  $C_0$  spacing changes are shown in Fig. 3 over the same temperature region as those for the previous experiment. The curves show the same general behavior noted in the case of the "a" axis dimensional changes. An error of  $\pm 4 \times 10^{-3}$  A is assigned to the  $C_0$  spacing measurement. Within this error, the data are best represented as a series of straight lines on a plot of " $C_0$ " spacing versus log time. As in the case of the dimensional changes, the slope of such a line increased with increasing temperature. After 3 min at  $3000^\circ\text{C}$ , the  $C_0$  spacing was nearly that of the single crystal value of 3.37 A. After 1 min at  $2740^\circ\text{C}$  and  $3000^\circ\text{C}$ ,  $C_0$  changes of  $4 \times 10^{-3}$  A and  $42 \times 10^{-3}$  A were noted. The  $C_0$  spacing was found to vary with position within the parent block, ranging from 3.42-3.43 A. The more ordered material is that which is initially produced, i. e., the material next to the mandrel.

On the basis of these preliminary data, the following conclusions are drawn:

- 1) Gross dimensional changes in pyrolytic graphite occur within minutes at temperatures in excess of 2600°C.
- 2) The rate of change becomes progressively more rapid with increasing temperature. At 3000°C, almost all changes are completed within 3 min.
- 3) The "a" axis expansion and the C<sub>o</sub> spacing show similar behavior. On the basis of these data, it is not possible to discern any difference in the temperature dependence of the two phenomena of ordering and layer-straightening.

## B. SPACE ENVIRONMENTAL EFFECTS

### 1. Introduction

An understanding of the behavior of materials under space conditions is essential for reliable space systems. Unfortunately, simulation of the space vacuum has been limited by the state of vacuum technology. Recent developments, however, permit vacuums of  $10^{-9}$ - $10^{-10}$  torr to be realized in chambers sufficiently large to perform experiments of a reasonable size. The present program will utilize this newly developed technology to study the behavior of aerospace materials under space vacuum. Initial studies will be of the ultraviolet degradation of polymers under high vacuum. Proposed experiments will investigate such phenomena as friction and self-welding.

### 2. Background

Under space conditions, adsorbed films which are normally present will be removed by mechanical abrasion, erosion, and evaporation. Due to the high vacuum, there will be essentially no re-forming of the monolayer (Ref. 5). The behavior of this clean surface cannot be inferred from data on the "dirty" surfaces normally encountered. An adequate description of the effect of the space environment on surface sensitive effects, particularly friction, wear, and ultraviolet degradation, is difficult since very little experimental data are available for pressures low enough to insure that a "clean" surface exists (Refs. 6 and 7).

Ultraviolet radiation studies in both vacuum and air, for example, indicate that the high rate of polymer film degradation usually associated with the effects of ultraviolet light depends on the presence of an oxygen-bearing atmosphere and oxygen absorption in the material (Ref. 8).

The atoms in organic materials are held together by strong exchange forces that arise from the sharing of electrons or a covalent bond. Ionizing radiation can break these bonds by means of an excitation process. The result is a change in physical properties. An increase in solar absorption is typical for thermal control surfaces resulting in increased spacecraft temperatures. Elastomers tend to harden and increase in brittleness due to crosslinking of the chain-like molecules. Cements or seals which depend upon elastic properties will become less effective (Refs. 2, 9, and 10).

One of the major problems at present is the combined effects of radiation and high vacuum on the characteristics of polymeric and oxide coatings. Such information is currently almost nonexistent in the  $10^{-9}$  torr range (Ref. 11)<sup>1</sup> and lower. This presents serious problems in a combined environment such as that found in space. Because of the outgassing problems that will be enhanced by radiation degradation, special considerations will have to be given to the vacuum system design so that a low enough pressure can be attained.

### 3. Experimental

The rate at which a monolayer re-forms is dependent on the pressure, temperature, and binding energy of the adsorbed molecules. If it is assumed that any molecule sticks that strikes the surface, then some simple kinetic theory considerations suggest that at a pressure of  $10^{-9}$  torr, it will take about 25 min for a monolayer to re-form; at  $10^{-11}$ , it will take about two

---

<sup>1</sup> The torr is the recommended international unit for pressure in vacuum technology. It differs from the unit mm Hg by only one part in seven million. For a more detailed description see Ref. 11.

days (Ref. 5). Pressures of  $10^{-9}$  torr or lower, therefore, seem necessary to assure that a clean surface is maintained for reasonable periods of time.

In any simulation technique, the effect of chamber walls must be considered. Where a surface is completely exposed to the space environment, molecules that leave the surface have a nearly zero probability of returning. The probability of return can greatly increase within an enclosure, depending upon geometry, chamber surface area, specimen surface area, and the effective pumping aperture into the chamber.

In a clean, empty chamber with an ideal vacuum pump, the pumping speed (volumetric rate) remains constant with time and density while the outgassing (mass rate) is constant with atmospheric density, but is a direct function of wall temperature (Ref. 12). Outgassing also decreases slowly with time. To reduce the atmospheric density by a decade, the pumping speed must be increased by a decade. To increase the pumping speed, a larger pump must be added. The addition of a larger pump also increases the pump surface area, which, in turn, increases outgassing in the system. Therefore, the actual increase in pumping speed is less than the ideal increase. The solution to this is to utilize the chamber walls to pump the gases. This increases pumping speed and decreases outgassing. The nearly completed apparatus shown in Fig. 4 uses this principle.

The inner 6-in. diam chamber is cooled with liquid helium. Depending upon the heat input, the chamber temperature will be between  $4.2^{\circ}\text{K}$ - $8^{\circ}\text{K}$ . The lower 6-in. diam chamber is constructed of copper and the rest of the chamber is stainless steel. A getter-ion pump will be used to pump noncondensable gases and high vapor pressure condensates. Hydrogen is the primary constituent in this class. The outer chamber is evacuated and maintained at a high vacuum by the cryopumping action of the inner chamber wall and a getter-ion pump. The outer chamber will be cooled with liquid nitrogen to reduce the heat transfer to the inner chamber. A vacuum-insulated transfer

tube will supply liquid helium to the cooling coils (not yet installed) on the inner chamber. The test specimen will be attached to the 6-in. blank, along with any electrical and fluid feedthroughs. To change from one experiment to another, we need to change only the blank.

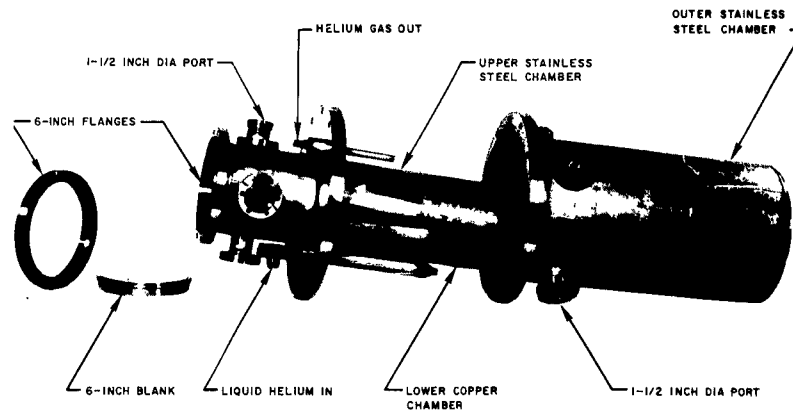


Figure 4. Ultrahigh Vacuum System

For ultraviolet irradiation experiments, the specimen will be suspended opposite a Suprasil quartz (high ultraviolet transmission) window mounted in one of the upper 1.5-in. diam ports. The source will be an air-cooled, 900 w mercury-vapor lamp. Although the density may be higher in the upper portion of the chamber, ultraviolet irradiation of the cryopump surface will increase sublimation of condensed gases. This precludes the mounting of the specimen in the lower chamber. A friction experiment, however, could be performed in the lower chamber without affecting cryopump performance, provided that the heat output is small.

Instrumentation to be used with this apparatus includes an ultrahigh vacuum, Redhead-type, cold cathode ionization gauge that can measure pressures to less than  $10^{-13}$  torr, and a mass spectrometer residual gas analyzer with a

sensitivity of  $5 \times 10^{-11}$  torr and unit resolution to mass 150. The gas analyzer will provide information on the type and quantity of volatile materials emitted by a specimen during an experiment. This should give some indication as to the nature of the chemical processes taking place.

Instrumentation is currently being evaluated in an existing chamber at pressures into the  $10^{-9}$  torr range. An exposed gauge, without an envelope and designed to extend into the chamber, has been successful. Although the use of a "nude" gauge is quite common, this has involved the attachment of purchased elements to a standard Ultek flange in the laboratory. Gauge geometry will probably limit the lower pressure reading to between  $5 \times 10^{-10}$  -  $1 \times 10^{-10}$  torr. As soon as the Redhead gauge power supply is received, the Redhead gauge will be checked out. Comparison of various gauges and calibration against a McLeod gauge at pressures down to  $10^{-5}$  or  $10^{-6}$  torr will provide a nearly absolute calibration. The McLeod gauge uses mercury to compress a known volume of gas to a smaller known volume. The initial pressure can be calculated from the final pressure. Because ionization gauge calibration is dependent upon gas composition, the gas analyzer can be used to verify the composition. Calibration of the analyzer for quantitative partial pressure measurement can be accomplished through the use of standardized ionization gauges and purging of the vacuum system with each gas of importance.

### C. EMISSIVITY STUDIES

#### 1. Introduction

Thermal control of missile systems and space vehicles requires exact knowledge of the thermal emittance of the skin. In addition, the detection of re-entry vehicles can depend on the infrared and visible emission spectrum from the hot vehicle. There is a dearth of knowledge regarding the emissivity of materials at elevated temperatures. Most data are primarily engineering in nature and, in many cases, discrepancies occur in data reported by several investigators.

Studies have begun in two areas:

- a) the total and spectral emittance of pyrolytic graphite
- b) the effect of surface roughness on the emittance of metals

This report will describe the construction of the emissometer and the development of experimental techniques needed to measure the total emittance.

## 2. Background

Emissometers, which are normally used in the determination of total emittance, consist of an evacuated chamber with blackened and cooled walls. The specimen is usually in the form of a long electrically-conducting strip or tube. It is held by electrodes inside the cell and heated by running a measured constant current through it. When the heat-radiation rate equals the heat-generation rate, the specimen reaches temperature equilibrium. The surface temperature at the center where the heat flow is radial is then recorded as well as the current and the voltage as read from potential probes along the length of the specimen.

The exchange of radiation between the specimen and the walls is described by a complex expression which simplifies and can be integrated over all wavelengths, giving Stefan's Law

$$Q = A \epsilon_t \sigma T^4 \quad , \quad (1)$$

provided the walls are black absorbers and are kept much colder than the specimen. In Eq. (1),  $Q$  is the power radiated by the test section of the specimen that has an area  $A$ , a total hemispherical emittance  $\epsilon_t$ , and an absolute temperature  $T$ . An error analysis shows that the determination of the surface temperature will be the primary source. This is because an error in this measurement will result in four times the proportional error in the value of  $\epsilon_t$ .

Thermocouples are used from room temperature to 1500°C except where limited by incompatibility with the material under test. The overlap with the pyrometer range provides a convenient double check on temperatures arrived at by pyrometry, and also enables calibration intercomparisons with pyrometers in a special furnace. Due to calibration uncertainties, the use of thermocouples higher than 1500°C is limited.

To obtain the surface temperature of the specimen, pyrometry must be used whenever thermocouples are inadequate. All pyrometry, whether it is monochromatic, multicolor, total radiation, or two-temperature, is subject to excessive errors without our prior knowledge of the specimen emittance characteristics (Ref. 13). Several techniques, however, can be employed to minimize these errors.

A technique described by Worthing (Ref. 14) can be used if the specimen is in the form of a thin-walled tube. In this method the inside wall temperature is measured by means of a small reference blackbody hole through the tube wall. Using the radial heat flow equation (Refs. 15 and 16) for thin-walled tubes, we can calculate the surface temperature. This method is quite useful with metals where the temperature drop is quite small and the thermal conductivity is well-known. It is of limited use in the case of pyrolytic graphite cylinders with the "a" planes forming the cylinder walls. In the latter case, the temperature drop across the walls is several orders of magnitude higher than for metals because of the very poor thermal conductivity in the "c" direction. Since the thermal conductivity is not well-known, such large temperature drops will lead to significant errors in the surface temperatures.

The method of Allen, Glasier, and Jordan (Ref. 17) will be used for pyrolytic graphite. In this method both the spectral and total emittance can be determined from a measurement of the brightness temperature  $T'$ , the power radiated  $Q$ , and the derivative of the brightness temperature with respect to the radiated power  $dT'/dQ$ . An initial approximation  $T_1$  to the surface

temperature  $T$  can be obtained from

$$\frac{1}{T_1} = \frac{4Q}{(T_1)^2} \frac{dT_1}{dQ}$$

This value of  $T_1$  is then used to calculate the first approximations  $(\epsilon_\lambda)_1$  and  $(\epsilon_t)_1$  to the spectral emittance  $\epsilon_\lambda$  and the total emittance  $\epsilon_t$  with

$$\ln (\epsilon_\lambda)_1 = \frac{C_2}{\lambda} \left[ \frac{4Q}{(T_1)^2} \frac{dT_1}{dQ} - \frac{1}{T_1} \right]$$

$$(\epsilon_t)_1 = \frac{Q}{\sigma A T_1^4} \quad ,$$

where  $C_2$  is the second constant in the Planck equation.

The second approximations  $T_2$ ,  $(\epsilon_\lambda)_2$  and  $(\epsilon_t)_2$  are obtained from:

$$\frac{1}{T_2} = 4Q \left[ \frac{1}{(T_1)^2} \frac{dT_1}{dQ} - a_1 \right]$$

$$\ln (\epsilon_\lambda)_2 = \frac{C_2}{\lambda} \left[ \frac{1}{T_2} - \frac{1}{T_1} \right]$$

$$(\epsilon_t)_2 = \frac{Q}{\sigma A T_2^4}$$

where

$$a_1 = \frac{\lambda}{C_2 (\epsilon_\lambda)_1} \frac{d(\epsilon_\lambda)_1}{dQ} - \frac{1}{4 T_1 (\epsilon_t)_1} \frac{d(\epsilon_t)_1}{dQ}$$

The following approximations are obtained from the same equations because more reliable values for  $\epsilon_{\lambda}$  and  $\epsilon_t$  permit calculating successively more accurate values for  $\alpha$ . This reiterative technique is repeated until the desired degree of convergence is attained.

The greatest difficulty with the measurement of pyrolytic graphite is the inhomogeneous nature of the surface itself. Observations of the "a" surface of a pyrolytic graphite specimen reveal the discrete structure of the material. Hot spots, corresponding to areas between growth cones, stand out against the lower brightness temperature of the growth cones. This distribution cannot be observed in detail yet because the pattern is too small for conventional pyrometry. Initial work on the total emittance will be made on pyrolytic graphite with barely "nascent" growth cones, where temperature nonuniformities will be minimized. A photoelectric pyrometer with higher magnification and resolving power is being developed to check the temperature profiles on these surfaces.

### 3. Experimental

#### a. Emissometer

An emissometer capable of measuring total emittance from room temperature to 2000°C has been constructed and is being calibrated. It consists of a stainless-steel chamber 20 in. long and 10 in. in diameter immersed in liquid nitrogen. Initial experiments will utilize flat samples which can be self-heated. The samples can be in the form of thin plates 6 in. long and 0.5 in. wide.

The specimen is clamped within the emissometer in a rigid electrode at one end and in a bellows-mounted insulated feedthrough at the other end. The bellows allows for thermal expansion. The feedthroughs are mounted at either end of the chamber and are there connected to the external circuitry. This arrangement differs advantageously from that in other emissometers in which both feedthroughs enter the chamber side by side. In the latter case, one end of the specimen fastens to a feedthrough and the other end

extends into the chamber. The other electrical lead then has to travel through the chamber to be fastened to the other end of the specimen. The disadvantage of this is two-fold:

- 1) The lead runs parallel to the specimen and exerts a force on it due to induction when the current is on, causing it to bend.
- 2) This same lead is not cooled as the walls are, violating the radiation void assumption for the specimen surroundings.

b. Supply and Measurement of Power

The power supplied to the specimen is 60-cycle alternating current rather than direct current. The use of direct current leads to errors in thermocouple readings whenever the two legs of a thermocouple do not lie exactly on the same equipotential line of the sample. This dc error on the thermocouple voltage can be corrected by reversing the direction of the heating current. Unfortunately, this reversal leads to undesirable temperature transients which are difficult to control. In the alternating current case, 60-cycle voltages superimposed on the thermocouple signal do not affect the readings of the potentiometer because they are integrated to a net zero dc bias by the galvanometer. This conclusion can be verified with a digital voltmeter by controlling the gate time. Alternating current can be controlled to a very fine degree at a fraction of the cost. The ripple in the specimen temperature due to the 60-cps power is negligible for the samples of the size being studied.

The specimen current passes through a standard shunt outside the chamber. A voltmeter reads the potential drop across the shunt, giving an accurate measurement of the current. Another voltmeter is used to measure the voltage level at each of several potential probes fastened along the length of the specimen. Single thermocouple legs can serve as potential probes in the case of metal specimens. The potential probes and thermocouples are brought out of the chamber through insulated vacuum feedthroughs.

Temperature excursions can be limited to  $\pm 0.05$  percent by keeping variations in the voltage supply to  $\pm 0.02$  percent. A 60-cps voltage regulator, which

can supply up to 10 kv-amp of power, regulates the supply voltage within  $\pm 0.1$  percent against line voltage changes. Only very short time-constant spikes in the line voltage can appear on the output of the regulator. Since the thermal inertia of most specimens is high, the specimen temperature does not follow the voltage spikes.

At power levels below 100 w, 60-cycle noise in the room prevents accurate measurement of the voltage. This problem was eliminated by using 1000 cycles of power supplied by means of an audio oscillator driving a 100-w audio amplifier. Both the oscillator and amplifier are operated from a stable voltage regulator.

Voltages are measured with two Fluke model 803 voltmeters whose accuracy is  $\pm 0.2$  percent from 0.5-500 v. These convert ac voltages to dc over a wide band of frequencies and then compare the dc with a very stable dc reference voltage by means of a bridge. The voltmeters are calibrated by the use of a thermal transfer standard that directly compares the heating power of an ac unknown to a dc reference voltage with high accuracy over a range from 0.3-1000 v.

c. Temperature Measurement

Thermocouples cool the portion of the specimen surface to which they are attached by conduction through the thermocouple legs. The resulting systematic errors in the temperature measurement can be calculated; indications are that 0.005-in. thermocouples are suitable in most cases, and that 0.003-in. thermocouples can be used in all cases. These conduction losses can be further reduced by attaching each leg of one thermocouple separately to the specimen surface.

A technique has been developed to weld thermocouples to a metal surface. Welding is accomplished by resistance-heating the thermocouple leg to sample junction by capacitor discharge. Figure 5 shows a 0.005-in. platinum/platinum-rhodium thermocouple welded to a stainless steel plate. This

technique cannot be used for pyrolytic graphite; other approaches such as "peening" are being investigated.

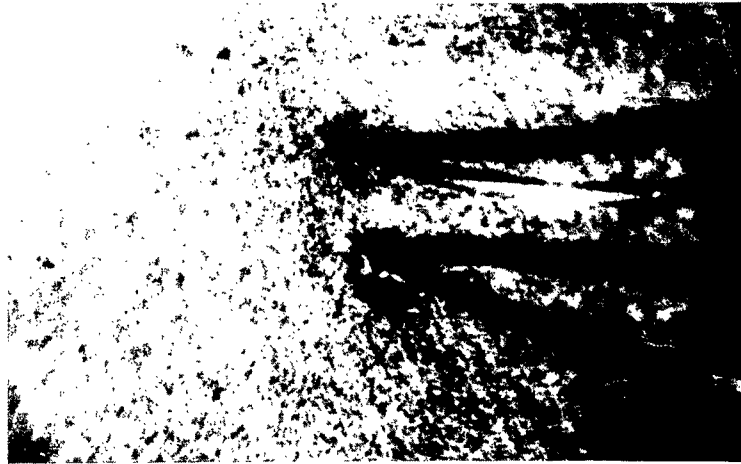


Figure 5. Thermocouple Welds

d. Coatings

So that the equation previously described may be used, it is necessary to surround the sample with a radiation sink. For this reason, the chamber walls are in the form of corrugations and, in addition, are coated with an optical black coating. The design of the walls is such that specular reflectances as high as 0.5 result in negligible errors after multiple reflections. In case of diffuse reflectance, the size of the chamber is such that values as high as 0.4, excluding the specular component, can be tolerated.

Platinum black is often used as a coating because of its high emissivity, 0.99 (Ref. 17). Difficulty of plating in the concave recesses of the corrugated wall prevented its use. Parson's Optical Black was used instead. Its optical

properties have been studied by a number of researchers<sup>2, 3</sup> and show it to be an efficient absorber from the ultraviolet to about 60  $\mu$  (Ref. 19). No spectral measurement has been made at wavelengths past 30  $\mu$ , and the emittance in that range can only be inferred from its use in total emittance measurements. However, because of the chamber geometry, it is expected that no significant errors will result.

Coatings of Parson's Black were tested for changes in their optical and mechanical properties as a result of thermal cycling. Stainless steel strips were coated with the black, air-dried, and heated to 300°C (maximum bake-out temperature of the emissometer) in a glass vacuum chamber. They were then immersed in liquid nitrogen repeatedly. No change in the specular reflectance from the visible to 20  $\mu$  was evident as a result of bake-out or liquid nitrogen submersion. Some cracking of the coating was visible under the microscope.

e. Vacuum System

Convection losses can be overcome by evacuating the emissometer to  $10^{-5}$  torr, because the mean free path at that pressure is 5 m, or much greater than the dimensions of the apparatus. The transfer of power away from the specimen by the residual gases is conductive rather than convective. This gas conduction loss is too small to affect the measurements with the specimen at room or higher temperatures. However, the contamination of surfaces by the backstreaming of diffusion oil vapors can be a serious problem. For this reason, the high-vacuum ion pump system shown in Fig. 6 was built.

This system is brought from atmospheric pressure to  $10^{-3}$  torr in a completely oil-free manner by means of a molecular sieve, which appears to the

---

<sup>2</sup> Private communication with W. J. Parker and R. S. Alger, Radiation Effects Branch, U. S. Naval Radiological Defense Laboratory, San Francisco, California.

<sup>3</sup> Information Sheets from Eppley Laboratory, Inc., Newport, R. I.

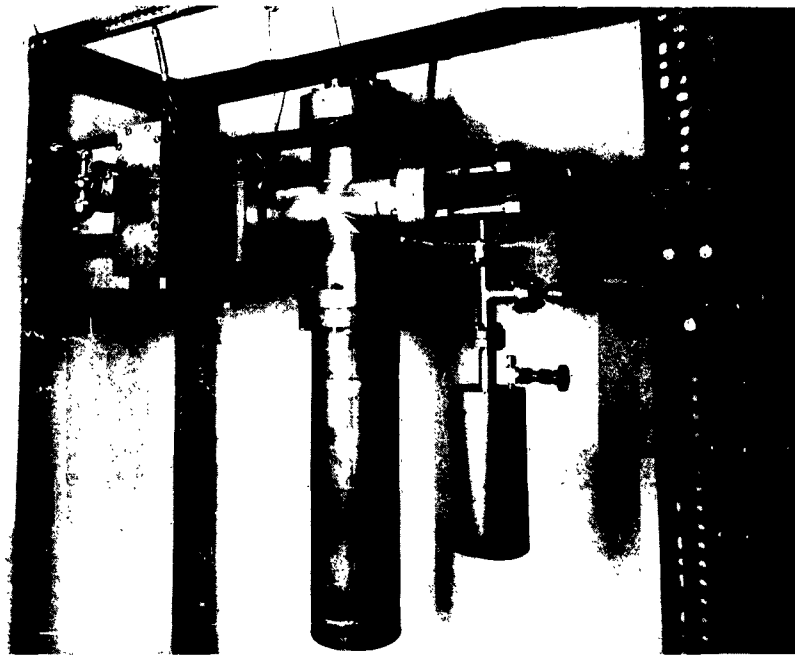


Figure 6. Emissometer Vacuum System

right, suspended by a valve from the main chamber. The ion pump is then turned on and an ultimate vacuum in the  $10^{-8}$ - $10^{-10}$  range can be reached, depending on the outgassing of the internal surfaces. Pressure is measured with Bayard-Alpert ionization gauges, and by a calibration of the pump collection current. A sensitive method of leak-checking the system has been worked out, through the use of the ion pump itself as a detector.

In order to protect the ion pump from possible irreparable damage, specimens suspected of severe outgassing will first be pumped down with a diffusion pump. This pump can also be used for initial outgassing of the empty chamber whenever the walls are freshly coated with black. A specially designed liquid-nitrogen cold trap is used between the diffusion pump and the chamber to

prevent contamination of the cell by the oil. The main 2-in. diffusion pump is backed up by a smaller diffusion pump to obtain higher and more reliable pumping speed at high vacuum.

#### D. EFFECT OF LASER BEAMS ON MATERIALS

##### 1. Introduction

The laser, or optical maser, provides a beam of coherent electromagnetic radiation which is relatively monochromatic, extremely intense, and highly directional. The latter two properties, the beam intensity and directionality, have made the laser one of the most promising new tools for materials research. The laser is not only of importance as a potential destruction weapon itself; as a laboratory tool it will provide higher power density of electromagnetic radiation than was previously available.

##### 2. Background

It is well-known that a laser beam can produce a hole through thin materials such as razor blades. When the material is thicker, the interaction of the beam can produce significant amounts of blowoff. This blowoff will result in impulsive forces being imparted to the body. Since laser technology is in its infancy, essentially no experimental literature exists by which a meaningful evaluation of such laser effects can be made.

When electromagnetic radiation strikes a solid surface, a portion of the radiation is reflected. The remaining portion penetrates the material and, in the case of opaque materials, is absorbed. The distance at which the intensity of the beam is reduced to  $1/e$  of its value is called the penetration depth. If the material has a high absorption constant (i. e., a short penetration depth), the main portion of the beam can be absorbed within a short distance of the surface. In the case of laser radiation, the beam is very intense. When this radiation is absorbed, it can vaporize the material, thus producing blowoff. This will, in turn, give rise to impulsive loads on the surface.

The magnitude of the effect might be best illustrated by considering graphite. The energy density of the laser being used in this laboratory is about  $100 \text{ cal/cm}^2$ . Assume that all of this energy is absorbed within the penetration depth of graphite, which is  $0.05 \mu$  (Ref. 21); this means that there is an energy generation of about  $2 \times 10^7 \text{ cal/cm}^3$  or  $3 \times 10^7 \text{ cal/gm}$ . The heat content is only about  $1.5 \times 10^4 \text{ cal/gm}$  (Ref. 22). It is obvious that the heat-generation rates produced will result in catastrophic vaporization of the surface.

If all of the absorbed energy goes into vaporization, the amount of heat can be calculated from the heat content of the material. This heat content consists of the energy needed to heat one gram of the material to its vaporization temperature and then to vaporize it. The heat of vaporization is usually the biggest contributor to the heat content. For rough calculations it is often sufficient to use the heat of vaporization instead of the heat content.

The mass vaporized under this simple assumption should be given by the equation

$$M = \frac{P}{H}$$

where M is the mass vaporized, P is the energy in the impinging beam, and H is the heat content. Using this equation, we can show that 20 J of energy will vaporize approximately 300  $\mu\text{gm}$  of carbon.

### 3. Experimental

An optical maser system has been received from the Trion Instrument Company. It utilizes a ruby laser and has a nominal output of approximately 30 J with a peak power between 10-30 kw. Initial runs indicated that the cooling system was not adequate to cool the ruby. This has been modified and is now complete.

Experiments are planned to determine the blowoff and impulse produced by a laser beam. Initial experiments have been performed to determine the magnitude of the effects. Samples of titanium carbide, magnesium oxide, and aluminum oxide were hit by laser pulses. The energy of the beam was estimated to be about 20 J and 0.1-in. beam diam. Material losses were about 300  $\mu\text{gm}$  in the case of the TiC and about 500  $\mu\text{gm}$  in the case of the oxides. Such mass losses are quite easy to detect by using standard weighing techniques and no difficulty is expected in obtaining accurate values for the blowoff.

A relatively crude ballistic pendulum was constructed with an 8-in. suspension, using small rods of 1/8-in. diam and 1/2-in. length as the mass. Rods of carbon and iron were struck by the laser beam. Deflections of one inch were found for the carbon and one eighth inch for the iron. These data were used to design a new ballistic pendulum now under construction. In this apparatus, the deflections will be measured optically. The entire apparatus will be placed in a vacuum system to eliminate problems due to air currents.

Preliminary data suggest that there is a large variation of beam power from pulse to pulse. However, it is necessary to accurately determine the power in each pulse if one is to meaningfully evaluate either blowoff or the impulse experiments. For this purpose, a secondary calorimeter is being constructed which will monitor the beam. Approximately 10 percent of the beam will be reflected by means of a glass slide into this secondary calorimeter. Its construction is similar to that described below for the primary calorimeter except that it will be smaller and not as accurate. The secondary calorimeter will be calibrated in situ by means of the primary calorimeter.

The primary calorimeter consists of a hollow copper chamber 1-in. long, 0.5 in. in diameter, and a wall of 0.040 in. A 90-mil hole in one end permits the converging beam to enter the chamber. The interior of the chamber is designed to minimize losses from the entry hole by reflection. The temperature of the chamber will rise  $0.3^{\circ}\text{C}$  for each joule of energy

absorbed. Since the nominal output of the laser is approximately 30 J, a maximum temperature rise of  $10^{\circ}\text{C}$  is expected. The calorimeter is placed in a vacuum chamber to prevent losses due to convection and gas conduction. Radiation losses at this temperature can be shown to be negligible. Temperature will be measured by means of a chromel-alumel thermocouple. Ambient temperature fluctuations will be cancelled through consideration of only the temperature difference between the active calorimeter and equivalent dummy calorimeter. A sensitivity of about  $10\ \mu\text{v}/\text{J}$  for the calorimeter has been calculated. A precision of  $\pm 1$  percent in determination of the energy of the beam is expected.

#### E. REFERENCES

1. J. H. Richardson and E. H. Zehms, "Materials and Structures, Physical Measurements Program, Pyrolytic Graphite, Semiannual Technical Report, 1 January-30 June 1962," TDR-69(2240-64)TR-2, Aerospace Corporation, El Segundo, Calif. (1 October 1962).
2. R. H. Bragg and C. M. Packer, "X-Ray Investigation of Heat Treated Pyrolytic Graphite," J. Appl. Phys. (to be published).
3. R. J. Tharn and G. H. Winslow, "Radiation of Thermal Energy from Real Bodies," Temperature, Its Measurement and Control in Science and Industry, Vol. III.
4. J. D. Plunkett and W. D. Kingery, "The Spectral and Integrated Emissivity of Carbon and Graphite," Carbon; Proceedings of the Fourth Conference, Pergamon Press, New York (1960), pp. 457-72.
5. J. H. Atkins, et al., "Effects of the Space Environment on Materials," WADD TR 60-721 (December 1960).
6. L. D. Jaffee and J. B. Rittenhouse, "Behavior of Materials in Space Environments," TR No. 32-150, Jet Propulsion Lab., Pasadena, Calif. (1 November 1961).
7. C. G. Goetzel and J. B. Singletary, "Space Materials Handbook," Lockheed Aircraft Corp., Missiles and Space Div., Sunnyvale, Calif. (January 1962).
8. L. A. Wall and J. D. Michaelson, J. Research Nat. Bur. Standards **56**, 27 (1956).

9. L. A. Wall and R. E. Florin, "Polytetrafluoroethylene-A Radiation Resistant Polymer, J. Appl. Polymer Sci. 5 (2), 251 (1959).
10. Space Radiation Effects on Materials, STP 330, American Society for Testing Materials, Philadelphia.
11. American Vacuum Society, Glossary of Terms Used in Vacuum Technology, Pergamon Press, Inc. New York (1958).
12. S. Dushman and J. M. Lafferty, Scientific Foundations of Vacuum Technique, John Wiley and Sons, Inc., New York (1962).
13. A. G. Emslie and H. H. Blau, Jr., J. Electrochem. Soc. 106, 177-80 (1959).
14. A. G. Worthing, Phys. Rev. 28, 190-210 (1926).
15. M. F. Angell, Phys. Rev. 33, 421 (1911).
16. A. G. Worthing and D. Halliday, Heat, John Wiley and Sons, Inc., New York (1948), p. 176.
17. R. D. Allen, et al., J. Appl. Phys. 31, 1382-7 (1960).
18. "Radiation Instruments and Measurements," IGY Instruction Manual, Pergamon Press, Inc., New York (1958), p. 436.
19. W. R. Pohl, Optics and Atomic Physics, Springer-Verlag, Berlin (1954), p. 147.
20. A. Goldsmith, et al., "Thermophysical Properties of Solid Materials," WADC TR-58-476 (August 1960).

METALLURGY AND CERAMICS RESEARCH

(JO 3240-31)

Prepared by

E. G. KENDALL

## ABSTRACT

Progress of studies on refractory metals, refractory metal carbides, and refractory oxides during the report period is reviewed.

The major effort in dispersion-strengthening of tungsten has involved establishing techniques for powder-handling, mixing, blending, hot-pressing, sintering, and annealing. The studies undertaken indicate considerable promise for use of both mechanical mixing and internal oxidation methods; future work will be conducted in the tungsten-hafnium system, which will involve controlled oxidation of the hafnium in situ. As a model for dispersion-hardened tungsten, some studies were undertaken on dispersion-hardening of Type 304 stainless steel by addition of aluminum oxide. Interesting microstructures were obtained; mechanical properties have not yet been determined.

Laboratory equipment required for preparation of refractory metal carbides was assembled. Initial studies were undertaken on the titanium-carbon system. Bodies have been prepared with between 20-30 wt % carbon. Preliminary evaluation indicates unusual properties of material in the neighborhood of 23-26 wt % carbon. This material exhibits unusually high compressive strengths compared to previously reported values for stoichiometric TiC. The existence of the reported eutectic between TiC and carbon has been confirmed. An analysis of microstructure and additional testing is underway.

Initial studies on refractory oxides have involved the use of a NaCl model to determine hot-pressing behavior. Initial indications are that NaCl may markedly depart from the hot-pressing behavior of a number of other solids.

## CONTENTS

ABSTRACT . . . . .	7-i
A. INTRODUCTION . . . . .	7-1
B. REFRACTORY METALS . . . . .	7-1
1. Background . . . . .	7-1
2. Tungsten, Hot-Pressed . . . . .	7-2
3. Tungsten, Cold-Pressed and Sintered . . . . .	7-9
4. Thoriated Tungsten Minor Phase Identification . . . . .	7-9
5. Internal Oxidation Alloys . . . . .	7-12
6. Dispersion-Hardening, Type 304 Stainless Steel . . . . .	7-15
C. REFRACTORY CARBIDES . . . . .	7-24
1. Background . . . . .	7-24
2. Synthesis and Fabrication . . . . .	7-25
3. Transverse Rupture Tests . . . . .	7-27
4. Compressive Strength Tests . . . . .	7-29
5. Elastic Moduli . . . . .	7-30
6. Hardness . . . . .	7-30
7. Density . . . . .	7-30
8. Metallography . . . . .	7-31
D. REFRACTORY OXIDES . . . . .	7-34
1. Background . . . . .	7-34
2. Hot-Pressing of Sodium Chloride . . . . .	7-35

## FIGURES

1	Tungsten Powders Used in Hot-Pressing Studies . . . . .	7-3
2	Typical Carbide Case Resulting from Hot-Pressing Tungsten Powders . . . . .	7-6
3	Variation in Porosity and Grain Growth in Hot-Pressed Tungsten . . . . .	7-7
4	Hardness versus Density of Hot-Pressed Tungsten . . . . .	7-8
5	Thoriated Tungsten Samples Sintered at 2800°C and Hot-Extruded prior to Tensile Testing at 1650°C in Vacuum . . . . .	7-11
6	Columbium + 5 Wt % Hafnium Alloy . . . . .	7-13
7	Columbium + 5 Wt % Hafnium Alloy . . . . .	7-14
8	Pure Columbium Cold-Pressed and Vacuum Sintered 1 hr at 2150°C . . . . .	7-16
9	Stainless Steel Cold-Pressed and Sintered, Type 304 . . . . .	7-18
10	Stainless Steel Cold-Pressed and Sintered, Type 304 . . . . .	7-19
11	Stainless Steel Cold-Pressed after Hydrogen Treatment and Additions of Al <sub>2</sub> O <sub>3</sub> . . . . .	7-22
12	-325 Mesh Type 304 Stainless Steel + 2.5 Wt % Al <sub>2</sub> O <sub>3</sub> Hot-Pressed at 900°C and 4500 psi for 3 hr, Showing Large Graphite Inclusions . . . . .	7-23
13	Ultimate Flexural Strength versus Wt % Carbon for TiC Alloys . . . . .	7-29
14	Ultimate Compressive Strength versus Wt % Carbon for TiC Alloys . . . . .	7-30
15	Elastic Modulus versus Wt % Carbon for TiC Alloys . . . . .	7-31
16	Slightly Hyperstoichiometric Material Showing Granular Structure . . . . .	7-32
17	Hyperstoichiometric TiC Showing Distinct As-Cast Columnar Structure . . . . .	7-32
18	Hyperstoichiometric TiC Showing the Free Flake Graphite Within the Matrix . . . . .	7-32
19	Microstructure of Hyperstoichiometric TiC Showing Essentially Pure TiC in Outer Chill Zone . . . . .	7-33

20	Microstructure of Hyperstoichiometric TiC Showing Fine Lamellar Eutectiv in a Matrix of TiC . . . . .	7-33
21	Microstructure of Hyperstoichiometric TiC Showing Free Graphite Flakes in a Matrix of TiC-C Eutectic . . . . .	7-33
22	Ram Motion versus Time for Hot-Pressed NaCl at 200°C . . . . .	7-36
23	Ram Motion versus Time for Hot-Pressed NaCl at 249°C . . . . .	7-36
24	Ram Motion versus Time for Hot-Pressed NaCl at 297°C . . . . .	7-37

TABLES

1	Data for Five Grades of Tungsten Powder Hot-Pressed for Two Hours at 5000 psi in Graphite Dies . . . . .	7-5
2	Data for Type 304 Stainless Steel Either Hot- or Cold- Pressed and Sintered for One Hour at Indicated Temperatures . .	7-20
3	Variance in wt % Carbon from Starting (Nominal) Composition to that Analyzed in the Final Casting . . . . .	7-28
4	Densities of Hot-Pressed NaCl . . . . .	7-38

## VII. METALLURGY AND CERAMICS RESEARCH

### A. INTRODUCTION

The Metallurgy and Ceramics Research program became a fully unified and integrated program during the past fiscal year. In the previous fiscal year this program was represented by three separate programs, namely, the Applied Metallurgy Research program, the Applied Ceramics Research program, and the Beryllium-Containing Materials Research program. Because of their common interest and similarity in goals and objectives, these three programs were integrated for optimization of technical direction and laboratory operation.

The Metallurgy and Ceramics Research program's primary objective is to conduct basic and applied research in the field of refractory materials. The materials of interest fall into five main classes, specifically, the refractory metals, carbides, oxides, borides, and beryllides. Within these classes of materials, significant problem areas have been delineated and are being studied. The research activity may be summarized as follows:

- 1) Within the refractory metal field, attention is being given to the development of tungsten-base alloys through the mechanism of dispersion-strengthening for high-temperature structural use to temperatures of 3000°C.
- 2) Within the area of refractory carbides, the titanium-carbon system is being investigated for the preparation and fabrication of TiC-base alloys which may be useful as solid propellant rocket nozzle materials as well as have re-entry applications.
- 3) Within the area of high-temperature oxides, attention is being given to the problem of thermal shock through investigations into prestressed ceramics.

### B. REFRACTORY METALS

#### 1. Background

The research effort in refractory metals is directed to the development of high-strength materials useful at the elevated temperatures characteristic

of current and future missile systems. Work has been initiated to improve substantially the strength of promising alloy systems at temperatures approaching their melting points. To increase strength at these temperatures, dispersion-strengthening (i. e. , incorporation of a finely dispersed inert second phase) offers the greatest potential.

Two different methods of achieving the fine uniform dispersion required are currently being employed:

- a) mechanical mixing of the powdered materials
- b) internal oxidation of a finely divided alloy

To date, nearly all of the effort has gone into developing means of handling, mixing, and consolidating the ultrafine powders involved.

Basically, the major effort involves tungsten. However, some studies have been carried out on stainless steel. These pilot studies were initiated at a time when laboratory facilities for handling tungsten were not available. In addition, preliminary studies on internal oxidation were carried out on the columbium-hafnium systems, with the hafnium being oxidized. Future studies on internal oxidation will be done in the tungsten-hafnium system.

Both hot- and cold-pressing and sintering were investigated for fabrication of dispersion-hardened tungsten. Some work was carried out on pure tungsten to optimize processing variables and to provide samples for comparison during subsequent evaluation.

When mechanical properties are being determined, a careful analysis will be necessary to correlate microstructural characteristics with the test data. This should not only delineate the proper course for further improvement but also add significantly to the somewhat nebulous theory of dispersion-hardening.

## 2. Tungsten, Hot-Pressed

A study of the feasibility of hot-pressing 3/4-in. bars from tungsten powder has been carried out on five different grades of tungsten powder. Three

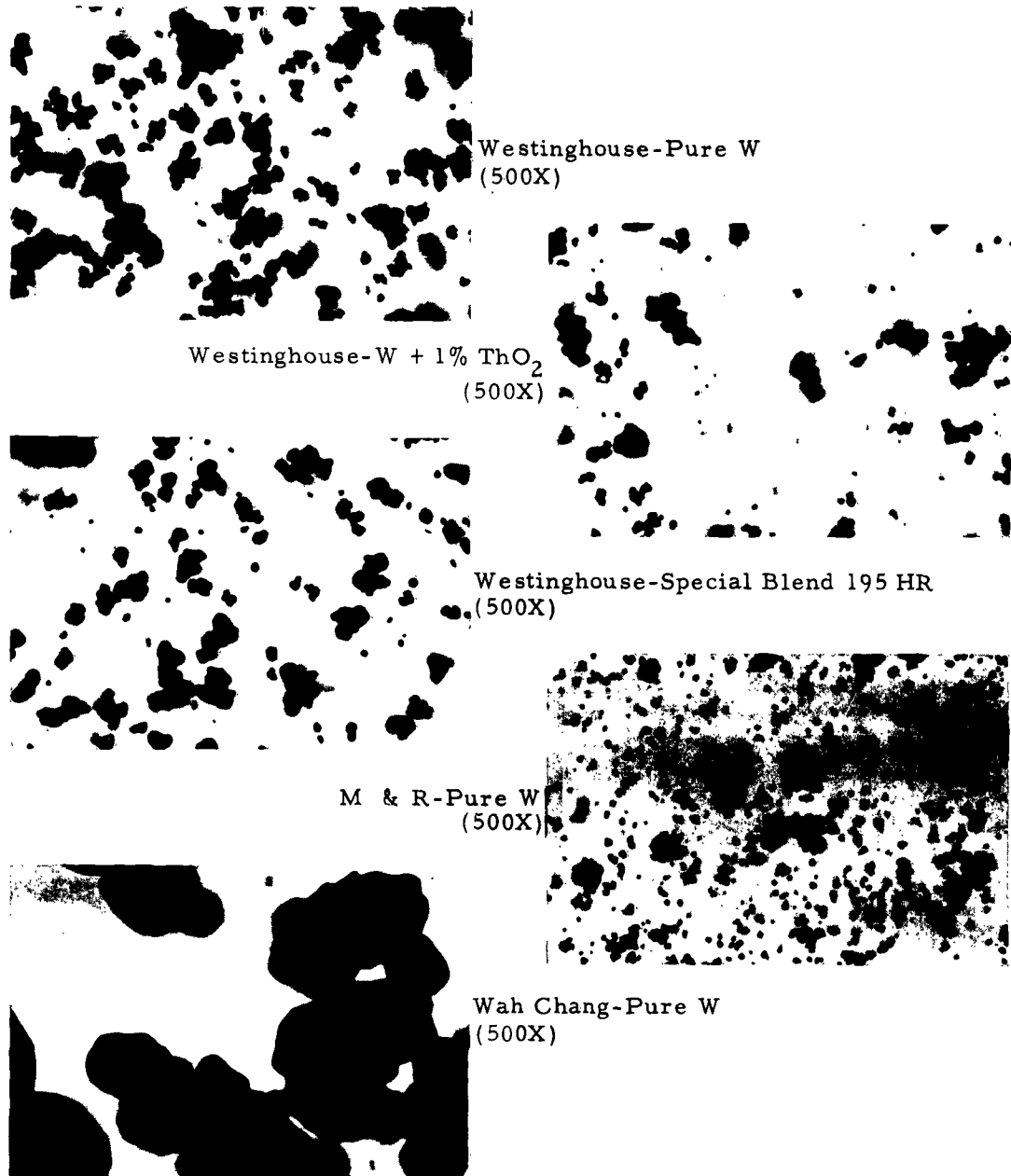


Figure 1. Tungsten Powders Used in Hot-Pressing Studies

grades were supplied by the Westinghouse Corporation, and one each by the Wah Chang Corporation and the M & R Refractory Metals Corporation. Photomicrographs of these powders appear in Fig. 1.

Forming was accomplished by first cold-compacting the tungsten powder at 36,000 psi to 3/4-in. diam pellets, approximately 1/2 in. long. The prestressed pellets were then loaded into split graphite dies. With the use of thin graphite spacers, as many as five pellets could be hot-pressed at one time. Pressure was either applied after reaching temperature or applied slowly as the dies were heated by induction; thus we attained full pressure of 5000 psi a few hundred degrees centigrade below the maximum holding temperature. Pressing temperatures ranged from 1400°C-1780°C at a constant pressure of 5000 psi. Holding time was generally two hours, with one run as short as 10 min at maximum temperature. Slow-cooling under pressure tends to add to the effective time at temperature.

Pressing in graphite dies results in the formation of a carbide case on the surface of the tungsten. This case is composed of both WC and W<sub>2</sub>C, with WC being the outermost layer. The depth of this layer varies with particle size and temperature as shown in Table 1. The sharp delineation after an electrolytic etch with 8 percent NaOH as well as the influence of particle size on the characteristics of the carbide case is shown in Fig. 2.

In general, the hardness and density presented in Table 1 increases with hot-pressing temperature. A notable exception is the apparent decrease in hardness and density at 1780°C. Conceivably, this could have resulted from pressure being applied after the hot-pressing temperature is reached. Prior to the application of pressure, a significant amount of presintering may have occurred which could hinder the subsequent pressure-induced plastic flow.

Initial particle size appears to be a rather critical factor in densification over this temperature range as shown by the poor results on the 10-40 μ size powder. For the finer powder size, a temperature of about 1525°C

Table 1. Data for Five Grades of Tungsten Powder Hot-Pressed for Two Hours at 5000 psi in Graphite Dies

Composition	Particle Size ( $\mu$ )	Hot-Pressed Temperature ( $^{\circ}$ C)	Carbide Case Depth (in.)	Hardness ( $K_{500}$ )	% Theoretical Density	Remarks
Pure W*	2-8	1780	0.013	321	89.2	Prestressed- 36,000 psi Green density- 57%
	2-8	1700	0.006	406	92.8	
	2-8	1600	0.006	354	87.0	
	2-8	1525	0.007	321	87.8	
	2-8	1460	0.007	293	82.5	
W (195-HR)*	2-8	1400	0.009	142	65.0	Prestressed- 36,000 psi Green density- 59.5%
	2-8	1780	0.020	325	87.0	
	2-8	1700	0.012	310	88.2	
	2-8	1525	0.011	306	87.8	
	2-8	1460	0.013	202	71.4	
W + 1% ThO <sub>2</sub> *	2-8	1400	0.006	87	61.2	Prestressed- 36,000 psi Green density- 55%
	2-8	1780	0.015	458	94.1	
	2-8	1700	0.010	463	97.1	
	2-8	1460	0.009	354	79.4	
	2-8	1400	0.008	109	60.7	
Pure W**	1-2	1780	0.018	241	80.0	Prestressed 36,000 psi Green density- 53%
	1-2	1700	0.010	329	88.4	
	1-2	1525	0.006	356	90.0	
Pure W***	10-40	1780	0.040	103	73.2	Prestressed- 45,000 psi Green density- 62.8%
	10-40	1700	0.024	144	70.6	
	10-40	1525	0.012	176	74.6	
	10-40	1460	0.013	100	71.0	
	10-40	1400	0.012	98	66.0	

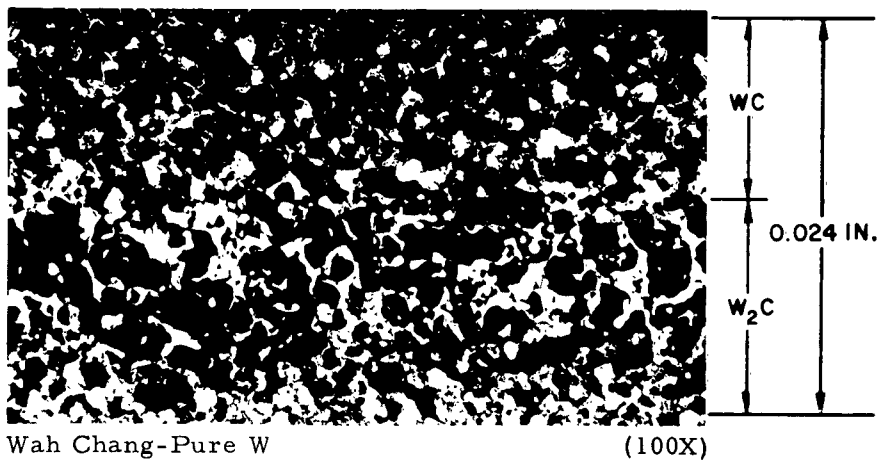
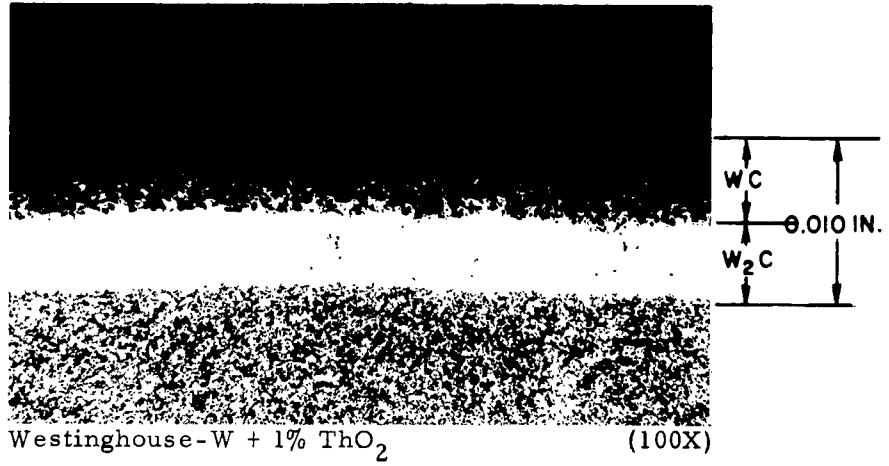
\* Westinghouse Corporation

Holding time = 10 minutes

\*\* M R Refractory Metals

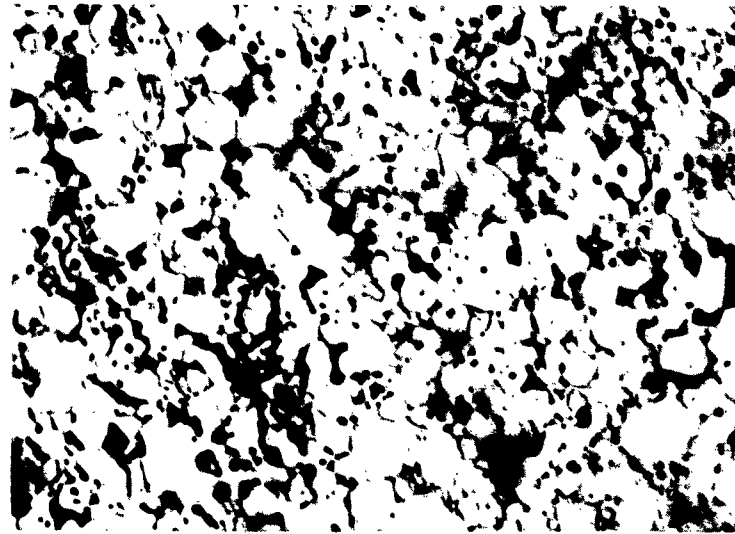
Pressure applied after reaching temperature

\*\*\* Wah Chang Corporation



Hot-Pressed 2 hr at 1700°C Etched with 8% NaOH Electrolytic

Figure 2. Typical Carbide Case Resulting from Hot-Pressing Tungsten Powders



Hot-Pressed 2 hr at 1400°C,  $\rho = 65\%$  TD (2000X)



Hot-Pressed 2 hr at 1780°C,  $\rho = 89.2\%$  TD (2000X)

Etched with 8% NaOH Electrolytic

Figure 3. Variation in Porosity and Grain Growth in Hot-Pressed Tungsten

was necessary to achieve final densities on the order of 90 percent. From the limited data, it seems that there is little advantage in holding temperature and pressure beyond approximately 10 min. The 2-hr holding periods, even at higher temperatures, resulted in very little more densification than the samples held 10 min at 1525°C.

Typical photomicrographs of the hot-pressed samples are shown in Fig. 3. Here the extremes in temperature of 1400°C and 1780°C result in a wide variation in void content. Poor densification and almost complete preservation of the initial powder grains at 1400°C is contrasted with low porosity and considerable grain growth obtained at 1780°C.

Hardness measurements, where the impression is large enough to cover several grains, correlate very nicely with density, as shown by the plot in Fig. 4. This relationship allows a quick and easy estimate of the density range in question by taking a few hardness readings across the specimen.

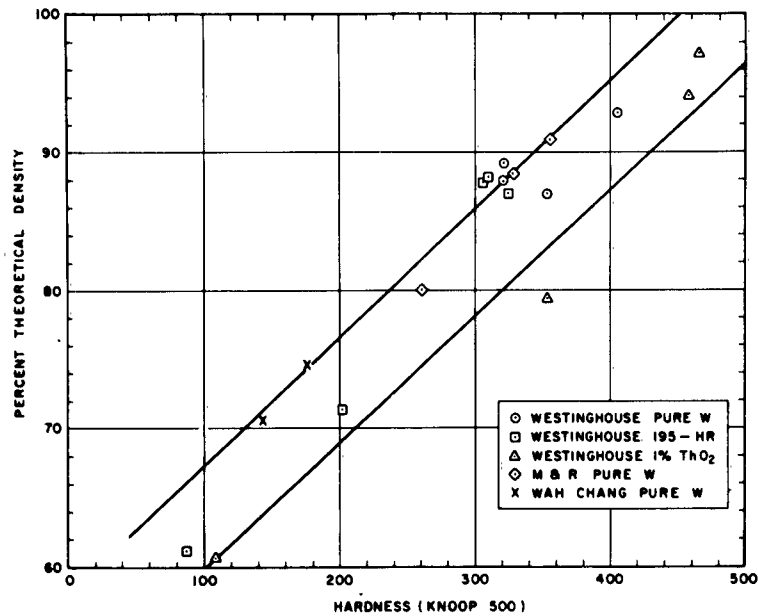


Figure 4. Hardness versus Density of Hot-Pressed Tungsten

### 3. Tungsten, Cold-Pressed and Sintered

Although the results of the hot-pressing studies have been very encouraging, cold-pressing and sintering are also being evaluated as an important means of consolidating tungsten powder. This method offers several advantages over hot-pressing in that no carbide case or carbon contamination is obtained, and a variety of atmospheres including hydrogen and vacuum can be used to effect purification during sintering. The difficulty in obtaining crack- or lamination-free cold-pressed parts and the high temperatures required for sintering are the major disadvantages.

Two grades of fine pure tungsten powder are being used for the initial evaluation: a 1-2  $\mu$  particle size obtained from the M & R Refractory Metals Co., and a 0.1-0.01  $\mu$  particle size from the Union Carbide Metals Corporation. Preliminary data on hydrogen sintering at 1800°C indicate that densities above 95 percent of theoretical can be obtained with these fine powders. Future work includes vacuum-sintering.

Mixing of fine tungsten powders with MgO by mechanical means to achieve an optimum dispersion is also being evaluated through hydrogen-sintering of the cold-pressed M & R and Union Carbide tungsten powders. A tumbling-mixing technique was found to give rather poor distribution due to agglomeration of the MgO. Mixing with a high-speed rotary blender results in a much better dispersion, but more work is necessary to work out blending times and speeds and to eliminate water vapor and static electricity which promote agglomeration.

### 4. Thoriated Tungsten Minor Phase Identification

Phase-identification studies were undertaken on material obtained from the Westinghouse Corporation in an attempt to explain the high-temperature strengthening mechanism operating in thoriated tungsten (W + 2% ThO<sub>2</sub>). The material included tensile specimens that had been tested to fracture

at 3000°F and a sample of the original thoriated tungsten powder for comparison purposes. Photo micrographs (Fig. 5) show the appearance of the tungsten sample; Fig. 1 shows an example of W + 1% ThO<sub>2</sub> powder.

By dissolving the tungsten matrix away from the nonmetallic secondary phases with 75% HNO<sub>3</sub>-12% HF-13% H<sub>2</sub>O, we obtained extracts for x-ray identification. X-ray patterns of the residues from both the tested samples and the starting powder showed evidence of ThO<sub>2</sub> only. However, the x-ray patterns showed that the crystalline perfection of the ThO<sub>2</sub> in the tested samples was much better than in the starting powder. This indicates that exposure to 2800°C during fabrication resulted in considerable perfection of the ThO<sub>2</sub> lattice, which had apparently undergone significant disregistry during synthesis of the original powder.

Because an increase in lattice perfection could be the result of solution and reprecipitation resulting in agglomeration of the ThO<sub>2</sub> particles, the higher magnifications of the electron microscope were necessary to disclose any change in size, shape, or distribution of the particles. Using carbon replicas of the sample surface, which gave good resolution up to 60,000X magnification, we observed no ThO<sub>2</sub> particles greater than 1.0 μ in major dimension. Since this is the approximate size of the initial powder, it is believed that the difference in x-ray patterns was not due to solution and reprecipitation during preparation or testing of the samples.

At the magnifications obtained with the electron microscope, an additional phase was observed with a particle size of 0.1 μ (Fig. 5). These particles were too fine to give an x-ray diffraction pattern, therefore identification was accomplished by electron diffraction using carbon extraction replicas. Several very good patterns were obtained from these particles, which were identified as being characteristic of W<sub>2</sub>C. The particle size, shape, and distribution of this phase is fine enough to contribute to high-temperature strength. Before definite conclusions can be drawn, however, the solution temperature of this phase, as well as the conditions under which precipitation takes place, must be determined.



Sintered 1 hr at 1300°C, Yield Stress-23,000 psi, 5% Elongation  
473 K<sub>500</sub>, Etched with 8% NaOH Electrolytic

Figure 5. Thoria-tungsten Samples Sintered at 2800°C and Hot-Extruded prior to Tensile Testing at 1650°C in Vacuum

## 5. Internal Oxidation Alloys

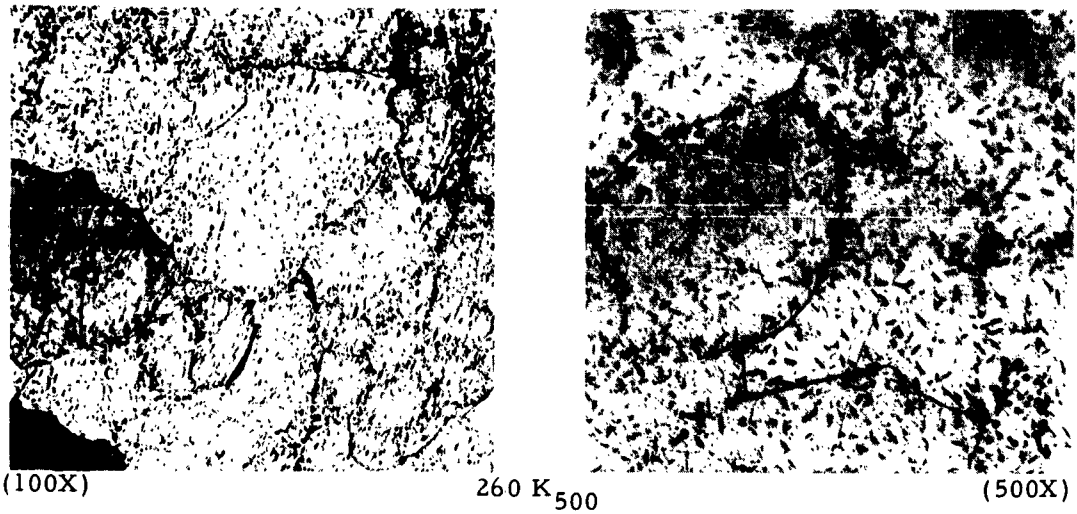
Dispersion-hardening through internal oxidation requires that one component of an alloy have a much higher oxidation potential than the other. When the alloy is doped with oxygen, the metal with greatest oxygen affinity will become oxidized while the other remains metallic. Under the proper conditions, a very fine oxide dispersion can be obtained. Of the refractory metals, two alloy systems (Cb-Hf and W-Hf, where Hf is the element with high oxidation potential) have been selected as offering the greatest potential.

In the absence of high vacuum-melting facilities, a Cb-5 wt % Hf alloy was prepared by arc-melting under argon. Although considerable oxide formation occurred during melting, work was conducted on this alloy to determine workability, recrystallization, and oxide stability characteristics.

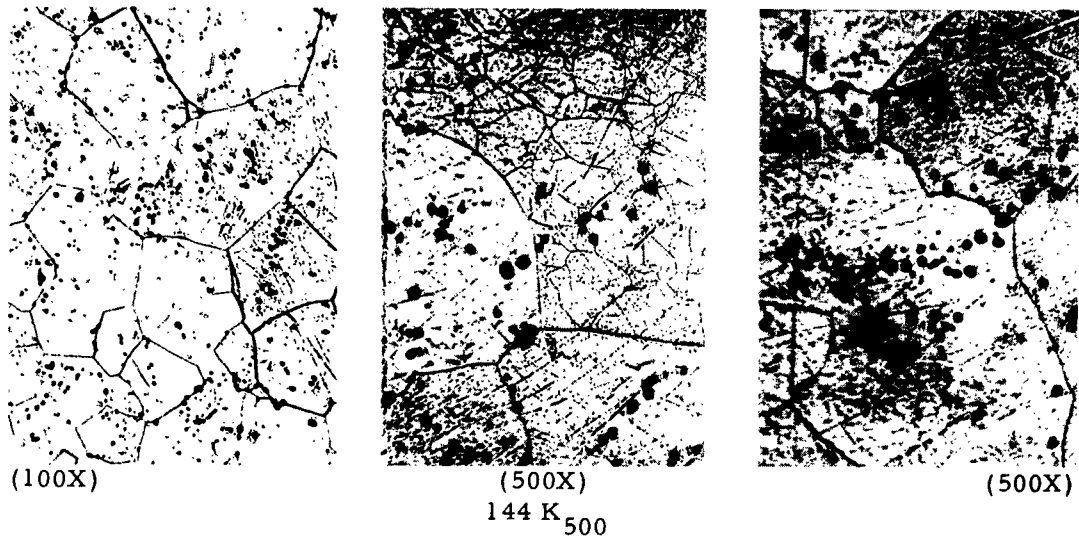
The structure and hardness of the alloy as melted appears in Fig. 6a. Analysis of this alloy with an electron micro probe x-ray analyzer showed that both of the two kinds of precipitate contained more Hf than the matrix. The large round particles had more Hf than the needle-like particles. X-ray patterns of residues from acid extraction showed evidence of only  $\text{HfO}_2$ . A vacuum anneal of one hour at  $2150^\circ\text{C}$  resulted in an equiaxed grain structure as well as solution of the needle-like particles. The microstructure in Fig. 6b also shows a slight increase in size of the round black particles, indicating that  $\text{HfO}_2$  is becoming somewhat unstable at  $2150^\circ\text{C}$ .

The alloy was quite malleable in that it was cold rolled from  $3/8$  in. to 0.016 in. with edge-cracking occurring only early in the deformation. Microstructures of this material as-rolled and after a subsequent treatment of one hour at  $2150^\circ\text{C}$  in vacuum are presented in Fig. 7.

The hardness values are also presented in these figures to give an indication of the work-hardening, recrystallization, and purification during the vacuum anneal at  $2150^\circ\text{C}$ . The high hardness of the starting material,  $260 K_{500}$ , is



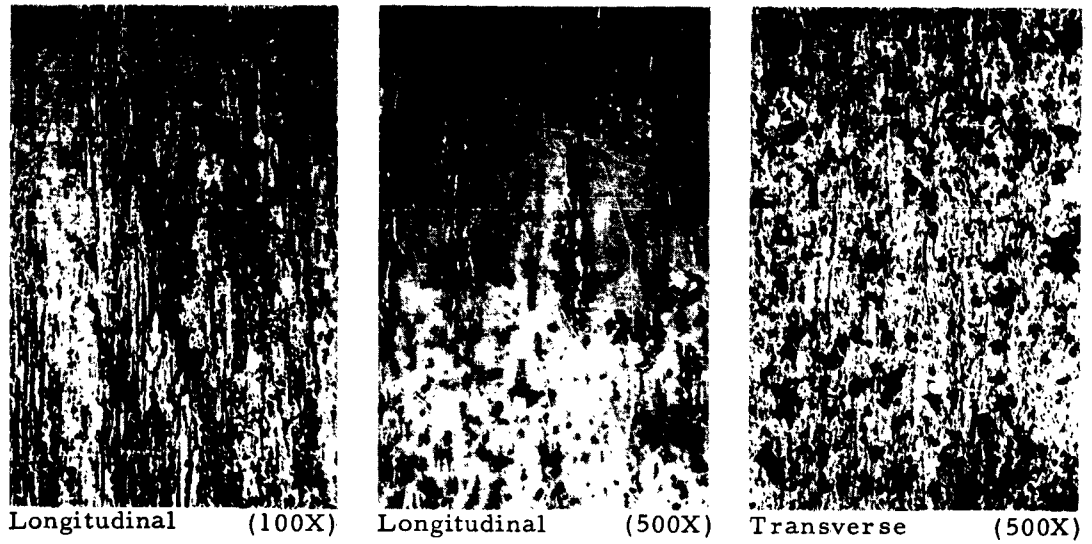
(a) Arc-Melted in Argon Atmosphere



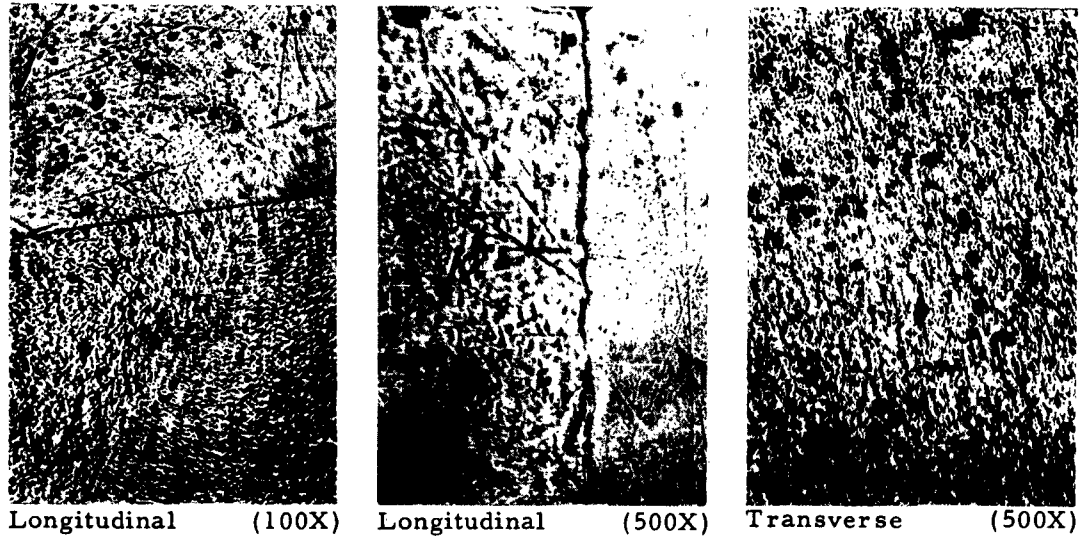
(b) Vacuum-Annealed 1 hr at 2150°C

Etched with 5 parts  $H_2SO_4$ , 2 parts HF, 2 parts  $HNO_3$

Figure 6. Columbium + 5 Wt % Hafnium Alloy



(a) As-Rolled



(b) Vacuum-Annealed 1 hr at 2150°C

Etched with 5 parts  $H_2SO_4$ , 2 parts HF, 2 parts  $HNO_3$

Figure 7. Columbium + 5 Wt % Hafnium Alloy

indicative of high interstitial impurities, primarily oxygen. The rolled sheet work-hardened very little, if any, during the drastic cold reduction. The loss of oxygen during the vacuum anneal caused the hardness to drop to 144 K<sub>500</sub> in the annealed condition. Extensive recrystallization and grain growth caused a further drop to 136 K<sub>500</sub> after the cold-worked sheet was vacuum-annealed.

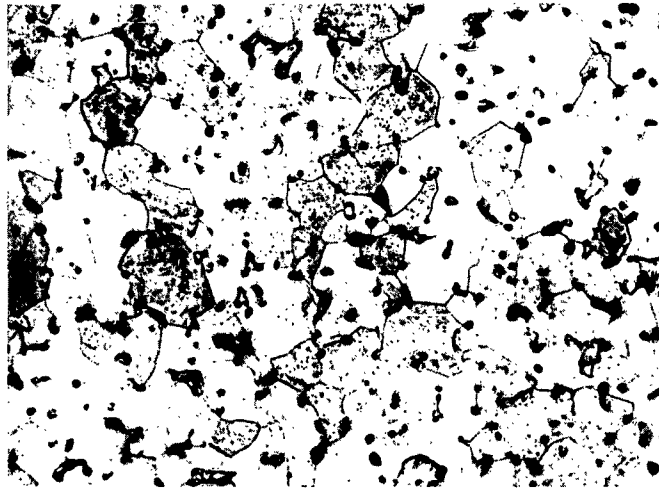
Because internal oxidation studies will involve oxygen-doping of alloy powders, the pressing and sintering of columbium powder was evaluated. Pure Cb powder (-325 mesh) yielded a density of 91 percent of theoretical by cold-pressing at 56,000 psi and vacuum-sintering 1 hr at 2150°C. The microstructure of the pressed and sintered material appears in Fig. 8.

Since oxygen can be removed from columbium at these temperatures in vacuum, a hardness traverse was made to check the depth of purification in this pellet. The hardness values showed a uniform hardness range from about 100 K<sub>500</sub> at the surface to a value of 150 at the center of the 3/4-in. pellet.

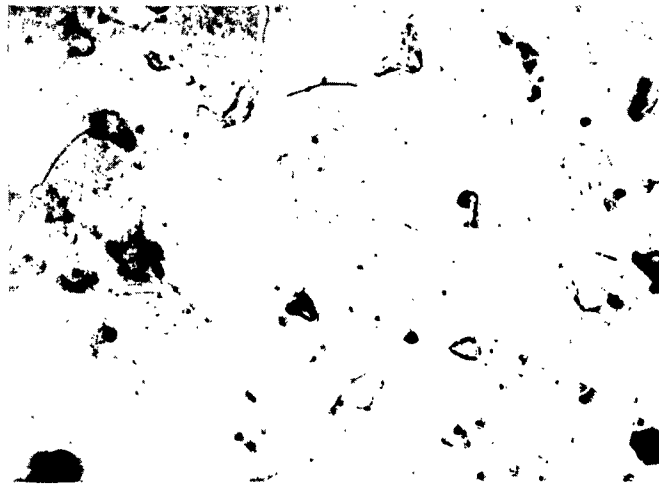
Future work in the area of internal oxidation will be conducted on Cb-Hf and W-Hf alloys melted under a vacuum of  $10^{-5}$  torr or more. The ingot will be comminuted to powder finer than 40  $\mu$  and doped with oxygen to form HfO<sub>2</sub> internally. The powder will be either hydrogen- or vacuum-annealed to remove excess oxygen from solution. The possibility of nitrogen-doping to form HfN will also be investigated. Final consolidation will be conducted according to powder methods previously evaluated.

#### 6. Dispersion-Hardening, Type 304 Stainless Steel

Powder consolidation methods have been developed to facilitate dispersion-strengthening of austenitic stainless steel by a mechanical blending with such refractory materials as Al<sub>2</sub>O<sub>3</sub> and MgO. The study has included several methods of cold-pressing and sintering as well as hot-pressing of 3/4-in. diam pellets. Different means of mixing the powders to achieve optimum



(100X)



(500X)

Etched with 5  
parts  $H_2SO_4$ ,  
2 parts HF,  
2 parts  $HNO_3$

Hardness: surface-100  $K_{500}$ , center-150  $K_{500}$

Figure 8. Pure Columbium Cold-Pressed and Vacuum Sintered  
1 hr at  $2150^{\circ}C$

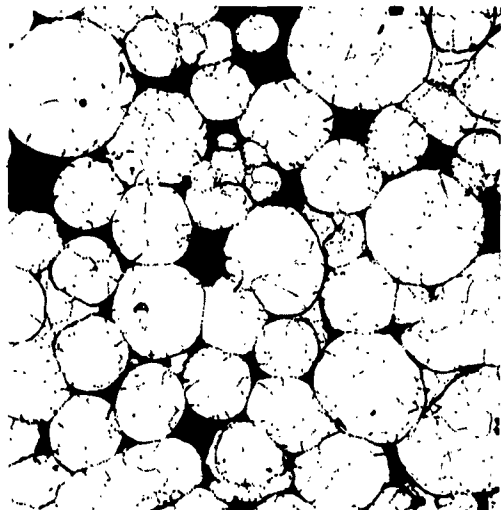
dispersion of the refractory second phase have been tried. Fabricability of selected alloys by either hot- or cold-rolling has also been checked.

Initial cold-pressing was conducted on rather coarse material (-100 + 270 mesh, i. e. , 70-200  $\mu$ ) over the range of 60,000-140,000 psi. A considerable amount of force was required to remove the pellets from the cold-press dies, which made it necessary to use a binder material to obtain sound parts. After removing the binder, the pellets were sintered in argon for 1 hr at 1200 or 1300°C. Microstructures of these samples appear in Figs. 9 and 10. Tabulated density and hardness data are presented in Table 2. From Fig. 9, it is apparent that good compaction accompanied by some deformation of the powder particles is obtained at or above 100,000 psi.

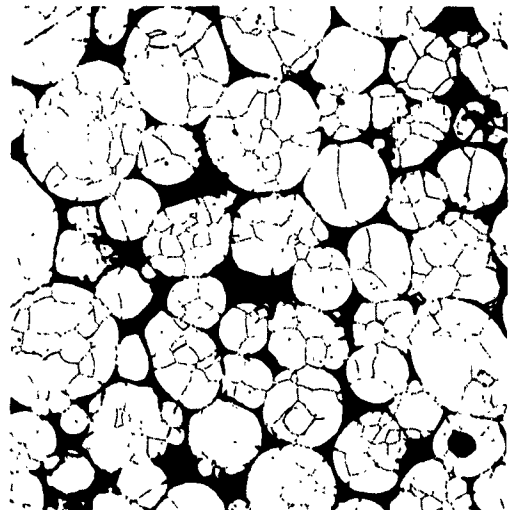
The density range of 80-88 percent is not extremely good; however, adequate sintering had occurred at the lowest sintering temperature of 1200°C shown by good interparticle bonding and the cold workability of these samples by rolling. Cold-rolling 30 percent with flat rolls, which resulted in surprisingly little edge-cracking, increased the density of all samples above 90 percent. A subsequent anneal for 1 hr in argon at 1100°C increased the density to 95 percent and accomplished recrystallization throughout the samples. This indicates that good densities can be obtained by a series of working and annealing steps from parts having initially an 80 percent density.

The rather high hardnesses reported in Table 2 are somewhat misleading in that they are micro-measurements (from an outside firm) made entirely in the large initial particles; they are certainly not indicative of the bulk material containing up to 20 percent voids.

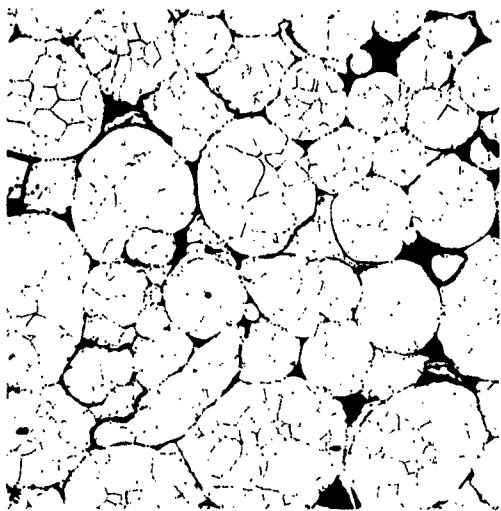
To avoid using a binder during cold-pressing, we used finer powders. Compaction was accomplished through the use of a split die or isostatic pressing, facilitating removal of the part after pressing. Although the maximum pressure on the isostatic press was only 18,000 psi, two good



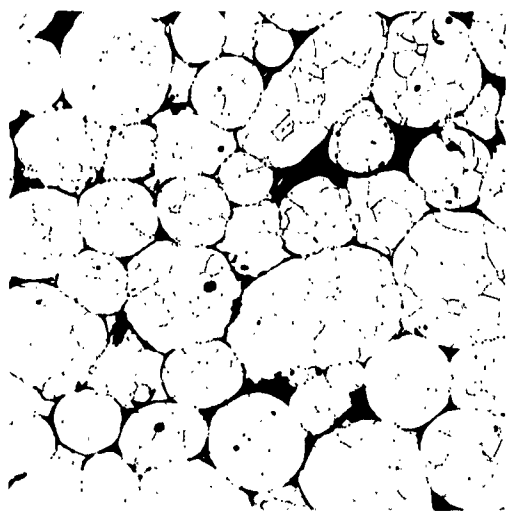
80,000 psi



100,000 psi,  $\rho = 85.3\%$  TD



120,000 psi,  $\rho = 87.9\%$  TD

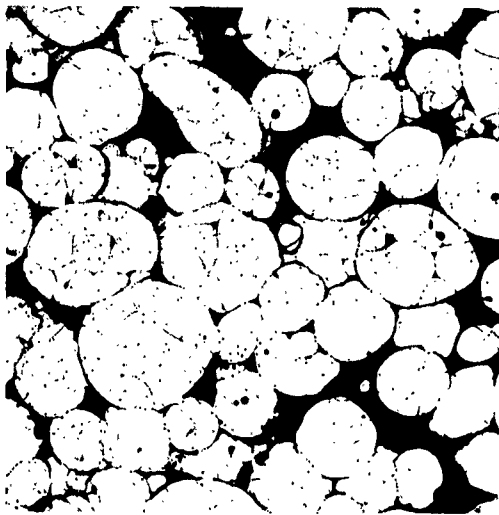


140,000 psi,  $\rho = 87.6\%$  TD

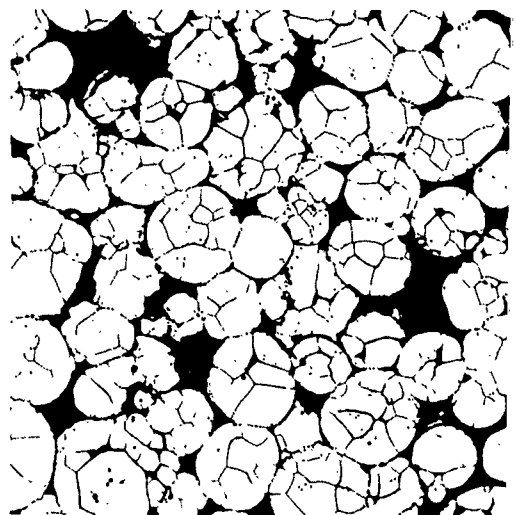
Etched with 68%  $\text{HNO}_3$  Electrolytic

Sintered 1 hr at  $1200^\circ\text{C}$  (150X)

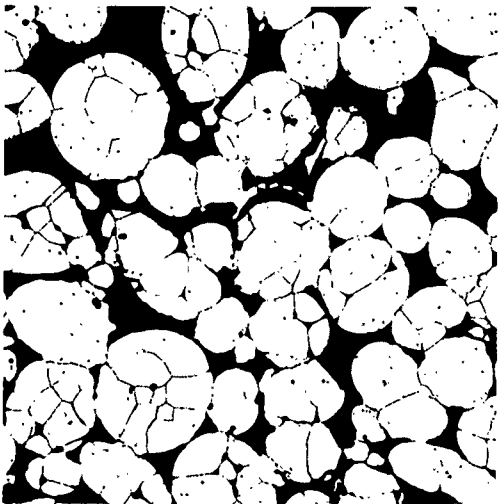
Figure 9. Stainless Steel Cold-Pressed and Sintered, Type 304



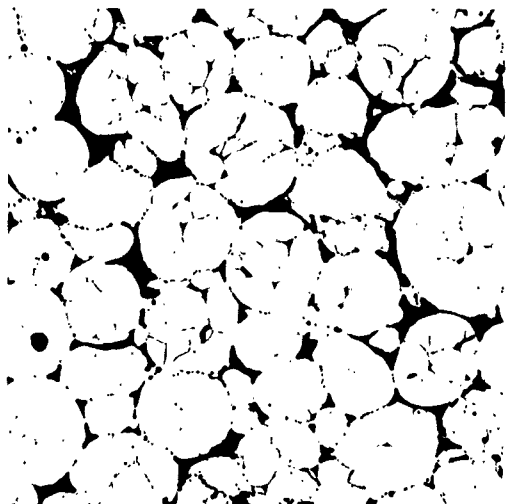
60,000 psi,  $\rho = 80.6\%$  TD



80,000 psi,  $\rho = 82.5\%$  TD



100,000 psi,  $\rho = 83.8\%$  TD



120,000 psi,  $\rho = 86.6\%$  TD

Etched with 68%  $\text{HNO}_3$  Electrolytic

Sintered 1 hr at 1300°C (150X)

Figure 10. Stainless Steel Cold-Pressed and Sintered, Type 304

Table 2. Data for Type 304 Stainless Steel Either Hot- or Cold-Pressed and Sintered for One Hour at Indicated Temperatures

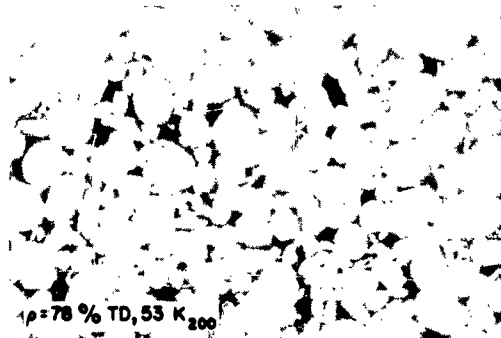
Particle Size and Composition	Pressing Conditions (psi)	Sintering Temperature (°C)	Final Density (% Theor.)	Hardness (K <sub>500</sub> )	Remarks	
-100 + 270 mesh	80,000	1200	85.3	188	Nopco binder CD-108 used during cold-pressing, burned out in 1 hr at 425°C. Sintered in argon.	
-100 + 270 mesh	100,000	1200	87.9	181		
-100 + 270 mesh	120,000	1200	87.6	185		
-100 + 270 mesh	140,000	1200	80.6	199		
-100 + 270 mesh	60,000	1300	82.5	181		
-100 + 270 mesh	80,000	1300	83.8	188		
-100 + 270 mesh	100,000	1300	86.6	184		
-100 + 270 mesh	120,000	1300		175		
-325 Mesh	18,000	1250	83.0	--	Isostatic pressing; Sintered in argon.	
-325 Mesh + 2.5 % Al <sub>2</sub> O <sub>3</sub>	18,000	1250	93.5	--		
-325 Mesh	60,000	1110	78.0	53	Sintered in hydrogen.	
-325 Mesh	60,000	1225	78.5	58		
-325 Mesh hydrogen cleaned 1 hour at 850°C	60,000	1110	83.4	75		
-325 Mesh hydrogen cleaned 1 hour at 850°C	60,000	1225	88.6	78		
-325 + 2.5 % Al <sub>2</sub> O <sub>3</sub>	60,000	1110	86.0	74		
-325 + 2.5 % Al <sub>2</sub> O <sub>3</sub>	60,000	1225	90.2	50		
-100 + 270 mesh	4500-900°C	--	82.0	--		Hot-pressed in graphite for 3 hr.
-325 Mesh + 2.5% Al <sub>2</sub> O <sub>3</sub>	4500-900°C	--	80.6	--		

pellets were obtained from -325 powder, one of which contained 2.5 wt %  $\text{Al}_2\text{O}_3$ . While pressing the third pellet, the press experienced a failure of the sealing cap, thus halting abruptly this phase of the investigation. This effort will continue when the press is again working. The density of the two pellets sintered in argon at  $1250^\circ\text{C}$  was quite good, indicating that this method may be very useful.

Pressing -325 mesh stainless steel powder in a two-way split die still results in the tendency of the pellet to split or crack when being removed from the die. However, cleaning the powder in hydrogen for one hour at  $850^\circ\text{C}$  increases the pressability so that sound pellets can be obtained. To evaluate the influence of conducting the final sintering operation in hydrogen, we pressed a series of pellets from the -325 mesh powder at 60,000 psi in the split dies. The three conditions used were: without the hydrogen cleaning operation, with the hydrogen cleaning operation, and the uncleaned powder plus 2.5 wt %  $\text{Al}_2\text{O}_3$ . The hardness and density measurements of these samples sintered for one hour in hydrogen at  $1110^\circ\text{C}$  or  $1225^\circ\text{C}$  are presented in Table 2. It is apparent that the hydrogen precleaning has increased the properties significantly; however, the properties resulting from sintering in hydrogen do not appear significantly better than those resulting from sintering in argon. The addition of  $\text{Al}_2\text{O}_3$  results in a considerable increase in density by filling up interparticle areas that are voids in the pure stainless. Microstructures of these materials showing the superior interparticle bonding of the hydrogen-cleaned material as well as the  $\text{Al}_2\text{O}_3$  distribution appear in Fig. 11.

While the pure stainless sintered compacts were cold-worked without difficulty, the addition of  $\text{Al}_2\text{O}_3$  made even hot-working at  $1000^\circ\text{C}$  in the flat rolls very difficult because of extreme cracking. The  $\text{Al}_2\text{O}_3$  distribution shown in Fig. 11 explains this behavior. The complete  $\text{Al}_2\text{O}_3$  network around the stainless steel particles allows very little interparticle bonding

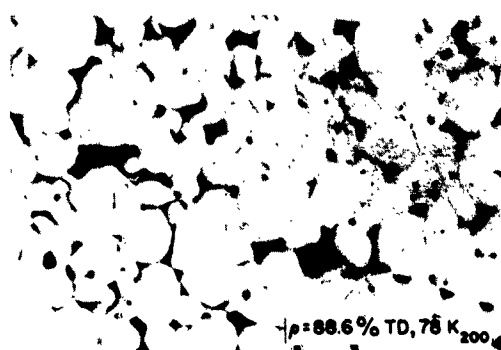
a) Hydrogen-Sintered 1 hr at 1110°C



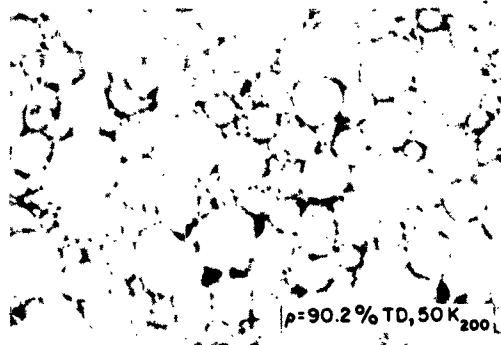
b) Hydrogen-Sintered 1 hr at 1225°C



As-Pressed and Sintered



Powder Precleaned in Hydrogen 1 hr at 850°C

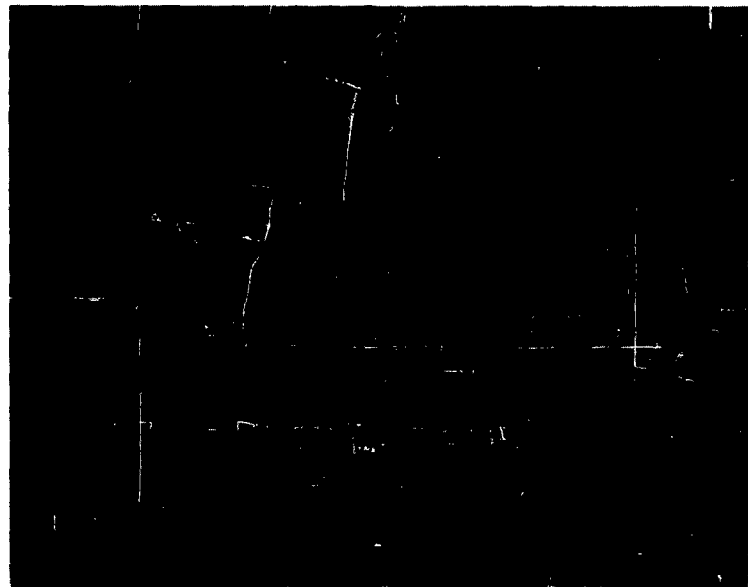


Plus 2.5 wt % Al<sub>2</sub>O<sub>3</sub>

Figure 11. Stainless Steel Cold-Pressed after Hydrogen Treatment and Additions of Al<sub>2</sub>O<sub>3</sub>

so that internal cracking is very prevalent even at low strains. This network must be broken up by hot-extrusion or swaging with a restraining can to achieve complete densification and optimum second-phase dispersion.

Hot-pressing was investigated as a possible means of consolidating the operation as well as keeping the temperature low enough so agglomeration or phase-changes in the second-phase material would be minimized. Powder was poured into closed 3/4-in. graphite dies and pressure applied gradually as the temperature was increased. This reached 4500 psi before the holding temperature of 900°C. After 3 hr, the pressure was released and the power turned off to allow the sample to cool slowly. A protective argon atmosphere was maintained at all times.



Unetched

250X

Figure 12. -325 Mesh Type 304 Stainless Steel+ 2.5 wt %  $\text{Al}_2\text{O}_3$  Hot-Pressed at 900°C and 4500 psi for 3 hr, Showing Large Graphite Inclusions

Two varieties of stainless steel powder were used: a coarse -100 + 270 mesh powder and a -325 mesh powder + 2.5 wt %  $\text{Al}_2\text{O}_3$ . The final densities obtained (approximately 80 percent of theoretical) were somewhat lower than expected. Although the microstructures generally looked very good, a considerable amount of large gray inclusion particles (found to be graphite) appeared (Fig. 12). The graphite, which is largely responsible for the low density, is apparently abraded from the die walls during loading or during compacting as pressure is applied. To avoid this, pellets will be cold-pressed prior to loading or compacting to minimize abrasion and ram travel.

Future work will be devoted to 1) obtaining finer starting powders by centrifugal classification or by milling and 2) upgrading the means of blending the powders.

### C. REFRACTORY CARBIDES

#### 1. Background

The refractory metal carbides, being the most refractory of all classes of materials, warrant an investigation within the scope of the metallurgy and ceramics research program aimed at improving their use for propulsion, re-entry, and spacecraft applications. A literature survey and analysis has been completed, emphasizing methods of synthesis and fabrication and subsequent determination of physical and mechanical properties. As a result of this analysis, it is quite apparent that existing data, to a large degree, have been based on material of inferior purity and density. On this basis, an investigation to determine selected mechanical and physical properties of the refractory carbides based upon high-purity, high-density material was initiated. It has been decided to synthesize the carbides by combining high-purity elemental materials. In addition, fabrication will be done in such a manner that the highest density possible results. The methods under consideration are:

- a) arc-melting and casting
- b) hot-pressing

Recent work has indicated the potential of the refractory carbides when used in conjunction with a lower modulus material. The refractory carbides suffer from poor thermal shock resistance, but when used in conjunction with a material such as graphite (which has much better thermal shock resistance), an improved material would possibly result. Another major problem concerns failure because of brittle fracture. Aerospace studies have emphasized the hyperstoichiometric region. The titanium carbon system was selected for initial studies because: a) it has the lowest melting point and, thus, fabrication problems are minimized, b) pure materials can be obtained at minimum cost, and c) studies to date in this system have been numerous, making possible data-verification of initial results.

Of possible interest in the titanium-carbon system is a reported eutectic between titanium carbide and carbon.

## 2. Synthesis and Fabrication

All alloys in this study were prepared from high-purity titanium sponge and high-purity nuclear grade graphite (grade AGOT). The titanium sponge was obtained from the Titanium Metals Corporation of America and was graded as 120 BHN material, indicating low oxygen and nitrogen content. The chief impurity listed was hydrogen, which is evolved during the vacuum-melting operation. Nuclear grade AGOT graphite is considered to be one of the highest purity graphites available and it is also extremely low in total impurities.

These raw materials were alloyed in a dc nonconsumable electrode arc furnace powered by two rectifiers capable of generating up to 3000 amp at 30 v for short periods of time. The furnace crucible, electrode tip, hearth, and molds were all fabricated from ATJ grade graphite to avoid additional contamination of the alloys. A considerable carbon increase was expected over and above the starting or nominal composition of the alloy. However, it was felt that upon establishing a routine melting and casting procedure, prediction of this increase would be possible. This prediction did not

materialize. Because of the wide liquidus-solidus gap existing in the hypostoichiometric region, these alloys exhibited poor fluidity characteristics. To produce a nearly-homogeneous bulk material, the alloys had to be re-melted many times. Additional difficulty was experienced during the drop-casting (method used for specimen preparation) because of this same sluggishness. Poor castings resulted; the material had to be re-melted and re-cast, which resulted in carbon increase.

All alloy specimens were cast to right circular cylinder shape by the drop-casting technique for property measurements. This is accomplished by melting the homogeneous bulk material in a graphite hearth sufficiently long to create a large molten pool. At the point when a casting is to be made, the power level is increased. This enables the melter to burn through the molten pool and allow a thin graphite diaphragm holding this molten pool to be dissolved. Thus, gravity allows the molten material to pour into the mold suspended below. Furnace operator technique is vital in the successful accomplishment of this operation. A large amount of miscasts are the rule rather than the exception, and a more refined method is desirable.

Future studies of this alloy system will be on materials which will be melted and cast within a vacuum skull casting furnace (not operational over the past report period, but expected to be during the next) and will circumvent the problems associated with the drop-casting technique. Alloys will be melted and cast in a single operation. This will permit accurate prediction of the final carbon content.

Also observed during the casting operation was a decrease in the arc voltage from a starting value of 26-28 v to a low of 11-13 v at the end of the cycle. High voltage could be maintained only by constantly flushing argon through and bleeding it out of the furnace chamber through the vacuum pump. Because the boiling point of titanium metal has been calculated to be approximately 3200°C (approximately 200°C higher than that of the reported melting point of pure stoichiometric titanium carbide), it is reasonable to conclude that

titanium was being boiled off during the melting operation with the appreciable superheat imparted to the carbide alloys to make casting possible. The titanium vapor would cause the arc-stabilizing atmosphere to be more electrically conductive; thus the voltage required to supply the current would decrease. This decrease in titanium from the melt would also cause the apparent increase in carbon in the finished alloy.

A tabulation of the original or nominal % carbon content as well as the final carbon content of the finished alloys is presented in Table 3. It can be noted that for starting compositions up to 26 wt.% carbon, the final casting had an increased carbon content, and that for starting compositions of from 28-32 wt % carbon, all final castings had a decreased carbon content. It is obvious from these data that it becomes increasingly more difficult to dissolve the carbon within the molten titanium carbide base material at the reduced pressures. The maximum amount of carbon that can be introduced using these selected conditions is being reached. It appears that this level is in the vicinity of 30 wt % carbon. It will be interesting to see whether or not this holds true for the skull-casting method.

Cast ingots, after removal of the sprue, were surface-ground by using diamond wheels. Specimens for metallographic examination were removed from the top and bottom of the ingots by means of an elox electrical discharge machine tool.

Machined ingots were spot-checked to determine the presence of macroscopic cracks by using a dye penetrant.

### 3. Transverse Rupture Tests

The ingots were subjected to a transverse rupture test at a strain rate of 0.02 in./min until failure. Plots of deflection versus load were obtained. The deflection was measured with a linear differential transformer positioned between the upper and lower plates. Other specimens were tested at a strain rate of 0.025 in./min until failure. Again, plots of deflection versus load

Table 3. Variance in wt % Carbon from Starting (Nominal) Composition to that Analyzed in the Final Casting

Sample No.	Nominal % Carbon	Casting Analysis % (by weight) Carbon	Change in Carbon During Casting (%)
44	1	0.48, 0.47	
45	3	0.51, 0.52	
48	3	19.80	6.2
24	14	20.18	6.1
26	16	22.11	2.6
33	20	22.57	4.0
2	19	22.95, 23.13	9.4
10	14	23.35, 23.40	2.4
13	21	23.44	7.6
30	16	23.55, 23.91	5.6
7	18	23.60	11.8
23	12	23.78	12.0
27	12	23.97	14.0
21	10	23.99	5.0
3	19	24.03, 24.26	16.1
28	8	24.12, 24.5	14.3
22	10	24.29	4.3
12	20	24.28, 24.75	6.8
32	18	24.83	4.0
34	21	24.95	-2.3
39	28	25.70	6.8
31	19	25.83	1.1
38	26	27.12	3.1
35	24	27.13	3.8
29	22	25.91, 25.80	-2.8
41	30	27.24	-1.8
40	28	26.23	-3.2
43	32	28.82	1.1
42	30	27.12	

were obtained. In this case, however, the deflection was measured by direct reading of a dial gauge. Values of ultimate flexural strength as a function of carbon content are presented in Fig.

13. As can be seen, fairly constant values ranging from 25,000-35,000 psi over a range of 20-26 wt % carbon were obtained. Above this carbon content, however, a sharp decrease in the flexural strength is exhibited with values of approximately 10,000 psi existing from 26-29 wt % carbon. These are considered to be preliminary values and further work is planned. Additional data are desirable in the stoichiometric and hypostoichiometric region. Voids existing over the total range of composition will also be filled in.

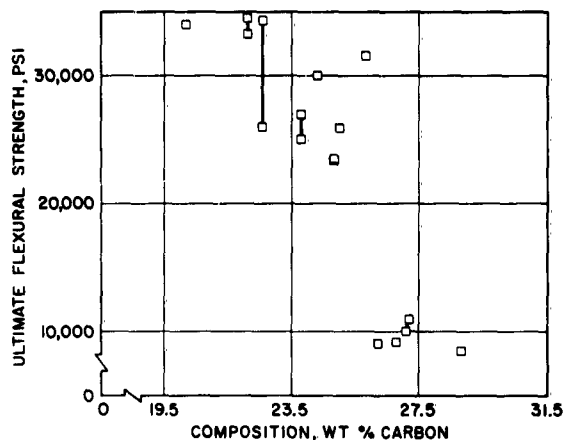


Figure 13. Ultimate Flexural Strength versus Wt % Carbon for TiC Alloys

#### 4. Compressive Strength Tests

When the transverse rupture tests were completed, the broken halves of the ingots were used for the purpose of determining the compressive strengths. These halves were machined by means of the elox electrical discharge machine to specimens having an approximate L/D ratio of 1. Care was taken to insure parallelism and perpendicularity. Early tests were made at a strain rate of 0.025 in./min until failure. Plots of deflection versus load were obtained (deflection was measured with a dial gauge). Following this, further tests were performed at a load rate of 10,000 lb/min. A stress-strain curve was established by use of an SR-4 strain gauge which was attached to the specimen parallel to the loading direction. The results of these tests are presented in Fig. 14. A constant value has been established at approximately 160,000 psi in the region of the stoichiometric TiC. This

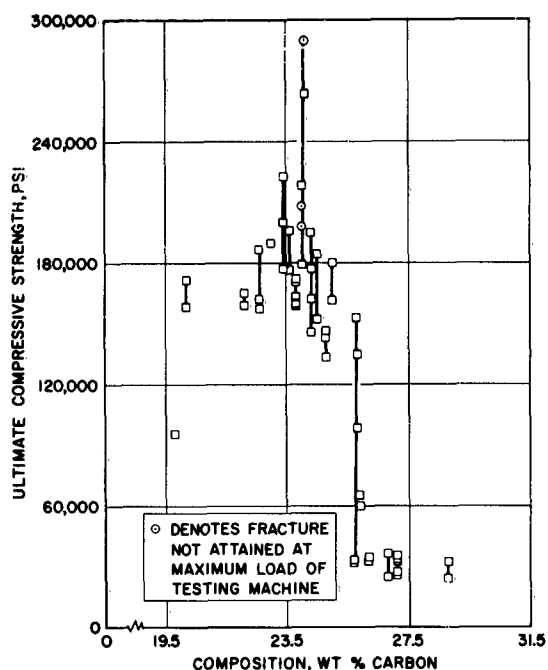


Figure 14. Ultimate Compressive Strength versus Wt % Carbon for TiC Alloys

value rises sharply and peaks in the vicinity of 300,000 psi at approximately 24 wt % carbon. It then decreases rapidly and levels off at approximately 30,000 psi above 25 wt % carbon. All values obtained from approximately 20-25 wt % carbon are considerably higher than the previously accepted value of 109,000 psi for stoichiometric TiC.

#### 5. Elastic Moduli

Figure 15 shows the elastic modulus obtained as a result of the compression tests. Values were obtained from the slope of the stress-strain curve. As can be seen, it shows a peak value at approximately 21 wt % carbon of  $69 \times 10^6$  psi.

#### 6. Hardness

Knoop hardness values were determined for the alloys over a range of carbon content. Tests on individual samples containing the TiC phase yielded  $K_{100}$  values ranging from 2390-3190. These values were for samples having a total carbon content ranging from 22.6-28.8 wt % carbon. These values agree well with those of  $K_{100}$  2470 to 3200 reported in the literature.

#### 7. Density

Densities have been determined by the displacement method for these alloys over a range of carbon content. Values range from 4.88 gm/cc for 23.4 wt % carbon to a value of 4.14 gm/cc at 26.8 wt % carbon. The theoretical

calculated value for stoichiometric 20 wt % carbon TiC is 4.92 gm/cc. Experimental values compare favorably with this value and indicate that the material in all the samples is near 100 percent theoretical density.

#### 8. Metallography

Figures 16, 17, and 18 are photomicrographs taken of the as-cast ingots at 10X original magnification after they have been subjected to the transverse rupture testing. The three structures represent different carbon contents as well as differences in structure due to freezing. As can be seen in Fig. 16 for material of 22.1 wt % carbon, a granular-type structure exists. In Fig. 17 for 25.8 wt % carbon, a distinct columnar-type structure exists. It has been determined that this structure represents that material exhibiting the highest compressive strengths. Lastly, in Fig. 18 the structure is representative of the hypereutectic-region material consisting of eutectic plus free carbon. The free carbon can readily be seen.

All samples have been examined metallographically at 100X magnification. Figures 19, 20, and 21 are representative of the microstructures existing in the titanium carbide region, the hypereutectic region, and the hypoeutectic region. Metallographic samples were prepared in the following manner: After mounting, the specimens were coarse-polished on diamond laps through 400, 600, and 1000 grit, using water as a lubricant. This was followed by a fine-polish through 8- $\mu$ , 3- $\mu$ , and 1- $\mu$  diamond paste, using metcloth. A finish polish consisted of a 0.25- $\mu$  diamond paste on microcloth. The microstructures shown are in the unetched condition. Figure 19 shows the

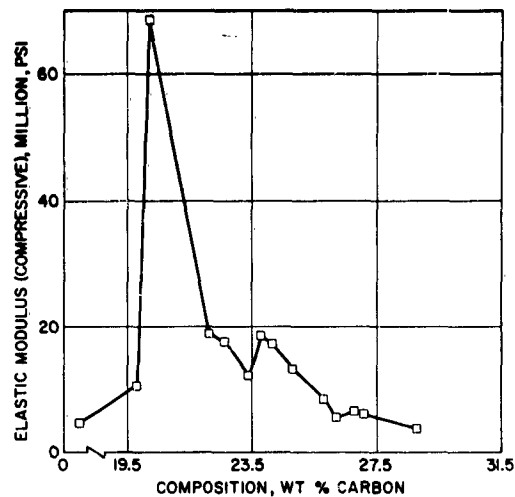


Figure 15. Elastic Modulus versus Wt % Carbon for TiC Alloys



Figure 16. Slightly Hyperstoichiometric Material Showing Granular Structure



Figure 17. Hyperstoichiometric TiC Showing Distinct As-Cast Columnar Structure



Figure 18. Hyperstoichiometric TiC Showing the Free Flake Graphite Within the Matrix



Figure 19. Microstructure of Hyperstoichiometric TiC Showing Essentially Pure TiC in Outer Chill Zone

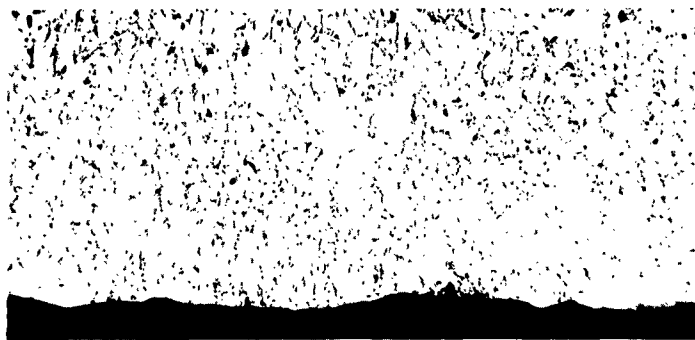


Figure 20. Microstructure of Hyperstoichiometric TiC Showing Fine Lamellar Eutectic in a Matrix of TiC



Figure 21. Microstructure of Hyperstoichiometric TiC Showing Free Graphite Flakes in a Matrix of TiC-C Eutectic

essentially 100 percent titanium carbide phase. Figure 20 shows a mixture of rich-in-titanium carbide with a small amount of fine eutectic and Fig. 21 shows that the hypereutectic region consists of the eutectic with the needle-like free carbon.

Future effort with respect to metallography will entail some investigation into suitable etchants. Those reported in the literature making use of sodium cyanide or boiling caustics are unsuitable for our use.

#### D. REFRACTORY OXIDES

##### 1. Background

The application of hot-pressing techniques to achieve rapid densification of inorganic powders has been quite successful in producing high-density compacts of refractory oxides. The mechanism or mechanisms whereby rapid rates of densification accrue are not fully understood. However, previous work on the hot-pressing of  $Al_2O_3$ , BeO, and tin powders indicates that a plastic flow mechanism may be a limiting process in a given density.

A limitation in carrying out a detailed investigation of the various parameters necessary to evaluate the densification mechanism in oxides is the high temperature requirement, i. e. , hot-pressing should be nominally carried out at  $\approx 0.5 T_{mp}$ . For this reason, it was felt that a study of the hot-pressing characteristics of an ionic solid with a relatively low melting point rather than an oxide would offer certain obvious advantages. Sodium chloride was selected as the material to investigate for the following reasons:

- a) It has the rock salt structure characteristics of at least one high temperature oxide (MgO).
- b) It has a melting point of  $801^{\circ}C$  which is easily attainable without special heating equipment.
- c) It is reported to exhibit ductile behavior in the polycrystalline form at temperatures above  $200^{\circ}C$ .
- d) The nature of the solid-state bonding is well understood.
- e) Fairly extensive information exists on the defect structure it exhibits when controlled impurity additions are made.

- f) Furthermore, the nature of solid-state diffusion processes occurring in NaCl has been studied in some detail.

## 2. Hot-Pressing of Sodium Chloride

The NaCl powder used was chemical reagent grade powder reduced to -325 mesh size by pulverizing in mortar and pestle. Samples weighing approximately 7 grams were loaded into a high-strength steel die 3 in. long and having a 1-in. diameter. Two plungers were used to locate the sample in the center of the die chamber. A split (clam-shell) furnace with nichrome element was used to heat the assembly to pressing temperature. A chromel-alumel thermocouple, used with a controller, sensed the element temperature, allowing control of specimen temperature to  $\pm 1.5^{\circ}\text{C}$  on a second specimen thermocouple located inside one plunger. Ram travel was determined by means of a dial gauge (reading to  $10^{-4}$  in.) which detected relative motion between the fixed platen and the ram of the hydraulic press system. Dial gauge readings were taken at fixed intervals of time beginning 1 min after the pressure was equilibrated for a given run. Pressings to date were carried out at effective pressures of 6400-9600 psi at temperatures ranging from room temperature to  $300^{\circ}\text{C}$  and for periods of four hours (except for one specimen pressed 16 hours).

At the end of a 4-hr pressing cycle, the furnace was turned off, the pressure released, and the die assembly cooled to handling temperature ( $< 50^{\circ}\text{C}$ ). The specimens were then pressed out of the die assembly and further cooled in a dessicator after which the density was determined by physically measuring the sample dimensions and then weighing the sample on a microbalance. A summary of these data is given in Table 4.

Figures 22, 23, and 24 show plots of relative ram motion versus time for the pressing cycles on specimens B-1 thru B-3. Two features which appear to characterize the limited number of pressings to date are noted from these plots. First, it is seen that the densities at 240-min pressing time are within a close range of values, i. e. , within a band of 2 percent theoretical density.

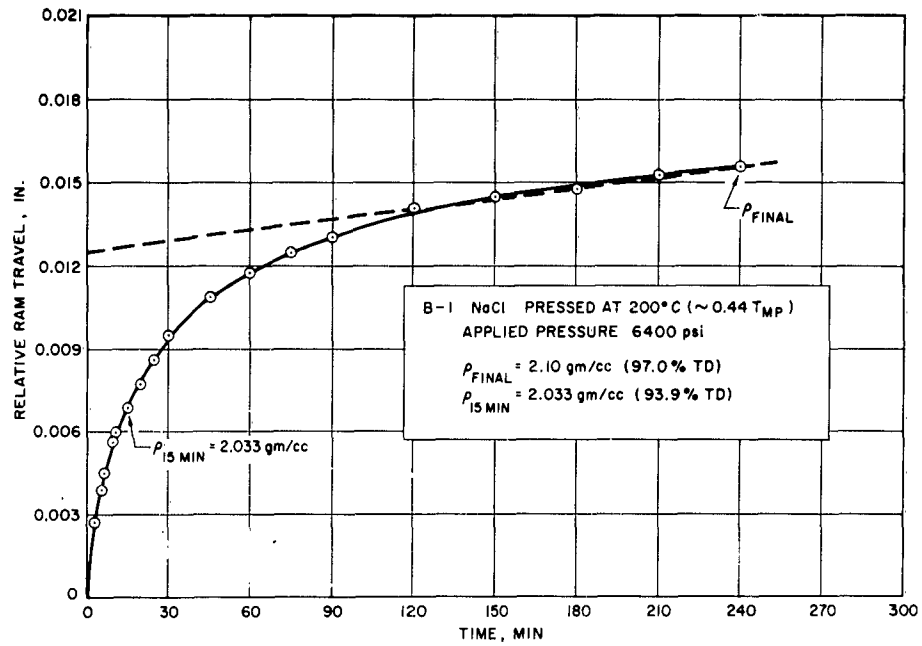


Figure 22. Ram Motion versus Time for Hot-Pressed NaCl at 200°C

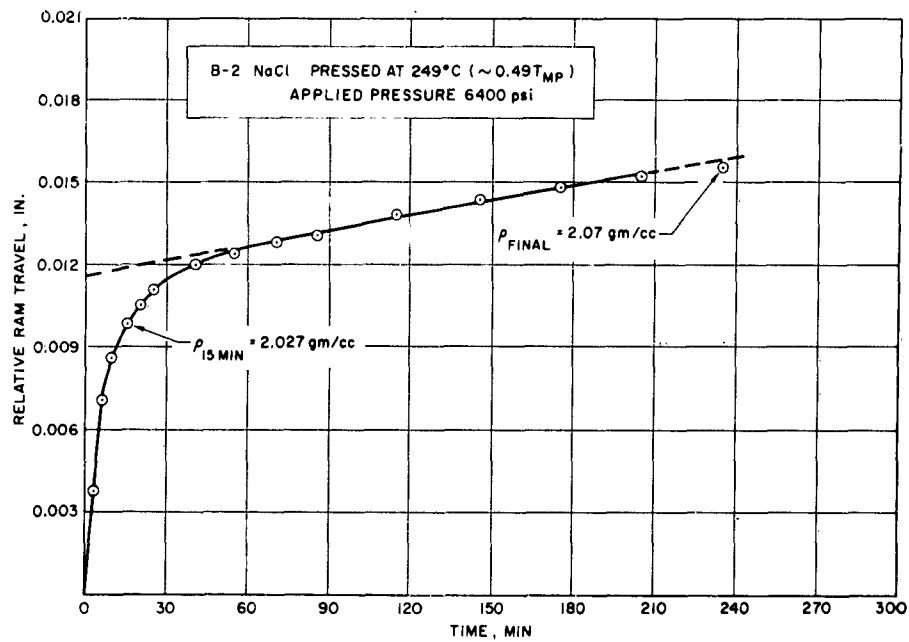


Figure 23. Ram Motion versus Time for Hot-Pressed NaCl at 249°C

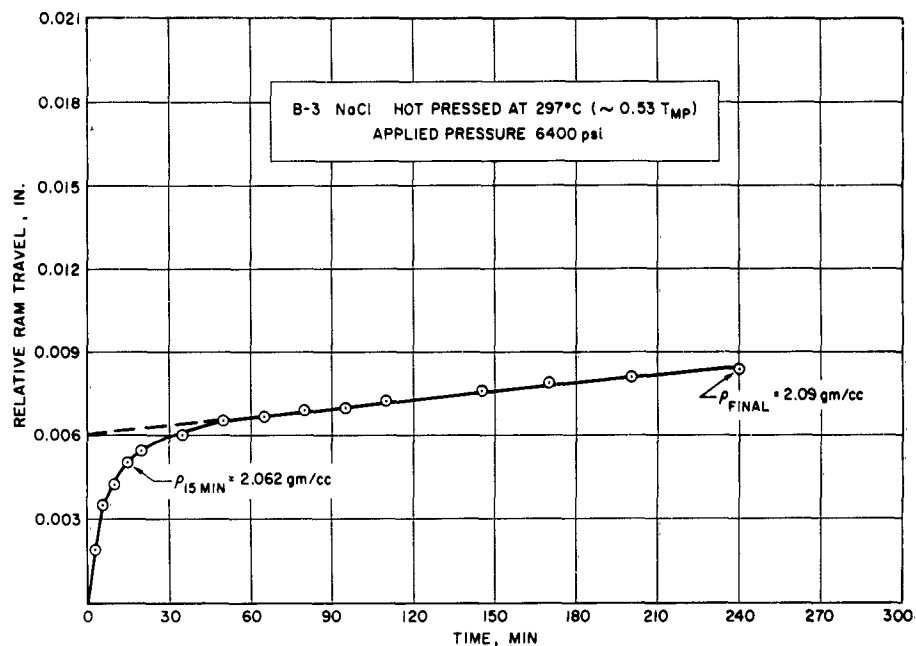


Figure 24. Ram Motion versus Time for Hot-Pressed NaCl at 297°C

Second, it is noted that the apparent steady-state densification rates (beyond 60 min for B-2 and B-3 and 120 min for B-1) are all of magnitude  $dD/dt = 1 \times 10^{-4} \text{ gm/cm}^3\text{-min}$ . Specifically, the values for 200°C and 298°C are  $1.1 \times 10^{-4}$  and  $0.8 \times 10^{-4} \text{ gm/cm}^3\text{-min}$ .

From Table 4 it is noted that specimens A-4 and A-5 fall within the same %TD band as specimens B-1 thru B-3. All five samples were pressed at identical pressure but at various temperatures, as indicated. Results on samples A-1, A-2, and A-3 are invalid due to contamination of the NaCl powder which occurred during reduction of particle size. Only one hot-pressing has been carried out at a higher pressure and for a longer time than 4 hr and, in this case, a marked improvement in density is noted, (see specimen No. 1).

Table 4. Densities of Hot-Pressed NaCl

Specimen No.	Temp (°C)	Pressure (psi)	Time (hours)	Film Density (gm/cc)	% TD	Color
B-1	200	6400	4	2.10	97	White
B-2	249	6400	4	2.07	95.6	White
B-3	297	6400	4	2.09	96.5	White
A-1	187 to 211	6400	4	2.15	99.31	Dark Brown to Black
A-2	248	6400	4	1.99	21.92	Light Brown
A-3	295	6400	4	1.92	88.68	Gray
A-4	298	6400	4	2.09	96.51	White (Coarse as received NaCl)
A-5	249	6400	4	2.08	96.07	--
1	200 Nominal	9600	16	2.131	98.4	Translucent (coarse powder)
2	27	~ 9600	16	1.934	89.3	White (coarse powder)

The extent of the investigation at this time is such that it must be regarded as exploratory. Any conclusions based on the results reported would, of course, be presumptuous; however, there are indications that NaCl may exhibit a marked departure from the hot-pressing behavior typical of a number of other solids. It is known, for example, that the principal requirement for plastic flow in polycrystalline ionic solids having the NaCl structure is the ability of the solid to deform by a wavy slip mode. This phenomenon is known to become the deformation mode of NaCl polycrystals at approximately 200°C, the temperature at which hot-pressing has produced high density (>96 %TD) NaCl specimens in the present investigation. Although it is not positively established that an endpoint density relation occurs in NaCl, the results to date would indicate that the characteristic displayed by BeO and Al<sub>2</sub>O<sub>3</sub>, for example, does not occur in NaCl. It should be pointed out that this may be a result of using a relatively high applied pressure in comparison with the flow stress of NaCl. Further experimental work is continuing to establish the express dependence of the hot-pressed density of NaCl on applied pressure and temperature.

UNCLASSIFIED

Aerospace Corporation, El Segundo, California. MATERIALS AND STRUCTURES PROGRAM. SEMI-ANNUAL TECHNICAL NOTE, 1 JULY - 31 DECEMBER 1962, prepared by Materials Sciences Laboratory, 20 May 1963. [158]p. incl. illus.

(Report TDR-169(3240)TN-1; SSD-TDR-63-76) (Contract AF 04(695)-169) Unclassified report

Progress during the report period on the study of the fundamental principles of crystal growth and the preparation of single crystals of laser and electronic materials for research purposes is reported in Laser and Electronic Materials. Studies on the effect of structure (crystal lattice and defects) on certain physical properties such as superconductivity, semiconductivity, laser activity, and mechanical behavior are reported in Materials Physics. The study of crystal growth is reported in Inorganic Chemistry. Results for electrochemical methods (over)

UNCLASSIFIED

UNCLASSIFIED

Aerospace Corporation, El Segundo, California. MATERIALS AND STRUCTURES PROGRAM. SEMI-ANNUAL TECHNICAL NOTE, 1 JULY - 31 DECEMBER 1962, prepared by Materials Sciences Laboratory, 20 May 1963. [158]p. incl. illus.

(Report TDR-169(3240)TN-1; SSD-TDR-63-76) (Contract AF 04(695)-169) Unclassified report

Progress during the report period on the study of the fundamental principles of crystal growth and the preparation of single crystals of laser and electronic materials for research purposes is reported in Laser and Electronic Materials. Studies on the effect of structure (crystal lattice and defects) on certain physical properties such as superconductivity, semiconductivity, laser activity, and mechanical behavior are reported in Materials Physics. The study of crystal growth is reported in Inorganic Chemistry. Results for electrochemical methods (over)

UNCLASSIFIED

UNCLASSIFIED

Aerospace Corporation, El Segundo, California. MATERIALS AND STRUCTURES PROGRAM. SEMI-ANNUAL TECHNICAL NOTE, 1 JULY - 31 DECEMBER 1962, prepared by Materials Sciences Laboratory, 20 May 1963. [158]p. incl. illus.

(Report TDR-169(3240)TN-1; SSD-TDR-63-76) (Contract AF 04(695)-169) Unclassified report

Progress during the report period on the study of the fundamental principles of crystal growth and the preparation of single crystals of laser and electronic materials for research purposes is reported in Laser and Electronic Materials. Studies on the effect of structure (crystal lattice and defects) on certain physical properties such as superconductivity, semiconductivity, laser activity, and mechanical behavior are reported in Materials Physics. The study of crystal growth is reported in Inorganic Chemistry. Results for electrochemical methods (over)

UNCLASSIFIED

UNCLASSIFIED

Aerospace Corporation, El Segundo, California. MATERIALS AND STRUCTURES PROGRAM. SEMI-ANNUAL TECHNICAL NOTE, 1 JULY - 31 DECEMBER 1962, prepared by Materials Sciences Laboratory, 20 May 1963. [158]p. incl. illus.

(Report TDR-169(3240)TN-1; SSD-TDR-63-76) (Contract AF 04(695)-169) Unclassified report

Progress during the report period on the study of the fundamental principles of crystal growth and the preparation of single crystals of laser and electronic materials for research purposes is reported in Laser and Electronic Materials. Studies on the effect of structure (crystal lattice and defects) on certain physical properties such as superconductivity, semiconductivity, laser activity, and mechanical behavior are reported in Materials Physics. The study of crystal growth is reported in Inorganic Chemistry. Results for electrochemical methods (over)

UNCLASSIFIED

UNCLASSIFIED	<p>used in the study of foreign metal ions in ionic solids are described in Electrochemistry of Solids. Work in High Temperature Chemistry during the report period consisted of studies in polymer synthesis and polymer mechanical properties and studies of the combustion of tetrafluoroethylene, which is the monomer and chief pyrolysis product of Teflon. Physical Measurements covers property changes in pyrolytic graphite for ballistic re-entry heat shields, space environment effects on prospective satellite thermal control surface materials, and laser effects on materials. Progress in studies on refractory metals, refractory metal carbides, and refractory oxides during the report period is reviewed in Metallurgy and Ceramics Research.</p>	UNCLASSIFIED
--------------	---	--------------

UNCLASSIFIED	<p>used in the study of foreign metal ions in ionic solids are described in Electrochemistry of Solids. Work in High Temperature Chemistry during the report period consisted of studies in polymer synthesis and polymer mechanical properties and studies of the combustion of tetrafluoroethylene, which is the monomer and chief pyrolysis product of Teflon. Physical Measurements covers property changes in pyrolytic graphite for ballistic re-entry heat shields, space environment effects on prospective satellite thermal control surface materials, and laser effects on materials. Progress in studies on refractory metals, refractory metal carbides, and refractory oxides during the report period is reviewed in Metallurgy and Ceramics Research.</p>	UNCLASSIFIED
--------------	---	--------------

UNCLASSIFIED	<p>used in the study of foreign metal ions in ionic solids are described in Electrochemistry of Solids. Work in High Temperature Chemistry during the report period consisted of studies in polymer synthesis and polymer mechanical properties and studies of the combustion of tetrafluoroethylene, which is the monomer and chief pyrolysis product of Teflon. Physical Measurements covers property changes in pyrolytic graphite for ballistic re-entry heat shields, space environment effects on prospective satellite thermal control surface materials, and laser effects on materials. Progress in studies on refractory metals, refractory metal carbides, and refractory oxides during the report period is reviewed in Metallurgy and Ceramics Research.</p>	UNCLASSIFIED
--------------	---	--------------

UNCLASSIFIED	<p>used in the study of foreign metal ions in ionic solids are described in Electrochemistry of Solids. Work in High Temperature Chemistry during the report period consisted of studies in polymer synthesis and polymer mechanical properties and studies of the combustion of tetrafluoroethylene, which is the monomer and chief pyrolysis product of Teflon. Physical Measurements covers property changes in pyrolytic graphite for ballistic re-entry heat shields, space environment effects on prospective satellite thermal control surface materials, and laser effects on materials. Progress in studies on refractory metals, refractory metal carbides, and refractory oxides during the report period is reviewed in Metallurgy and Ceramics Research.</p>	UNCLASSIFIED
--------------	---	--------------